Development of a Compact, Soft, Distributed 3-axis Hall Effect-based Skin Sensor: uSkin

ホール効果を利用したコンパクトかつ柔軟な分散型 3 軸スキンセンサー「uSkin」の開発

February 2019

Waseda University
Graduate School of Creative Science and Engineering
Department of Modern Mechanical Engineering,
Research on Intelligent Machines

Tito Pradhono TOMO
トモ　ティト　プラドノ

Abstract

Tito Pradhono TOMO

Development of a Compact, Soft, Distributed, 3-axis Hall Effect-based Skin Sensor: uSkin

Our dream is to have robots inside our house or office that can help us performing useful manipulation tasks (handling objects/ utilizing tools). Currently, robots are still far from perfect in terms of manipulation. One of the reasons is the lack of tactile sensing ability. Without this, robots will not have any information related to the contact location, grasping power, and force direction. Available tactile sensors in the market have some problems that make the implementation of tactile sensing for robots be difficult. Those problems are the rigid body, lack of shear forces information, low density of sensing points, and bulky hardware & electronics. Additionally, they are not affordable and the maintenance can be difficult.

This thesis will propose a method for developing uSkin, a tactile sensor that can cover many robot parts (skin sensor). uSkin achieved something that other skin sensors could not achieve previously: soft, 3-axis force measurement, high density (4.7 mm center-to-center distance), and compact in a single module. Despite the sensor's ability to have these features simultaneously, uSkin has 1 gf - 1800 gf range, 4.6% hysteresis, 500 Hz sampling rate, 72 dB Signal to Noise Ratio (SNR), and 0.4 gf & 0.04 gf resolution for normal & shear forces respectively. These specifications are more than enough for manipulating everyday objects that usually are in the range of 200 - 500 g. Moreover, the sensor is easy to produce and low cost in terms of manufacturing and labor effort. uSkin has been successfully mounted on the Allegro Hand, EzGripper, and iCub's hand for performing tasks such as object recognition, slip prevention, and tactile exploration.

The current implementation is limited to non-ferromagnetic objects only. This is because uSkin uses a Hall-Effect approach as its sensing principle. Although magnetic objects can influence the sensor's measurement, a compensation algorithm can be implemented. For example, the earth magnetic

field influenced the sensor's reading when the orientation of uSkin changed but could be eliminated by generating compensation values via kinematics.

Acknowledgements

First of all, I would like to thank my Professor, Shigeki Sugano, for accepting me to become a part of his laboratory, allocating his time for discussions despite his busy schedule, and giving feedback on my research. The journey of my doctoral degree would have never started without his support. And thanks to Associate Professor Alexander Schmitz for introducing me this wonderful laboratory, the Leading Program, this fantastic research topic, and connecting me to the IIT (Istituto Italiano di Tecnologia). My research finally became a product (uSkin), and we could establish our company, XELA Robotics as a result of that.

I also would like to say thank you to Dr. Sophon Somlor that has been becoming my mentor for developing a tactile sensor since I started my doctoral degree. Also my review of related work used his thesis as the basis for selecting the papers that I review in my own thesis. To Sensor team member (Harris Kristanto, Rawleigh Tucker, Prathamesh Sathe, Wai Keat Wong, and Jinsun Hwang). They helped me so much in the hardware development. Thank you to Satoshi Funabashi for always helping me translating Japanese. My Japanese language proficiency has been improving because of him. I would like to thank Kento Kobayashi for always putting his effort into managing our company, XELA Robotics despite being busy with his research. Without his help, the company would have never been established and my research would have never achieved this level. To Members of Sugano Laboratory, especially Alex Team, thank you for your help and support.

This research was partially supported by the JSPS Grantin-Aid for Scientific Research (S) No. 25220005 and JSPS Grant-in-Aid for Young Scientists (B) No. 15K21443.

Finally, I would like to thank my parents, family, and friends.

Contents

List of Figures

List of Tables

To my parents, family, and Ne.

Chapter 1

Introduction

1.1 Motivation

Humans have five basic senses: taste, smell, hearing, sight, and touch. Thanks to these, human can recognize and adapt to their unstructured world. Each sense associate to the others to give brain more information. For example, with a sight, human can quickly estimate the location of an object and grab it. However, without a touch sense, they will have a difficulty to maintain it from slipping as they cannot feel the contact location and force.

There are many things that can be done by using only the sense of touch alone. In case of there is no visible light, human can explore their world and figure out the location of the objects by gently touching them. They start to create a map in their mind. After they grasped an object, they can estimate its orientation and re-positioning it. When an unknown object hit or touched them, they can quickly react to it. These examples show a wide range capabilities of touch sensing.

As technology becomes more advanced, people start to use automation such as robots to save time and cost. In the future, the application will expand to pick and place objects in a warehouse and helping people in and around home (i.e. using tools). Versatile robots need to be able to manipulate any object for this kind of tasks. There are many competitions encouraging people to improve manipulation performance on robots. Amazon picking challenge and Toyota AI Ventures are some of the examples. The goal is to make robots safer, more useful, and more affordable.

To be able to manipulate objects, robots need to be equipped with an end-effector. The requirements can be different according to what kind of tasks should be accomplished. For example, for picking and manipulate objects in a warehouse, gripper seems to be enough. But for utilizing human tools, a multi-fingered robot hand is more suitable. Although their functionality

can be different, they need the same human-inspired ability that can lead to a successful manipulation: detecting contact locations and forces.

Vision is one important element for manipulation. With vision, robots can estimate the object position and orientation. However, for various reasons vision can fail or be insufficient. For example, the objects that are intended to be or being manipulated can be occluded and sometimes it is difficult to figure out their material properties and center of gravity. For this reason, relying on vision alone is often not enough.

Knowing the contact location, material properties, and the direction of the force are also important to achieve a successful manipulation. A tactile sensor is an interface modality to provide robots these abilities. By mounting tactile sensors intrinsically (embedded in the joints) or extrinsically (distributed in the skin) on robots, they can sense the objects they are in contact with. Regarding the intrinsic sensors, force sensors embedded in the joints can only sense the sum of all forces acting on the link and measure also substantial forces due to the robot's movement, and the joint angles only provide crude information about the contact with the object as well. Tactile sensors in the skin provide richer and more direct information than the sensors in the joints, which can be crucial for various applications. However, implementing distributed sensors in the skin is challenging.

1.2 Background

1.2.1 Importance of tactile sensing

In the future robots should share their workspace with humans and work in unstructured environments, and for safety and to perform adaptive tasks, a rich set of sensors is needed in such scenarios. Tactile sensors on the robot's surface can provide the most detailed and direct information about the contacts with the environment and are therefore a crucial component. Yet, the fact that they should be spread over the surface makes the implementation difficult. The importance of tactile sensors especially for robotic manipulation is reported in [1].

When designing tactile skin sensors, I consider that they should have the following characteristics: (i) soft, (ii) distributed, (iii) sensing the 3-axis force vectors and (iv) integrated electronics. (i) Softness of the robot's skin adds to the safety of the robot, because it adds a level of security that cannot be achieved with other methods. Active control schemes alone are typically too

slow for impacts. Compliant joints help, and are a crucial component as they can typically absorb more energy than soft skin, but they can only decouple the various links of the robot, while the inertia of the robot segments in contact with the human could still lead to harmful forces. Only soft skin can absorb impact energy directly at the collision site. Furthermore, soft skin in robot hands can enhance the grasp stability, and the Sugano lab previously found that soft skin also aids during manipulation [2]–[4]. (ii) Distributed skin sensors provide detailed information about the contacts with the environment, which can be used for example for tasks like tactile servoing or tactile object recognition [5]. Alternatives exist, like force sensors in the robot's joints, but they provide less information, as each sensor can only measure the sum of all the forces acting on it. (iii) While most distributed skin sensors only measure single axis force, measuring the force vector is required for tasks such as tactile servoing, and the Sugano lab has used such information for example for robust in-hand manipulation [3][6]–[8]. Distributed force vector measurements are useful in scenarios with more than one contact, a situation that is typically challenging for existing solutions that cannot measure distributed force vectors. (iv) When distributing many sensors in the robot's surface, without integrated electronics, a lot of wires would be required, which would require a lot of space and which would make the integration in the robot and their maintenance challenging. Distributed electronics can help, and several sensors should share a data line. Sending digital instead of analog information also makes the sensor signals less prone to interference from the environment.

1.2.2 Current state of tactile sensor development

A lot of different sensing principles have been used for tactile sensors [9], [10]. Most distributed skin sensors reported in literature can measure only 1-axis force for each sensor. This is because the sensors need to be arranged in a certain manner in order to be able to measure and distinguish multi-axis forces, which can be difficult to achieve in relatively thin robot skin. This review will focus on tactile sensing of multi-axis forces and Hall Effect-based sensors.

More broad reviews of tactile sensors were reported in [11]–[13]. Tactile sensing in both humans and robots is discussed in [9] and for human-robot interaction in [14], [15]. Recent reviews can be found in [16], [17].

TABLE 1.1: Comparison of different transduction technologies for tactile sensors

Sensing principle	Advantage	Disadvantage
Piezoresistive	• Many implementations • Robust	• Complex structure for 3D sensing required • Small-sized analog-digital converters not available
Hall Effect	• Small chip for 3D sensing available • Simple implementation	• Interference of external magnetic fields and ferromagnetic materials
Piezo electric	• Dynamic sensing with high sensitivity	• No sensing of static forces
Optical with camera	• Immune to electromagnetic interference • High density	• Large overall size due to camera
Capacitive	• Small chip for analog-digital conversion available • Good resolution possible • Robust	• Stray capacity • 3D sensing somewhat complex

Table 1.1 summarizes the benefits and disadvantages of various sensing principles. In particular, for most tactile sensors it is difficult to achieve dense 3-axis tactile sensing with a force range useful for manipulating everyday

objects.

(1) Piezoelectric-based sensors

One of the more common sensing principles for relatively thin robot skin is to use piezoelectric sensors. Polyvinylidene fluoride (PVDF) is commonly used as the piezoelectric material. Thin films can be produced which produce small amounts of electricity resulting from changes in force. These sensors are well suited to detect the onset of touch as well the small changes in force resulting from vibrations, and have been used for example to detect the texture of materials. To measure static forces, integration of the force changes must be conducted, which is prone to accumulate errors over time, and such sensors are therefore not best suited to measure static or slowly changing forces. Piezoelectric sensors have been implemented in robot hands [18]–[21] as well as in large scale skin to cover robot bodies; for example, the humanoid robot CB2 has 197 of such sensors distributed all over its body [22]. These piezoelectric films are not intrinsically soft, but can relatively easy be embedded in soft skin, as they are bendable.

While in the aforementioned skin sensors the force vector cannot be measured, a small and thin 3-axis tactile sensor based on MEMS piezoelectric elements is sold by Touchence [23], see Figure 1.1 (c). However, using this sensor for distributed skin sensing is challenging, as the sensor is rigid and the required additional readout electronics are rather bulky.

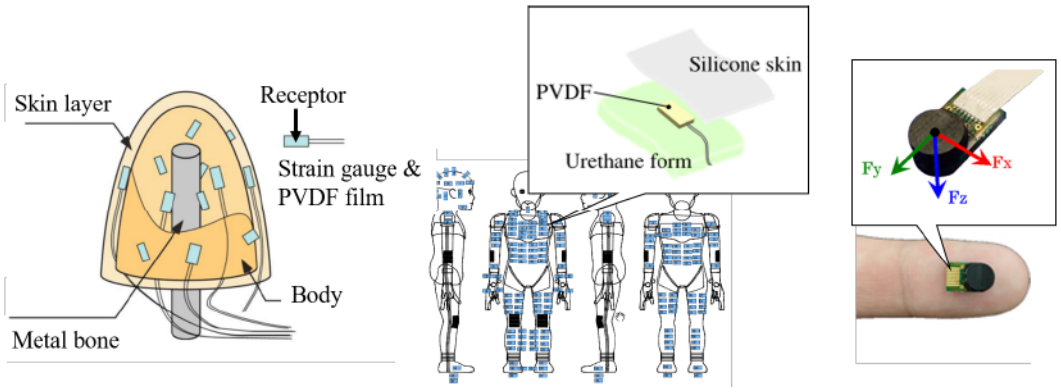

FIGURE 1.1: Related sensors based on piezoelectric sensing. (a) PVDF and strain gauges randomly distributed in fingertip. (b) CB2 humanoid robot covered with 197 piezoelectric sensors. (c) 3-axis sensor from Touchence. The pictures are taken from [21], [22] and [24], respectively.

(2) Optical-based sensors

Two different types of optical-based sensors are described in literature, and both of them have the potential to measure the force vector. The first type uses a camera to detect deformations in the skin membrane, for example [25], [26]. This type can achieve distributed force vector sensing with a high spatial density. It is suitable for the fingertip of robot grippers but is often too thick for other robot parts where the skin should be only several millimeters thick, because it requires a minimum thickness for the camera to be able to focus. The sensors in [27] use optical fibers and measure 3-axis force with high sensitivity, but the overall size is 42.6 mm high and 27 mm diameter. Another example is the TacTip series [28], see Figure 1.2 (a).

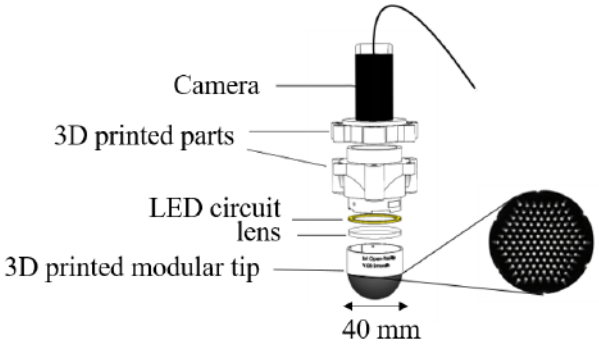

(a)

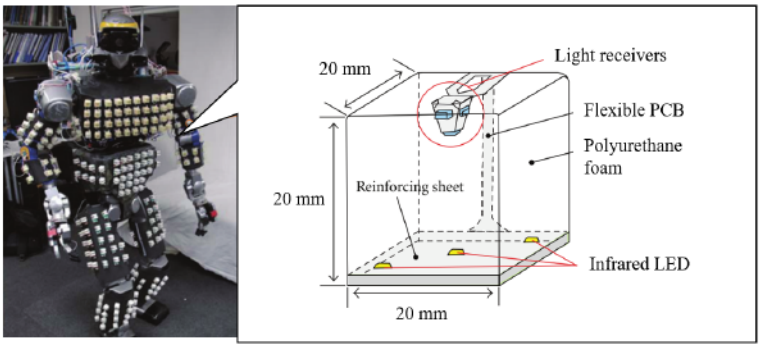

(b)

FIGURE 1.2: Related optical-based tactile sensors. (a) TacTip from Bristol. (b) 3-axis soft cubic sensor ShokaCube. The pictures are taken from [28] and [29], respectively.

The second type of optical-based sensors uses separate photoreceptors (not in the form of a camera) to measure light intensity; this type can measure the force vector in a slimmer package, however it does not achieve the high

spatial density sensing of the first type. The concept of a small sized 3-axis sensor for distributed sensing was introduced in [30]. A cubic optical 3-axis sensor with a size of 20x20x20 mm3 has been realized, using soft and light-weight polyurethane foam, and has been integrated in robots [29], see Figure 1.2 (b). Versions of this sensor are sold by Touchence. Optoforce sold a small-sized optical sensor (10 mm diameter and 8 mm high), but Optoforce is now part of OnRobot and this sensor does not appear on their website anymore [31]. All sensors mentioned in this paragraph require additional electronics, in particular for analog-to-digital conversion, which are typically bigger than the sensor itself, and make the integration of such sensors in high numbers on a robot challenging.

(3) Piezoresistive-based sensors

Strain gauges are a common method for force measurements. They are piezoresistive, as their electric resistivity slightly changes when being bent. Rather complex arrangements are needed to measure 3-axis or even 6-axis force/torque, which makes them typically too bulky for the integration in a thin skin. In the WENDY robot [32], robot covers were mounted to the robot via a 6-axis F/T sensor, and thereby forces acting on the robot cover could be sensed, see Figure 1.3 (a). Only one multi-axis force vector can be sensed, corresponding to the summation of all forces acting on the robot link. This is typically sufficient for applications such as to measure impacts and to ensure safety. Moreover, additionally, force-sensitive resistor (FSR) pads were put on the cover. The FSR pads can sense only 1-axis force. Several other robots use similar concepts, with distributed 1-axis sensors on the surface, and one multi-axis force measurement for one robot link. For example, [33], [34] uses 10x7.5x5.5 mm3 3-axis sensors in addition to skin sensors based on conductive rubber for each link of the MAC hand. The necessary electronics for analog to digital conversion are integrated in the hand a well. Another example is the TWENDY-ONE hand [35]: each fingertip has a multi-curved shape and integrates a 6-axis force/torque sensor, in addition to 241 distributed capacitive sensors covering the hands surface, see Figure 1.3 (b). However, the electronics for digitizing the sensor signals are rather voluminous and are not integrated in the fingers. While most force-torque sensors provide analog output and need additional electronics for analog to digital conversion, the 6-axis force/torque sensors in the DLR-HIT hand provide digital output [36], but the sensor is 16 mm long and has a 20 mm diameter, see Figure 1.3 (d). A rare example of a hand that manages to integrate a 6-axis F/T sensor in

each finger segment is the Robonaut 2 hand [37], [38], see Figure 1.3 (c). The Robonaut 2 hands overall is smaller than many other robot hands previously mentioned, and has a size more similar to a human hand. The electronics for the analog to digital conversion are not integrated in the fingers, but instead in the palm of the hand. The further away the analog to digital conversion happens from the transducer, the higher the susceptibility to noise, and the amount of wires increases.

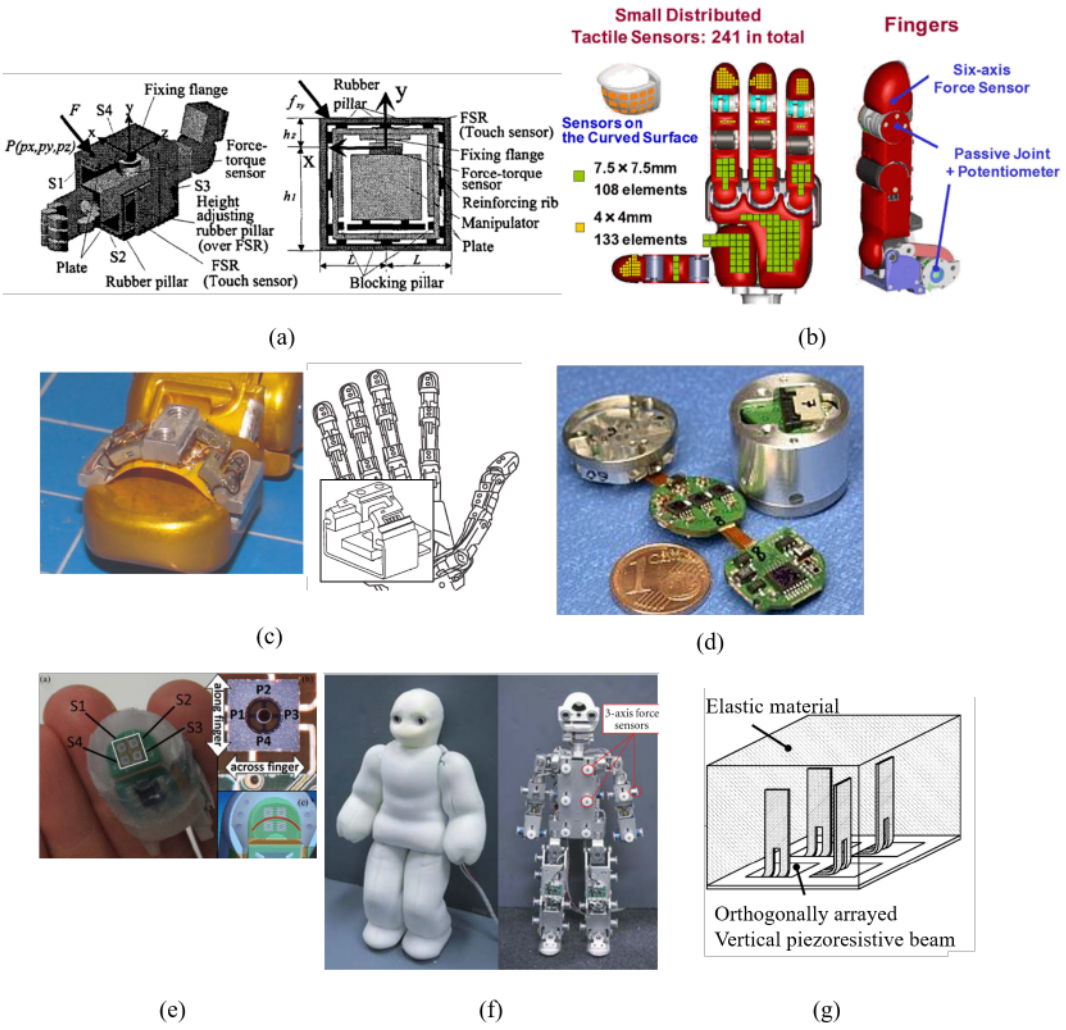

FIGURE 1.3: Related sensors based on piezoresistive sensing. (a) 6-axis force/torque sensor connected to WENDY cover. (b) TWENDY ONE fingertip with 6-axis force/torque sensor. (c) 6-axis force/torque sensor for Robonaut 2. (d) 6-axis force/torque sensor with digital output for DLR-HIT hand. (e) Fingertip with 4 tri-axial sensors. (f) Distributed 3-axis sensors for robot Macra. (g) A direct method to use strain gauges to measure shear force in soft skin. The pictures are taken from [29], [34]–[36], [38]–[40], and [41], respectively.

Distributed 3-axis sensors in robot skin were presented in [39], see Figure 1.3 (e). In particular, four 3-axis sensors for a robot fingertip were described, but the size of the additional electronics makes it difficult to cover larger areas with a high density. 3-axis sensors distributed over a wider area are shown in [29], see Figure 1.3 (f). This skin for the robot Macra is rather thick and would be difficult to use for robot hands. A concept for sensing multi-axis force with vertical arranged piezoresistive beams in an elastic material was described in [40]–[42], see Figure 1.3 (g). The production of each sensor was rather complicated, and the analog to digital conversion is not discussed.

(4) PSECR-based sensors

Another form of sensors based on resistive sensing, commonly used for skin sensors, use pressure-sensitive electric conductive rubber (PSECR). PSECR is well suited for realizing thin, pressure sensitive skin sensors, and they also have additional benefit for being inherently soft. To realize 3-axis sensing, a dome was placed on top of 4 such sensors [43], see Figure 1.4.

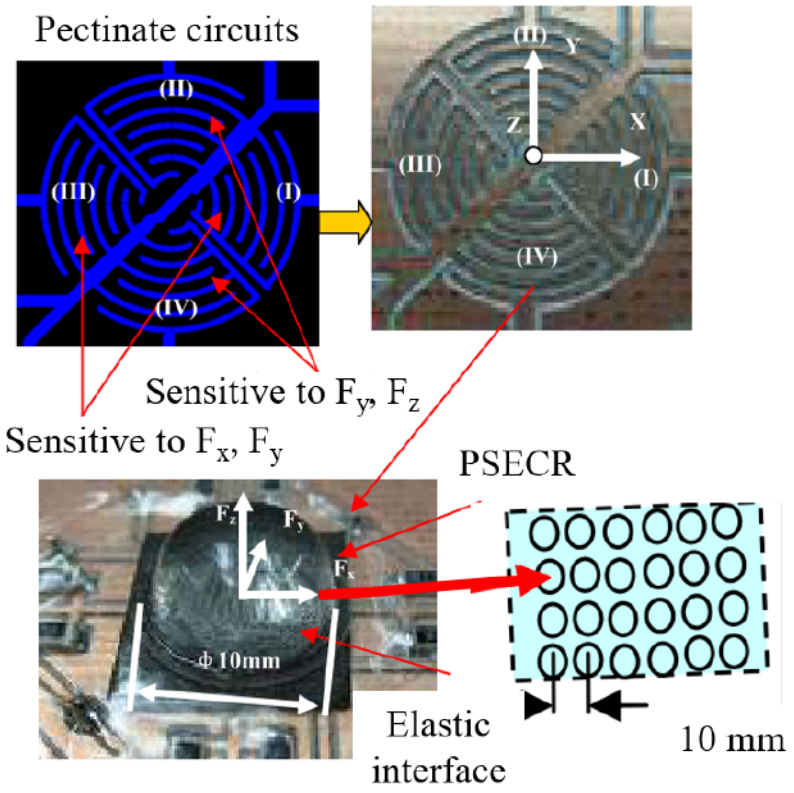

FIGURE 1.4: Related sensor based on pressure sensitive rubber. A dome is used so that the underlying sensor can measure shear forces. The pictures are taken from [43].

(5) Capacitive-based sensors

Capacitive sensors have been widely used as robotic skin sensors, and have good sensor characteristics in general [17]. However, making them into multi-axis sensors is challenging, similar to the other sensors discussed previously. A flat form factor for 3-axis sensing was achieved in [44], [45], see Figure 1.5 (a & c). Similar to [43] discussed previously, in [46], [47] a dome was added on top of four sensors to be able to sense shear forces, albeit only in the millinewton range, see Figure 1.5 (b). While these two sensors did not include small-sized analog to digital converters, small sized chips for capacitance to digital conversion are available and have been used for the skin in the humanoid robot iCub [48], [49], see Figure 1.5 (d). In general, for all these capacitive sensors the connection of the electrode on top of the compliant material and the shielding from stray capacitance is challenging. While the iCub skin only measures distributed single axis force, the chip used for the iCub skin could possibly also be used for the 3-axis sensors discussed previously. Indeed, our lab previously developed 3-axis capacitive sensors with digital output [50]–[52]. However, each 3-axis sensor had a size of more than 20x20x7 mm3, which is considerably bigger than the sensor developed in the current thesis, and was more time consuming to produce than the sensor that will be presented in this thesis. However, the sensor in [51] had the benefit of reliable shielding against electromagnetic interference. The skin in [51] used copper beryllium (CuBe2) plates, as did previously the Hex-O-Skin [53], to reduce the hysteresis and as a reliable top electrode. Each Hex-O-Skin module can measure proximity, temperature, 3-axis acceleration, and 3 normal forces, but not 3-axis force, see Figure 1.5 (e).

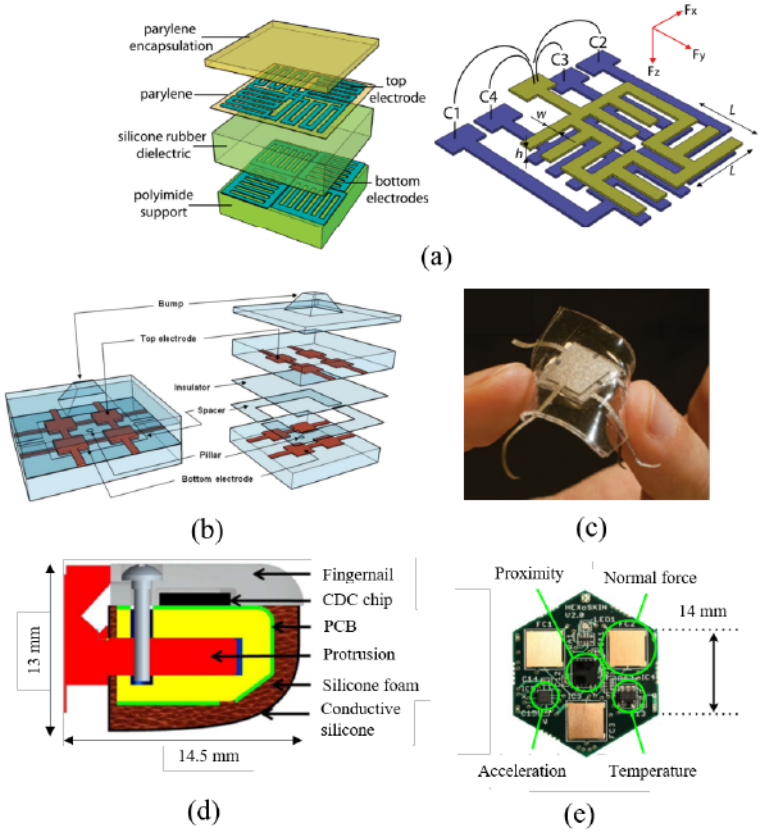

FIGURE 1.5: Related sensors based on capacitive sensing. (a & c) Flat capacitive 3-axis sensors. Shielding and analog to digital conversion is not included. (b) A small bump is used to detect 3-axis force. (d) Distributed 1-axis sensors for iCub fingertips with digital output. (e) Multimodal Hex-O-Skin module including 1-axis capacitive-based sensors. The pictures are taken from [44]–[47], and [53], respectively

(6) MEMS-based sensors

MEMS force sensors can be based on various sensing principles (for example piezoelectric [24] or capacitive [54]), but due to their special characteristics they are discussed separately. In particular, they are very sensitive, but their sensing range is also very small and they are fragile [54], [55], therefore they are typically not suitable as sensor skin for robots that grasp everyday objects.

(7) Hall Effect-based sensors

Hall Effect sensors together with a magnet have been used as skin sensors. A prototype 3-axis sensor with digital output was proposed [56], see Figure 1.6 (a). However, detailed sensor characterization, distributed sensing, and

the integration in a robot were all not performed. The robot James had such sensors integrated into its hands [57][58]. Each sensor measured 1-axis force, and an air-gap increased the sensitivity by making it easier for the magnet to move as a result of force being applied to the sensor, see Figure 1.6 (b). 3-axis sensors have also been proposed [59], [60]: A magnet was embedded in an elastic dome on top of 4 Hall Effect sensors, see Fig. Figure 1.6 (c). However, the output of the sensors was not digital, and the overall form factor was too big for thin robot skin.

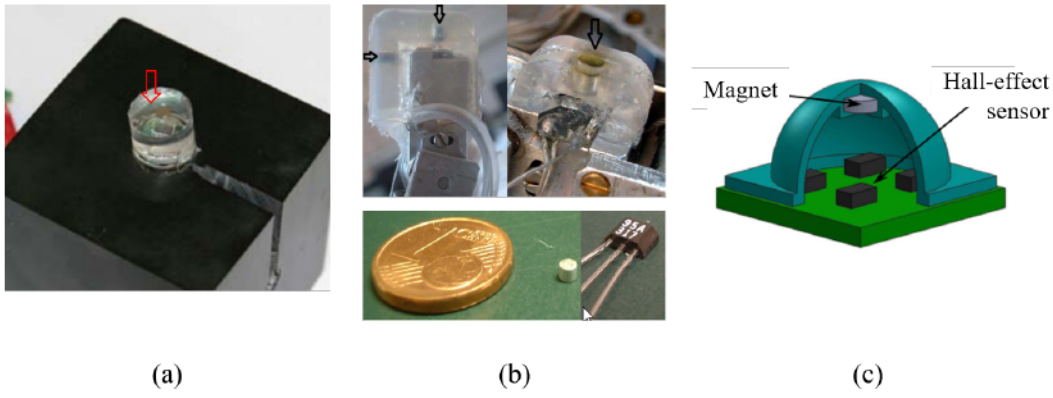

FIGURE 1.6: Related sensors based on Hall Effect sensing. (a) 3-axis sensor with digital output. (b) 1-axis sensor with air gap. (c) 3-axis dome-shaped sensor with 4 individual Hall Effect sensors. The pictures are taken from [56], [58], and [60], respectively.

(8) Summary of Related Work

Overall, currently existing sensors have the problem that it is difficult to make 3-axis sensors into a form factor suitable for robot skin. Furthermore, it is difficult to incorporate all the electronics to provide digital output in a small sensor package. However, if the sensors provide only analog output, many wires are required, which makes the integration of a large number of sensors in a robot difficult.

1.3 Objective

The goal of this research is to develop a skin sensor for robot hands and grippers that is affordable and accessible for everybody, yet applicable for dexterous manipulation tasks. Meanwhile, the sensor will be developed to meet main criteria below:

1. Soft: Beside it can act as a damper to reduce the impact force, a deformable surface can also increase the grasping stability during object manipulation. However, implementing soft materials will lead to problems such as hysteresis, causing measurement inaccuracies. Research on characterizing the crosstalk and hysteresis as well as how to reduce them will be conducted.

2. Measure normal and shear forces (3-axis). Although many skin sensors were successfully mounted on robots, only a few that can measure distributed 3-axis force. Shear (tangential) force can give more direct information such as the direction of the force and objects contour shape. Usually, achieving 3-axis with high spatial density will increase the overall size of the sensor itself. Therefore, the sensor and robot part usually must be integrated as one module (i.e. robot fingertip). A tactile sensor that can cover most of the robot parts (skin sensor) is preferable to avoid modification or replacing robot parts that are already available in the market.

3. Providing rich information (high density): The sensor will be developed to have a subcentimeter spatial density. By having distributed dense sensors, the contact location and geometry information can be more accurate.

4. Efficient implementation of distributed sensing (compact). Distributed sensors with many sensing elements typically cause integration problems that should be avoided. For example, the Sugano Laboratory has been developing the human-symbiotic robot Twendy-One since 2007. This humanoid robot has sophisticated hands covered with distributed soft skin sensor. It has 241 1-axis tactile sensors on each hand in total. Thanks to this sensor, Twendy-One could manipulate small objects such as straw and recognize multiple objects. However, large-scale tactile arrays usually correlated to an increasing number of wires used for delivering the data. Secondly, the analog measurements are converted to digital signals by relatively large sized additional electronics, that should be located close to the sensing site, and therefore further increase the space and weight requirements of the complete sensing system. These issues will also result in a high maintenance cost and labor effort. I2C connection will be implemented so that it can be easily integrated to a microcontroller. Moreover, I2C interface allows to chain

multiple chips in a single data line. This will significantly reduce the number of wires.

Additionally, the sensor developed in this thesis must be easy to produce and cheap. The sensor will be developed using a Hall Effect-based sensing. As mentioned before, this sensing principle allows us to achieve 3-axis sensing using a very simple construction without complex processing (i.e. image processing for optical sensor). Some 3D Hall Effect chips are also available and can be easily get in the market. The soft skin structure will be produced using a silicone material. Silicone is very cheap and can be easily purchased. It also gives more freedom to create any kind of shape. Recently, silicone also can be printed using a 3D printer making the prototyping is much easier and faster. High signal to noise ratio (SNR): A sensor with higher SNR value measures less noise, making it can have higher resolution. Fast response: Unlike a sensor in [61] that is aiming for an ultra high resolution for texture recognition, uSkin is developed mainly for a dexterous manipulation task that requires an agility. Therefore, higher sampling rate and faster response time are more important. According to [16], a tactile sensor should have more than 400 Hz of sampling rate for an in-hand manipulation task. uSkin will be developed to have a subcentimeter spatial density and also fast response time at the same time.

This thesis proposes a way to manufacture a compact, distributed, high density 3-axis soft skin sensor that can cover almost robot parts with few number of wires in low cost and effortless way.

1.4 Novel Contribution

As mentioned in Section 1.2.2, Hall Effect based skin sensors have been implemented previously, for example in [62], [63] and [56]. However, these works do not investigate the sensor characteristics in detail. Furthermore, as the semiconductor technology has evolved, small sized 3-axis Hall-effect sensors became commercially available. For example, MLX90393, a small 3D magnetometer (3x3x1 mm) chip can be purchased from Melexis. Since this chip has digital output, more than one sensor can be connected on the same data bus, reducing the numbers of physical wires. The chip can be directly connected to a microcontroller through I2C connection. As a result, the first skin sensor prototype using this chip was successfully developed in [64]. Also, for the first time, a mature characterization of the sensor such as its behavior against the temperature change, hysteresis, and crosstalk was

investigated. Compared to [57][58], the skin sensor in my work can measure not only normal force but also shear forces (3-axis).

The works in [60] [65] implement distributed tactile sensing using Hall Effect as their sensing principle. However, the center-to-center distance between the 3-axis sensors is more than 1 cm, therefore the previous work could not show that high density sensing truly can be implemented, especially when the sensors and permanent magnets are distributed in close vicinity. To prove the idea, the first distributed Hall Effect-based skin sensor where the distance between sensing points is less than 1 cm was developed for the first time in [66] for a flat surface, and in [67] for a multi-curved surface. As a result, 3-axis force sensing with a spatial density of 4.7 mm could be achieved. However, even though the sensor provides digital output, rather bulky readout electronics were used. Moreover, the magnets were embedded in conventional bulk silicone, causing severe crosstalk between the three measurement axis. To reduce the crosstalk between 3-axis measurements, I developed a new soft skin structure with air gaps in [68]. Several works are implementing an air gap structure for their skin sensors [65] [69]. However, they never investigated the importance of an air gap to reduce crosstalk. Instead, the air gap was used for increasing the sensitivity of the sensor [69]. Moreover, in [57][58][69] only one sensor for one finger phalange was implemented. Naturally, a high-density & distributed sensor will require a different structure than these related works.

In short, uSkin is the first compact, 3-axis Hall Effect-based soft skin sensor that is implementing distributed sensing using available 3D Hall Effect chip. The importance of air gap structure for reducing crosstalk in distributed sensing is also firstly investigated here.

1.5 Thesis Outline

This section provides the synopsis of each chapter in this thesis.

1.5.1 Chapter 2

The conceptual idea to achieve a low cost, small 3-axis soft skin sensor will be explained here. This chapter will show that 3-axis force measurement can be achieved by using MLX90393, a small 3-axis magnetometer from Melexis.

The idea is by using a permanent magnet to change the magnetic field surrounding the magnetometer (transducer). A small permanent magnet is implanted inside a soft structure such as silicon, floating above the transducer. When the surface of the uSkin is pressed, the permanent magnet will displace according to the force vector. This will cause changes in x, y, and z-axis of transducer's reading. Later this value can be converted into force or pressure through a calibration process. As the output of MLX90393 is already digital, an amplifier and ADC unit are not required. Moreover, this chip can communicate to a microcontroller through an I2C (Inter-Integrated Circuit) interface.

1.5.2 Chapter 3

In Chapter 3, uSkin with distributed sensing elements and its new structure will be shown. The transducer was successfully distributed every 4.7 mm. In a 25 x 25 mm area, 16 x 3-axis force data can be measured. The thickness can be reduced to 4 mm overall, reasonable enough to cover robot parts. Each module's measurements will be collected using a small microcontroller that can be daisy-chained through a CAN (Controller Area Network) protocol. Only one microcontroller needs to be connected to the main PC to read all sensor measurements. As a result, the number of final output wires that need to be used for communication is only 4.

In previous chapter, uSkin was developed using a simple, bulk structure. Because of this, there is no room for compression inside the silicon. When the sensor is pressed with a perpendicular force (normal force) to its surface, permanent magnets inside the silicone will also displace sideways. These uncontrollable movements are mistakenly detected as shear forces, affecting the x and y-axis measurements called a crosstalk effect. To reduce this effect, a new structure with an air gap was developed. Material selection is important to maintain the structure and reducing the hysteresis. For example, using too soft material will make the magnets attracting each other, deforming the whole structure. Using too hard material will reduce the sensitivity in shear forces measurement.

1.5.3 Chapter 4

In Chapter 4, the implementation of uSkin will be shown. This chapter will show that uSkin can be mounted on different robots to perform multiple

tasks. For example, uSkin was successfully mounted on the iCub, a humanoid robot developed by IIT (Istituto Italiano di Tecnologia) performing an object shape exploration task. Moreover, uSkin can also be mounted on commercially available robot hands/grippers, the Allegro hand and EzGripper for performing reactive grasping such as slip prevention.

1.5.4 Chapter 5

Chapter 5 will draw a conclusion, future works, and discussion. Although the sensor can be successfully developed, current implementation is limited to manipulation for non-magnetic materials. However, compensating magnetic influences is possible. For example, by having one sensor that does not measure displacements of a permanent magnet, the environmental of magnetic field can be detected. uSkin was initially developed to meet criteria for dexterous manipulation. But, the technology can also be implemented for covering other robot parts such as arm, torso, and legs. It can also be used for covering prosthetic limbs to help disabled people regain their ability to feel the touch through a tactile display.

Chapter 2

Hall-effect Based Skin Sensor

2.1 Background

This chapter presents an easy means to produce a 3-axis Hall effect–based skin sensor for robotic applications. It uses an off-the-shelf chip and is physically small and provides digital output. Furthermore, the sensor has a soft exterior for safe interactions with the environment; in particular it uses soft silicone with about an 8 mm thickness. Tests were performed to evaluate the drift due to temperature changes, and a compensation using the integral temperature sensor was implemented. Furthermore, the hysteresis and the crosstalk between the 3-axis measurements were evaluated. The sensor is able to detect minimal forces of about 1 gf. The sensor was calibrated and results with total forces up to 1450 gf in the normal and tangential directions of the sensor are presented. The test revealed that the sensor is able to measure the different components of the force vector.

2.2 Objective

The objectives of this chapter are:

1. Present an efficient way to produce a 3-axis Hall Effect–based skin sensor for robotic applications.

2. Discover the characteristics of the sensor and determine whether the sensor concept could be used for distributed sensing.

2.3 Sensor Description

2.3.1 Sensor Concept

The force vector can be detected by measuring a magnetic field change. To achieve that, a magnetometer (MLX90393) from Melexis [70] is used. A single MLX90393 chip is capable of providing 3-axis magnetic data and temperature data through the I2C fast mode protocol (four wires). The chip is mounted on a printed circuit board (PCB). I embedded the chip below a soft material, specifically silicone rubber, and implanted a small magnet above it as shown in Figure 2.1. The soft material acts as a compliant layer, and also transmits the force applied on the top surface. As a result, the small magnet will be displaced from its initial position when force is applied, causing a magnetic field change. For the experiments in this section, a PCB (the evaluation board from Melexis) with one single chip is used.

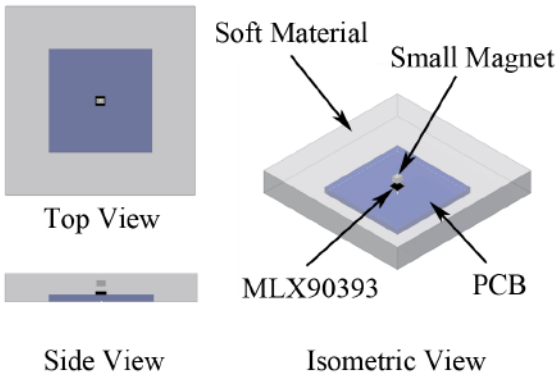

FIGURE 2.1: Conceptual image.

2.3.2 Soft Outer Layer

The following steps are required for the molding process. First, an MLX90393 chip is placed at the middle of a molding cast, supported with four guidance points and double-sided tape. The chip is covered by liquid silicone rubber (Ecoflex Supersoft from Smooth-On, shore hardness 00-30). To distribute the magnetic field evenly, the position of the magnet should be centered above the chip. A guidance lid (Fig. 2.2 a) is used to create a hole for placing a small magnet in the center. The magnet for the current implementation is a Neodymium magnet coated with nickel (Nd-Fe-B) with a dimension of 2

mm x 2.5 mm x 1.7 mm. After the first layer of silicone has cured, the magnet is placed inside the hole, and more liquid silicone rubber is used to cover it. The silicone layer above the PCB is 8 mm thick overall, with the small magnet covered by approximately 2 mm of silicone, as in Fig 2.3. In my experiments there was a good bond between the first and second layer of silicone. The silicone covers an area of 55 mm x 55 mm.

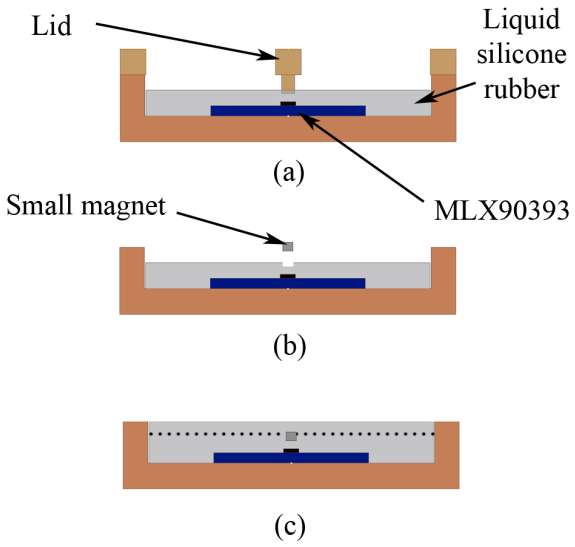

FIGURE 2.2: The molding process: (a) Liquid silicone rubber was poured into the molding cast; (b) A small magnet was placed inside the hole; (c) More liquid silicone rubber was poured above the first layer to cover the small magnet.

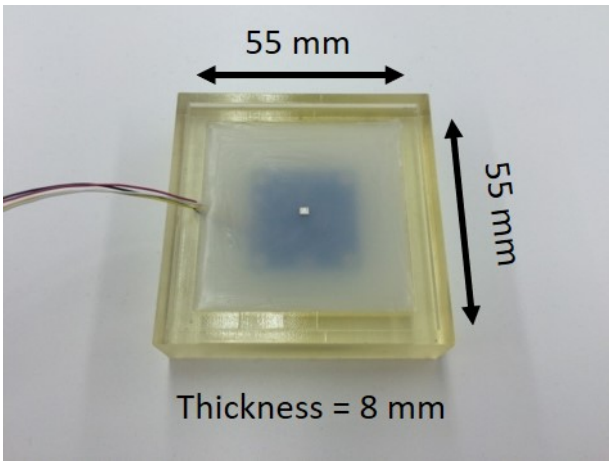

FIGURE 2.3: The prototype of the Hall effect-based skin sensor.

2.4 Sensor Characterization Method

Three experiments were conducted to understand the characteristics of the sensor. This section explains the experimental setups and procedures that were used during the tests.

2.4.1 Temperature Drift Test

This test studies the effect of thermal drift on the sensor reading. The skin sensor was placed inside an oven along with a Sparkfun TMP102, which is an I2C temperature sensor for measuring the temperature inside the oven during the test. The MLX90393 chip also includes a temperature sensor. The experiment started with the room temperature of 27° C, then the sensor was heated up until the skin sensor reached 40° C. Afterwards, the oven was turned off and the door of the oven was opened to let the temperature drop to around 30° C. The temperature value and the skin sensor's readouts were recorded using Arduino Due, stored in an SD (secure digital) card.

2.4.2 Hysteresis Test

A viscoelastic material such as silicone can introduce hysteresis in the sensor's force measurements. To evaluate the hysteresis, the skin sensor was placed on top of an acrylic platform table tilted 45 degrees in the y-axis direction. The sensor was pushed for 5 min with a load of 1450 gf (the maximum load that the experimental setup can achieve). To perform this, a voice coil motor (VM5050-190 from Geeplus), a linear bushing, an aluminum shaft adapter, a six-axis force/torque (F/T) sensor (Nano 1.5/1.5 from BL Autotech) for monitoring the pushing force during the experiment, and a 30 x 30 mm acrylic push plate, which is used to push on the proposed sensor, were utilized. The configuration for this test can be seen in Fig. 2.4. Two microcontrollers were required due to the different input voltage of my sensor (3.3 V) and the F/T sensor (5 V). The data from both sensors were recorded into the SD cards installed on Arduino Due and Uno with the synchronized sampling rate of 100 Hz in my experiments (the maximum sampling rate of the Hall effect sensor is about 240 Hz to measure all three axes). Finally, the voice coil motor applied no force on the sensor for one minute, and afterwards the acrylic push plate was retracted. The silicone is sticky, and therefore a force in the minus z direction is recorded when the acrylic push plate is removed.

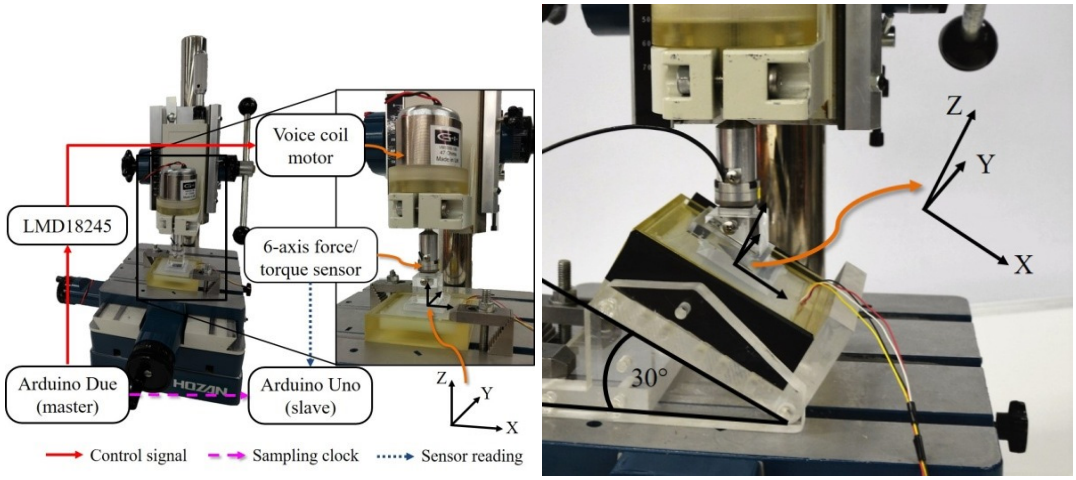

FIGURE 2.4: Experiment setup used in this section. The right side shows the addition of the adjustable angle tilt stage and the angle push plate, in particular the 30-degree setup where the stage is adjusted to 30 degrees and the 30-degree push plate is used.

2.4.3 Load Test

To calibrate the sensor and to evaluate its capability of tri-axial force measurement, two experiments were conducted. The first experiment was a normal force test where multiple magnitudes of normal force were applied on the sensor's top surface. In the second experiment, the sensor was pushed with both normal and shear force in different angles and with different force magnitudes.

The configuration for this experiment was similar to the hysteresis test. In the normal force experiment, the skin sensor was mounted directly on the flat and sturdy X-Y table. In the shear force experiment, the sensor was mounted on an adjustable angle tilt stage (Fig. 2.4). This acrylic stage was fixed to the X-Y table. The angle can be adjusted in three different positions that are 15, 30, and 45 degrees, and corresponding acrylic push plates with the same angles were used.

In both the normal and shear force experiments, the sensor was pushed by the voice coil motor with a stepwise force and its magnitude was increased every 10 seconds. The applied force was ranging from approximately 70 gf to 1450 gf. A Savitzky-Golay filter was utilized to filter all data (polynomial order = 4, frame size = 21). I performed the normal force test and the shear force tests with 15, 30, and 45 degree, in four directions (+/ x/y direction).

2.5 Results

2.5.1 Thermal Drift Evaluation

From Fig. 2.5 it can be clearly seen that the Hall effect sensor measurements change with the changing temperature, even though the temperature change measured by the chip was slower than the external temperature. A possible explanation for the change in the Hall effect measurements is an expansion of the silicone packaging with higher temperature. The test also revealed that the sensor reading in the z-axis was the most affected by the temperature change, but also the x-axis and y-axis measurements slightly changed; a closer look reveals that the y-axis is more affected than the x-axis. This is in accordance with the results presented in Section 2.5.3, which show that changes in the z-axis also affect the x-axis and y-axis, which might be due to a slightly misaligned magnet. The graph shows that the sensor changes are proportional to the temperature change measured by the chip, meaning that temperature compensation can possibly be performed.

A linear regression was conducted to find the coefficient k for calibrating the sensor's outputs. I selected a Huber robust model for this task. The temperature compensation was calculated as follows:

$$S_{i,T} = S_i - k_i \times \Delta S_T \tag{2.1}$$

where:

1. i is each axis of the skin sensor (x, y and z).
2. S_i and S_i,T are the skin sensor readout and compensated value, respectively.
3. ΔS_T is the temperature change measured by the MLX90393 built-in temperature sensor.

To evaluate the temperature compensation performance, another test was conducted. This time, the temperature was raised to 35° C. Fig. 2.6 shows a comparison between the sensor's readout before and after the compensation was applied. A moving average of the temperature was used for the compensation. After being compensated, the z-axis maximum value was around 600 digits (over a full scale of 65,500 digits), which corresponds to 120 g in my experiments (contact size 30 x 30 mm). Further improvements are likely possible by employing a high-pass filter. Furthermore, small steps can be seen

on S_y and S_z. The cause of those is not clear and will be further investigated in future work.

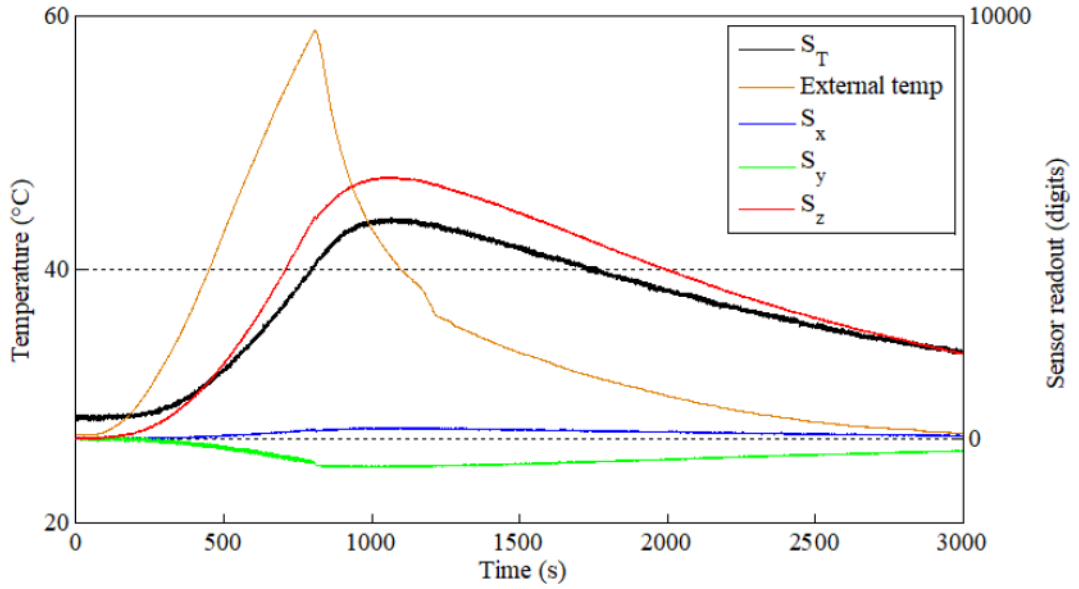

FIGURE 2.5: The effect of temperature changes on the sensor measurement.

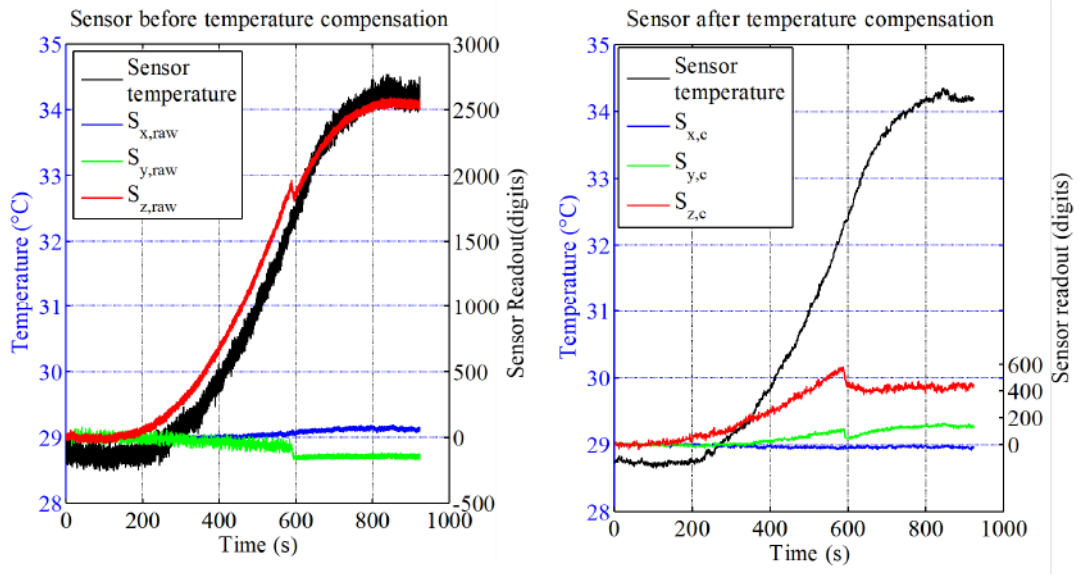

FIGURE 2.6: A comparison between the sensor's readout before and after temperature compensation was applied. The right figure also shows the moving average of the sensor temperature, which was used for calibrating the sensor.

2.5.2 Hysteresis Evaluation

As expected, there is hysteresis in the sensor measurements. In the result presented in Fig. 2.7, it took about one minute for the sensor to reach its quasi-static state, both while loading and unloading the sensor. The x-axis, which was not loaded, showed only a minor drift. Please note that an optimal soft material selection was not the focus of this study, and the hysteresis can probably be reduced with different materials, for example closed-cell foams.

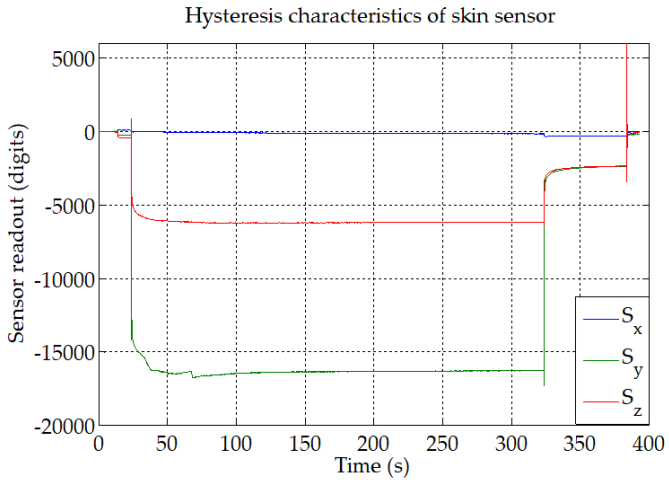

FIGURE 2.7: Hysteresis characteristics of the skin sensor.

2.5.3 Load Tests and Calibration

The results from the load test can be seen in Fig. 2.8. Fig. 2.8 a,b show the Hall effect and reference force sensor readout, respectively, when only a normal force is applied. Even though only normal force was applied, the Hall effect sensor also detected a magnetic field change in the y-axis. A related effect is also described in Section 2.5.1, and I suspect that the orientation of the small magnet was not perfectly aligned with the sensor and caused this. Furthermore, as silicone is soft but incompressible, forces in one axis can cause movements in another direction, as the silicone moves away from the pressure.

Fig. 2.8 c shows the Hall effect sensor response when a 45-degree shear force is applied in the y-axis. Even though no force was applied in the x-axis, as can be also seen from the measurements of the reference sensor in Fig. 2.8 d, the Hall effect sensor also detected a small magnetic field change in the x-axis direction. Furthermore, the y-axis Hall effect sensor measurements are bigger than the z-axis measurements, even though the force in the z-axis

was bigger. Due to this cross-talk and different magnitude of the skin sensor response, a calibration was performed.

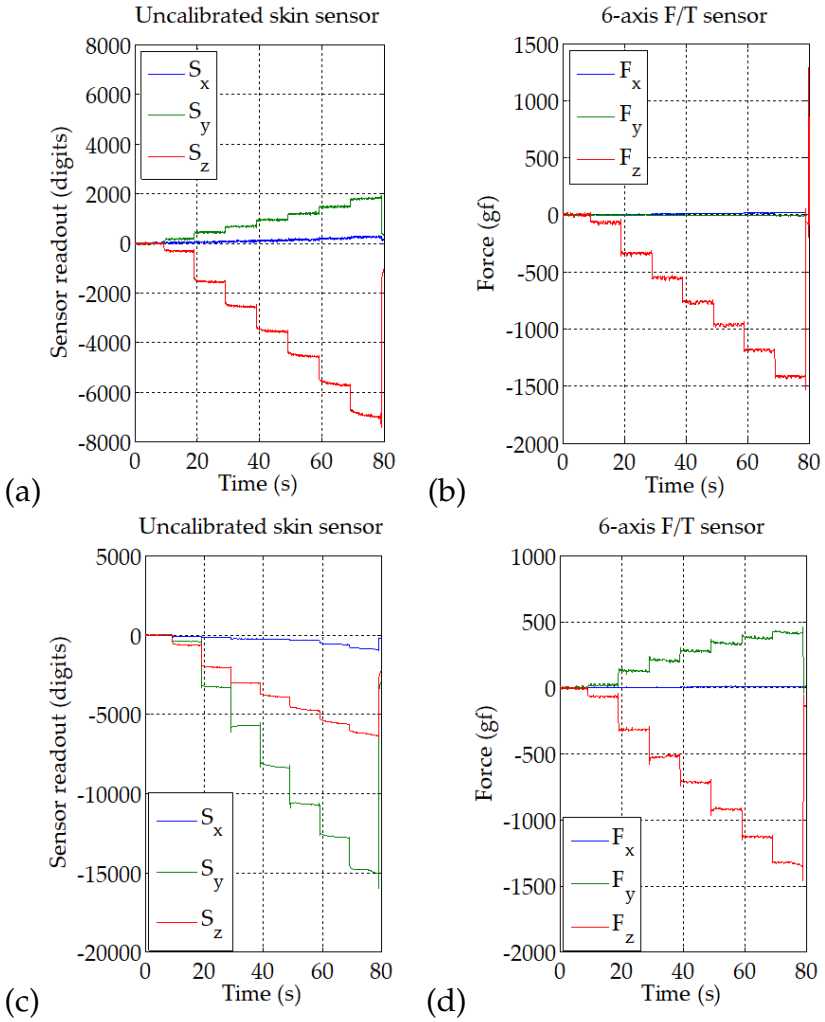

FIGURE 2.8: The sensor's readout (a) and the corresponding force from F/T sensor (b) when only normal force is applied; The sensor's readout (c) and the corresponding force from F/T sensor (d) when 45-degree shear force is applied in the y-direction.

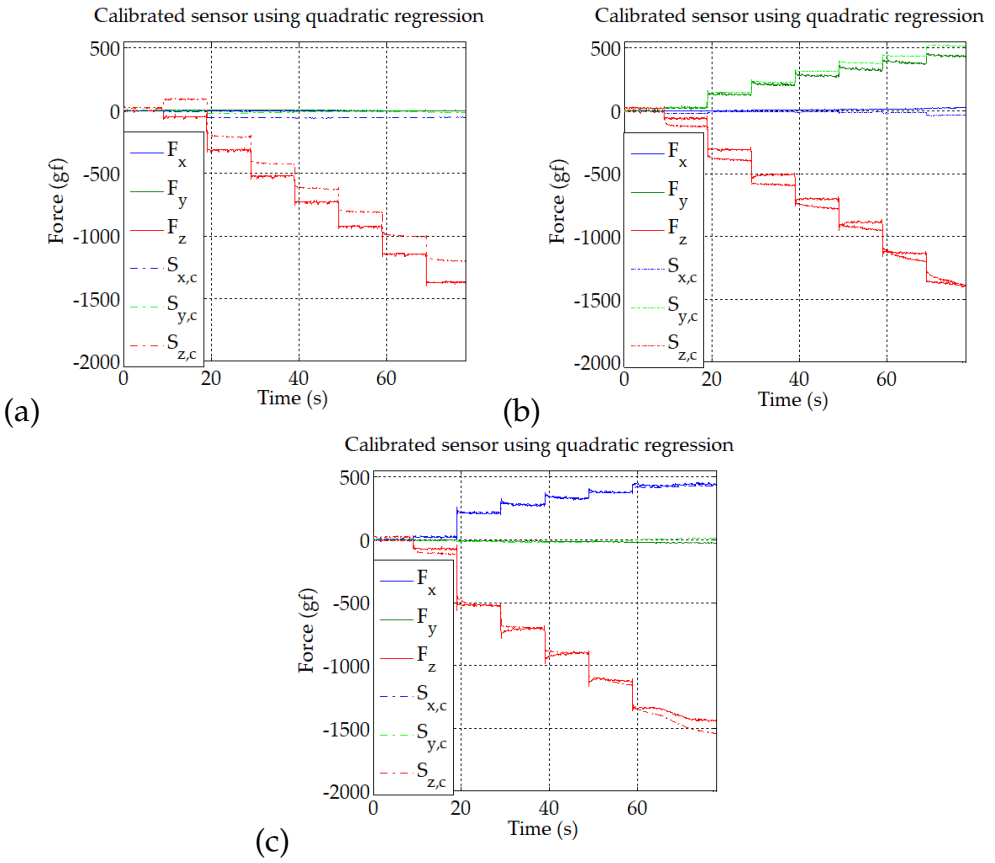

FIGURE 2.9: (a) Normal force; (b) 45-degree (y-axis direction); (c) 45-degree (x-axis direction) force calibration result. Sx,c, Sy,c and Sz,c are the calibrated skin sensor measurements.

Different models were used to calculate the x, y and z forces from the Hall effect sensor values, with the measurements of the six-axis F/T sensor as the reference. To calculate the parameters for the calibration, datasets from all angles were used. For the evaluation purpose, I used new datasets that were not used for the calibration. Robust Huber regression was used (MATLAB function LinearModel.fit); least squares regression performed nearly the same as the robust Huber regression. A quadratic model performed better than a linear model, as can be seen by higher R-square values in Table 2.1. Also, a neural network (one hidden layer with 20 hidden units) was trained with the same training data that I used for approximating the parameters of the linear or quadratic equation. The neural network performed better for the test case with only normal force, but overall the quadratic equation performed best. The calibration result using the quadratic model is shown in Fig. 2.9. The graphs show the comparison between the force detected using the F/T sensor and the force calculated using the skin sensor. A good correspondence between the measurements can be observed, with the biggest

TABLE 2.1: R-squared value for the normal force and shear force experiments.

	Linear + Huber	Quadratic + Huber	FNN
Normal Force	0.8634	0.8925	0.9368
Shear 45 – y	0.8634	0.9418	0.8275
Shear 45 – x	0.9272	0.9744	0.9644

differences in the normal load case for the z-axis.

As a final evaluation, the minimum detectable load was evaluated. Rubber weights with a diameter of about 1 cm were placed on the sensor and it was found that a force of about 1 gf in the z-axis produced sensor measurements that are higher than the observed noise of the sensor, as can be seen in Fig. 2.10. The calibration is slightly incorrect in this case, showing a measurement of 2 gf. This might be partially due to the different contact area than that during the calibration. Nevertheless, it can be seen that the sensor can already detect a 1 g weight.

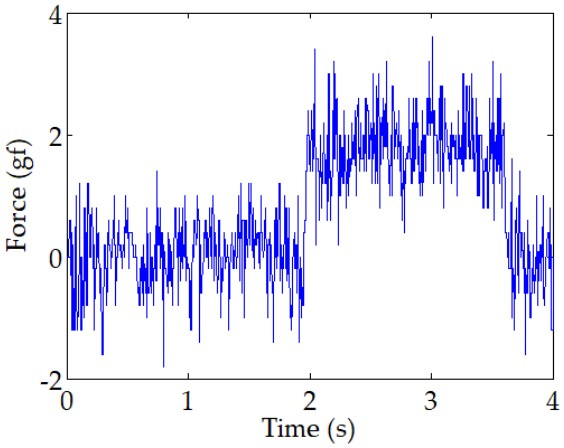

FIGURE 2.10: The z-axis calibrated sensor measurements (Sz,c) when a weight of 1 g (contact area of about 1 cm2) is placed on the sensor at a time of around 2 s.

2.6 Discussion

A sensor similar to my sensor prototype was introduced in [56]. The 3D Hall effect-based tactile sensor had a diameter of 15 mm, and it was claimed that it would be possible to reduce it to 10 mm. The sensor had digital output and the additionally required electronics such as microcontroller to read the sensor data are also small. However, the minimum thickness of the sensor was not mentioned. The uSkin prototype presented in this chapter has a size of 55 mm x 55 mm x 8 mm, but is possible to reduce the size to less than 5 mm x 5 mm x 4 mm, which will be proven in the next chapters. Although a rather bulky microcontroller was used for the experiments, uSkin can be connected to any kind of microcontroller through its digital I2C port without any further signal amplification. uSkin will be used with small sized microcontrollers in later chapters. The significant contribution on the research presented in this chapter compared to [56] and other related work is that a mature sensor characterization for a 3D Hall-effect based tactile sensor was performed for the first time. The tests in this chapter include observing the sensor's behavior when the temperature changes, investigating the cross-talk between each axis due to the incompressibility of silicone and proposing methods to eliminate it, and conducting hysteresis tests.

Although the concept of using the MLX90393 chip to develop tactile sensors could be successfully implemented, it is not certain that the sensors will still be able to work properly when the chips and permanent magnets are distributed in close vicinity to each other, especially with subcentimeter spatial density. For example, the permanent magnets can attract each other or interfere with neighboring Hall effect sensors. Therefore, the sensors' behavior when magnets are distributed with subcentimeter density needs to be investigated. Chapter 3 will introduce uSkin with distributed sensing elements as well as its characterization.

2.7 Conclusion

This chapter presented the design and characterization of a Hall effect–based soft skin sensor.

1. A soft, 3-axis skin sensor can be manufactured in low-cost and effortless way.

2. The temperature test shows that the skin sensor's readout in the z-axis direction was the one mostly affected by temperature changes (2500 digits at 34° C). Using a built-in temperature sensor, drift compensation was performed, reducing about 84% of the drift. Next, the hysteresis was evaluated. The sensor requires about one minute to reach its quasi-static state, both while loading and unloading the sensor. Indeed there is hysteresis in the sensor measurements, which is to be expected due to the use of silicone, which is a viscoelastic material. After the calibration of the sensor, when applying varying amounts of normal and shear force, the tests showed that the sensor can measure the components of the force vector. However, it is still difficult to determine whether the concept will work for a distributed sensing implementation at this stage. Therefore, the next chapter will investigate further about this issue.

Chapter 3

uSkin with Distributed 3-axis Sensing Elements

3.1 Background

In this chapter, uSkin that implements multi taxels will be introduced.

A good skin sensor should be able to cover not only a flat surface, but also a multicurved surface. There are two models that have been developed so far. The first one uses a rigid PCB for covering a flat area such as robot phalanges. The other model is uSkin with a flexible PCB for covering multicurved surface such as fingertip. They were developed based on the shape of the Allegro Hand, a commercially available robot hand from Wonik.

3.2 uSkin - Flat Module

3.2.1 Objective

In the previous chapter the prototype Hall effect sensor to measure a single 3-axis force vector was introduced; the drift due to temperature and a compensation algorithm using the integrated temperature sensor, minimal detectable normal force, and 3-axis calibration were discussed. The current section introduces sensor modules with 16 3-axis force vector measurements that are ready for the integration in a robot hand and evaluates the distributed force vector measurements.

In particular, the current section introduces distributed tactile sensors for the flat phalanges of the Allegro hand. Each module is 26 mm long, 27 mm wide and 4 mm high; each module can measure 16 force vectors with 16 3-axis Hall effect sensors. The output of each module is digital and requires only seven wires. The back of the sensor modules is flat so that they can be

attached to the Allegro hand straightforwardly. The sensor modules incorporate silicone (2 mm – 3.5 mm thick, depending on the location); softness for robot skin has been shown to be beneficial for safety and object handling. Furthermore, in addition to the 16 force vector measurements, each module also has eight 3-axis accelerometers and all 24 sensors also measure temperature. Therefore, the modules also provide multimodal information. These features expand the potential applications of this sensor for not only force control, ensuring grasp stability and for tactile servoing, but also for classifying the surface texture and enhanced tactile object recognition. This section focuses on the Hall effect sensors to measure the distributed 3-axis force vector. Experiments were performed to evaluate the crosstalk of the Hall effect sensors.

3.2.2 Sensor Description

(1) Design

In the previous chapter I developed the first prototype of a Hall effect based skin sensor with a single MLX90393 chip and successfully detected normal and shear forces. A single chip can provide 3-axis magnetic data and temperature data. A small magnet is placed above the chip, and the movement of the magnet can be acquired by measuring the magnetic field change, which corresponds to the 3-axis force. For the integration into a robot hand, especially for the purpose of in-hand manipulation, a distributed force measurement is beneficial. For this reason, I improved the skin sensor by developing a custom PCB mounted with 16 Hall effect sensor chips. The chips were distributed within a 26 mm x 27 mm area, placed 4.7 mm apart from each other as shown in Fig 3.1. 16 small magnets were embedded above the chips. A deformable material such as silicone is necessary to create a layer between the chip and the magnet. The MLX90393 has I2C fast mode protocol (4-wire). Each chip has a 7-bit address, and the last 2 bits can be configured by connecting the corresponding pin to either the power source or ground. For this reason, one data line (SDA) can share four chips at the same time. Four SDA lines are required to acquire force measurements from 16 chips. One module has seven cables including VCC (+3.3 V), GND, SCL, and four SDAs for communicating with a microcontroller. I used a multiplexer or I2C splitter with PCA95448A from BitWizard connected to the Arduino Due's SDA port.

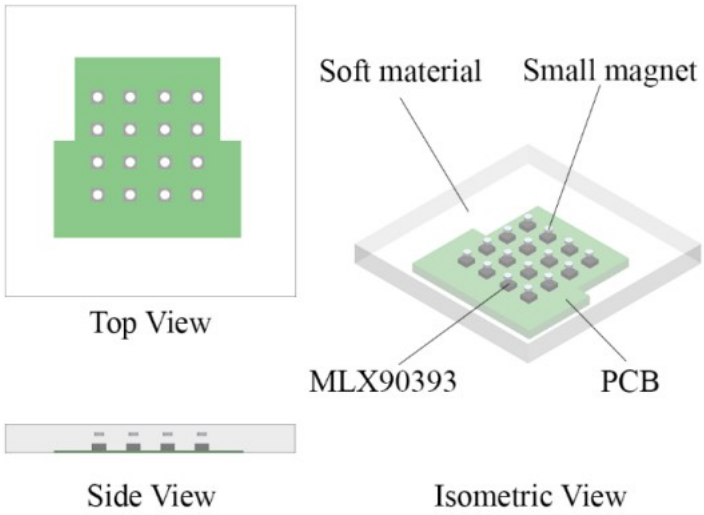

FIGURE 3.1: Conceptual design for flat module.

(2) Manufacturing Process

Fig. 3.2 shows the manufacturing process for the distributed skin sensor. First, the custom PCB with 16 MLX90393 chips was placed in the middle of a molding cast. The guidance lid (Fig. 3.2 (a)) for making 16 holes was placed on the top of it, ensuring the holes were placed in the center of each chip. Afterwards, enough liquid silicone rubber was poured for the silicone to cover all the PCB and touch the lid. After the silicone had cured, the lid was removed, leaving 16 small holes. 16 small magnets were placed inside the holes, floating about 1mm above the chips. The magnet for the current implementation was neodymium (grade N50) with a 1.59 mm diameter and a 0.53 mm thickness. It had an optimal pull of 226.8 g and 729 surface gauss. After the magnets had been placed inside the holes, more liquid silicone rubber was poured to cover the magnets with silicone. The overall thickness of the silicone layer above the PCB is 3.5 mm. Considering the thickness of the chip (1 mm) and the magnet, the silicone has a thickness of at least 2 mm. The prototype of the proposed sensor can be seen in Fig. 3.3.

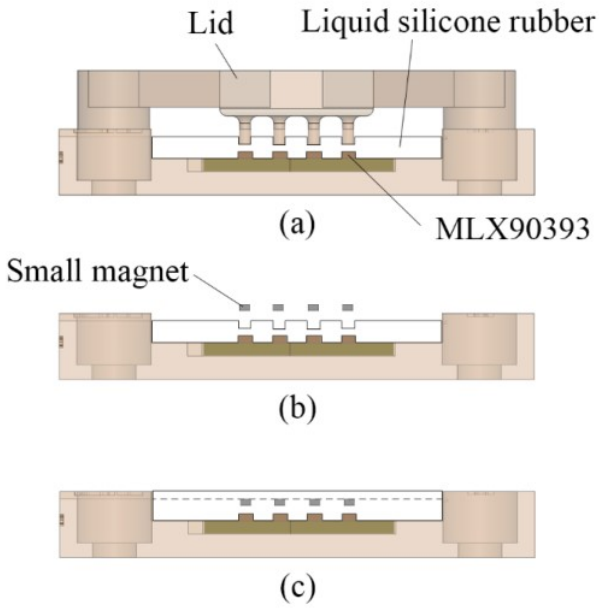

FIGURE 3.2: The molding process. (a) Liquid silicone rubber was poured into the molding cast. (b) 16 small magnets were placed inside the hole. (c) Another layer of liquid silicone rubber was poured above the magnets.

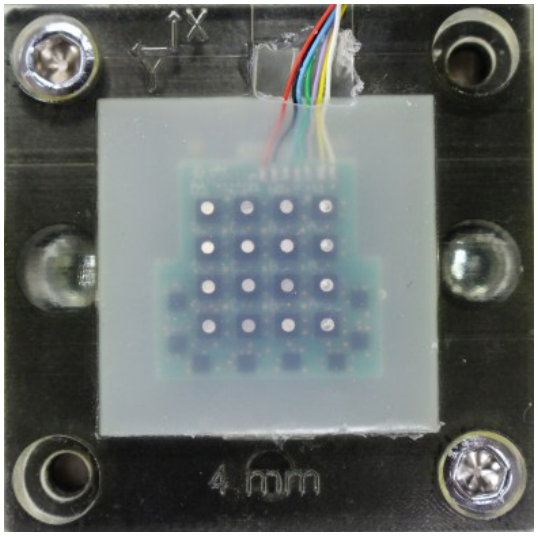

FIGURE 3.3: A distributed skin sensor embedded with 16 MLX90393 chips, providing 48 force data in total.

Ecoflex Supersoft 00-30 was used as the soft material. With a shore hardness of 00-30 this silicone is softer than human skin. Different materials with different hardness could be used to tune the sensor parameters, for example

to increase the sensitivity or increase the range. However, for this version of the sensor I did not optimize the material. Ecoflex 00-30 provided reasonable results regarding sensitivity and range, considering the possible application of grasping everyday objects, which are often less than 1 kg.

Moreover, compliant skin contributes to robust object handling and safety, as the force gets distributed over a wider area and impact forces are absorbed. At the same time, softness causes problems for the sensor characteristics, in particular it often leads to severe hysteresis in the sensor measurements. Therefore, I chose a soft material on purpose, to benefit from its softness for object handling and to be able to evaluate its negative effects for the sensor characteristics. Ecoflex 00-30 was the softest material that I had available and provided reasonable results. In particular, Ecoflex 00-10 is even softer, but even after curing an oily film remains on its surface.

(3) Integration in the robot hand

The sensor modules fit on the motors that constitute the phalanges of the fingers of the Allegro hand, as shown in Fig. 3.4. Another silicone mold compared to the one shown in the last section was used to create the silicone shown in Fig. 3.4, which surrounds the fingers of the Allegro hand. The thickness of the sensor module including a 0.5 mm thick PCB is 4 mm. The connections between the finger phalanges have to be made 4 mm longer than in the original hand in order for the fingers being able to bend without touching the sensors, thereby extending the length of the finger 12mm in total. Finally, while for the current experiments I use rather bulky electronics to collect the I2C measurements, small sized microcontrollers are available; for example, the microcontroller board used for the skin sensors in iCub is about 26x18x6 mm big, can collect measurements from four I2C buses, and is connected on a daisy chain CAN bus.

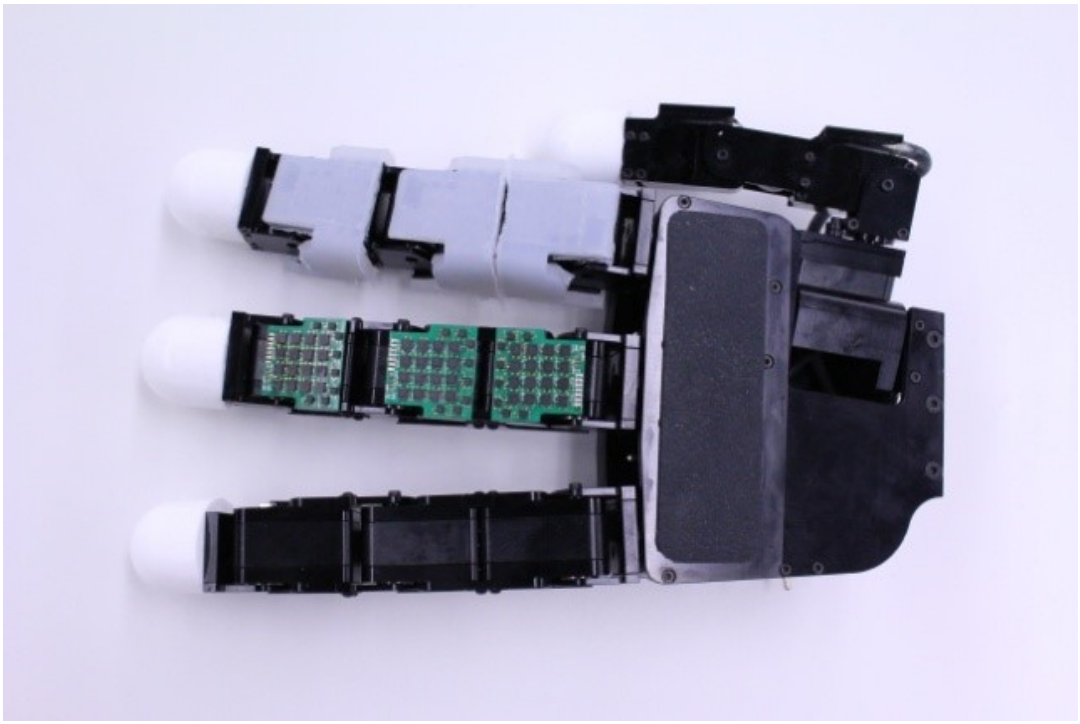

FIGURE 3.4: An Allegro Hand integrated with my proposed sensors (middle) and covered with skins (top).

Since a servo motor is installed in each joint, I considered that the magnetic field from the motor may interfere with the skin sensor readout. However, after conducting a test by activating the servo motors while the skin sensor was mounted, the result revealed that there was no magnetic field interference. The skin sensor reading was not affected by the rotation of the motor.

3.2.3 Evaluation Method

Three experiments were conducted to evaluate the performance of the skin sensor. In the first experiment the measurement of normal and shear force is tested; the second experiment investigates the crosstalk between the chips. In the third test I repeatedly push the sensor, to test it stability. SDA 1 was selected for the experiments, see Fig. 4.3.

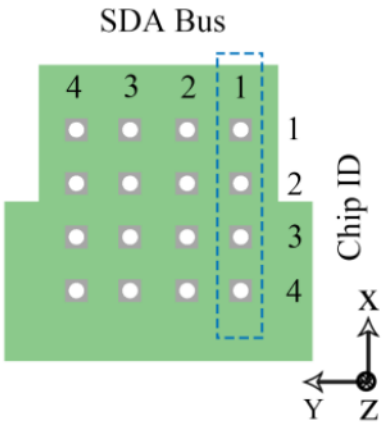

FIGURE 3.5: SDA bus and chip ID assignment for the skin sensor. SDA 1 was selected for the experiments.

(1) Experimental Setup

Fig. 3.6 shows the test setup. The test setup consists of a current controlled (without force feedback) voice coil motor (VM5050-190 from Geeplus) to apply normal force, a linear bushing, an aluminum shaft adapter, a 6-axis force/torque (F/T) sensor (Nano 1.5/1.5 from BL Autotech) for monitoring the pushing force, and a 12x12 mm 3D printed push plate with a flat surface. The load limit for the F/T sensor is 15 N for the x, y and z axis, respectively. Therefore, in my experiments the maximum load applied per axis is kept below 15 N. The orientation of the skin sensor was fine adjusted with a tilt stage to achieve a parallel contact with the push plate. I used an LMD18245 from Texas Instrument for changing the load force by controlling the current to the voice coil motor. The F/T sensor and my sensor required 5V and 3.3 V supply voltage, respectively. For this reason, I used two microcontrollers, Arduino Uno and Due. They were synchronized, and both data were recorded on SD cards with a sampling rate of 40 Hz. The skin sensor was mounted on a sturdy X-Y table; the position where to apply the force can be adjusted with the X-Y table; also shear force can be applied by moving the X-Y table after an initial contact with the push plate. Unfiltered sensor data was used for all experiments and is shown in the plots.

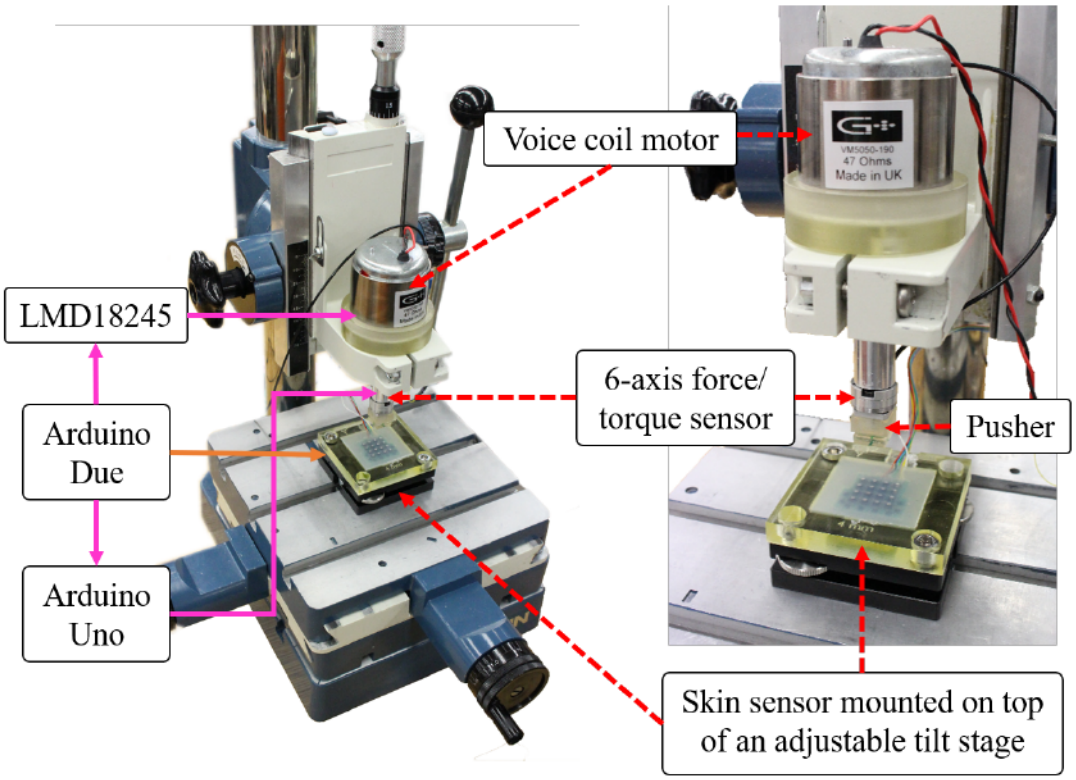

FIGURE 3.6: Experiment setup used in this section.

(2) Sensor Measurements before Calibration

Fig. 3.7 shows the result of the load test when a normal force was applied centered above a sensor. Before the calibration, as shown in Fig. 3.7 (a), my skin sensor shows some displacements in the x-axis (S_x, marked as blue) and y-axis (S_y, marked as green) even though only normal force was applied, see Fig. 3.7 (b). A possible reason for this is that the placement of the magnet was not perfectly centered, and due to the incompressibility of the silicone, causing a small sideward displacement of the magnet if it is not perfectly centered initially. I discovered a similar situation in Fig. 3.7 (c) and (d), which shows combined shear and normal force.

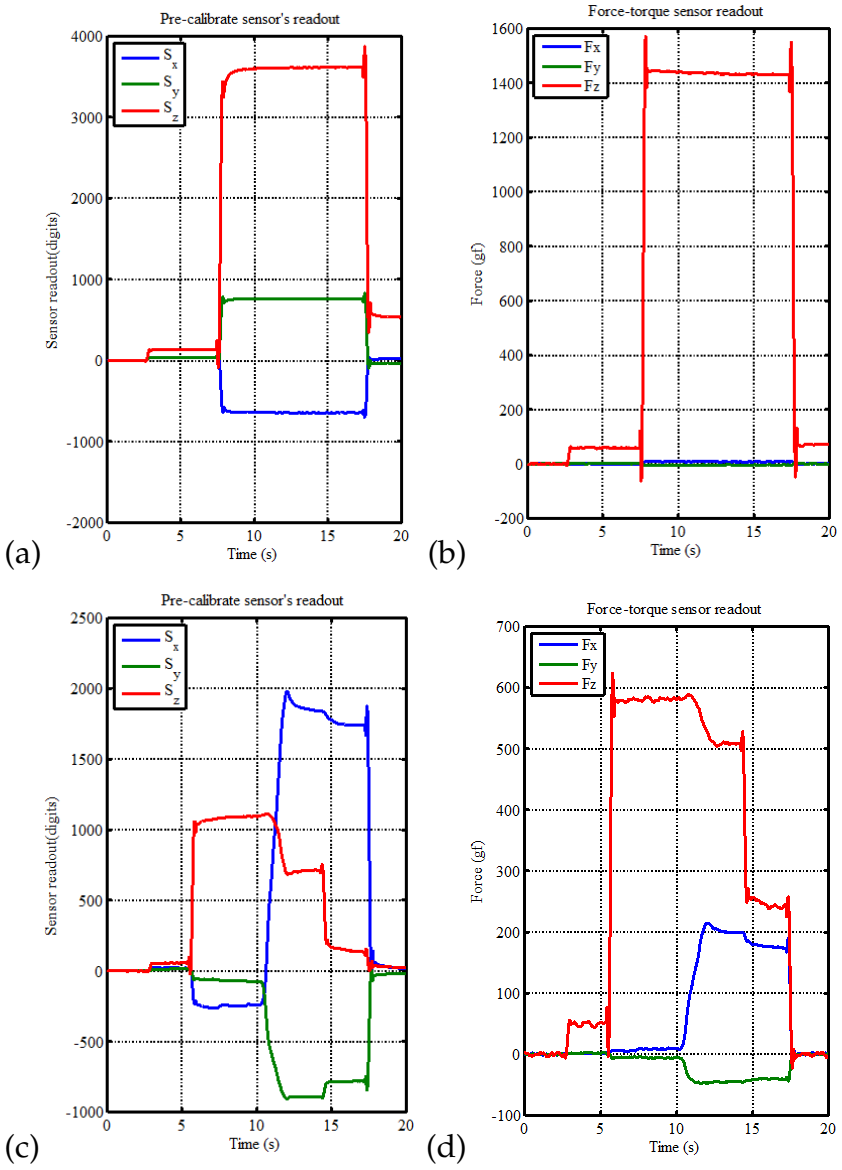

FIGURE 3.7: The sensor's readout (a) and the corresponding force from the F/T sensor (b) when shear force is applied (sensor 3 SDA1).

(3) Calibration

Load was applied to the sensor by stepwise increasing and subsequently decreasing the force on a single chip. The sensor was calibrated with data when applying force only in the x, y or z axis, respectively. In particular, three kinds of force (normal, shear in the x-axis, and shear in y-axis) were applied on the top of each sensor once each, resulting in three time series data to calibrate each Hall effect sensor. When applying force only in the z-axis, each step lasted 5 s and the force was changed by changing the reference

voltage of the LMD18245 in steps of 0.27 V. In total 21 steps were performed for increasing and decreasing the force, and at step 11 the maximum force of around 14 N was achieved. When applying force in either the x or y axis, each step lasted 6 seconds; a longer time interval was chosen because the force was applied manually by moving the X-Y table, which requires about 1 s. For each step, the X-Y table was moved 0.5 mm by turning the fine adjuster knob of the X-Y table. Overall, 10 steps were performed. Each taxel was calibrated independently. I used the MATLAB Curve Fitting Toolbox™, and a quadratic model with a robust Huber regression for calibrating the sensor. I removed 15 samples before and after each load change to clean the dataset from unwanted transient signals. I found that the prediction performance for test data increased when cleaning the training data in such a way. For each chip, all 3 sensor measurements are used to calculate each force in the x, y and z-axis, therefore 6 parameters for each axis have to be calculated for each chip.

(4) Crosstalk Test

To evaluate the magnetic field interference that can affect another Hall effect sensor measurement while one chip is being pushed, a crosstalk test was conducted. Bus no. 1 was selected for this experiment. A 14 N load was applied every 1.175 mm (a fourth of the distance between two chips) in the x-axis, starting from -4.7 mm away from the center of chip no. 1. The force was applied for around 10 seconds for each position; I waited sufficient between pushing at different positions to avoid the effect of hysteresis on this experiment. Twenty positions were recorded in total. Afterward, the mean value of the force was calculated.

(5) Repetitive Test

To evaluate the sensor reliability, I conducted a repetitive test. In this test, I repeatedly applied a normal force of 9.8 N on top of the sensor (Chip ID 4) for 1 second and retracted the pusher for 5 seconds in five cycles.

3.2.4 Results

(1) Calibration Result

For testing, I used data that was not used for calculating the calibration parameters. Fig. 3.8 shows a representative result when only normal force was applied, while Fig. 3.9 displays the calibrated sensor measurements when also shear forces in the x-axis and y-axis were applied, respectively.

For Fig. 3.9, the load was changed every 6 seconds: first the z-load was automatically changed every 6 seconds, and immediately afterwards for each step the shear force was changed manually. The figures compare the mean force measured by the F/T sensor to the mean value of the calibrated skin sensor in the x, y, and z-axis, respectively, for every step. Also the standard deviation (SD) for the skin sensor for each step is shown. Fig. 3.10 presents a zoom on the x-axis and shows that the sensor is sensitive also to low forces.

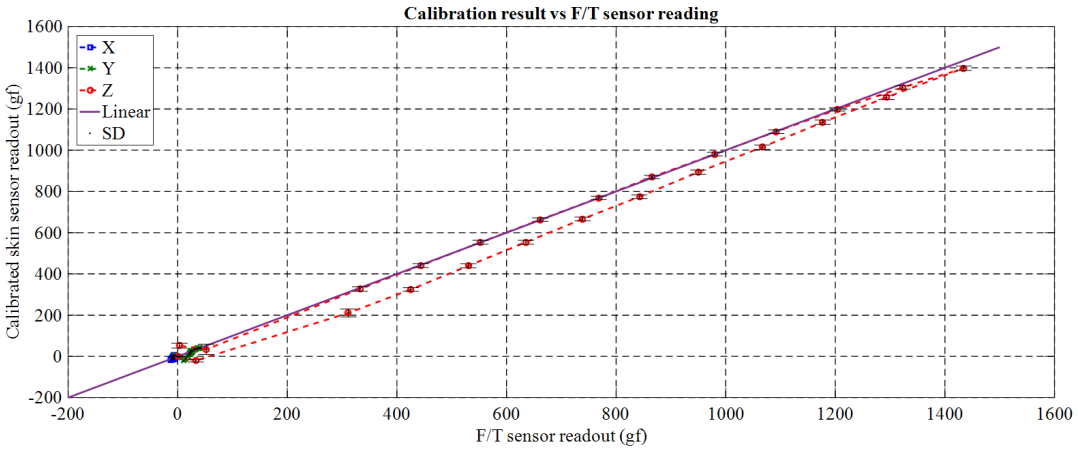

FIGURE 3.8: A calibrated sensor response when normal force applied (chip 3 SDA1).

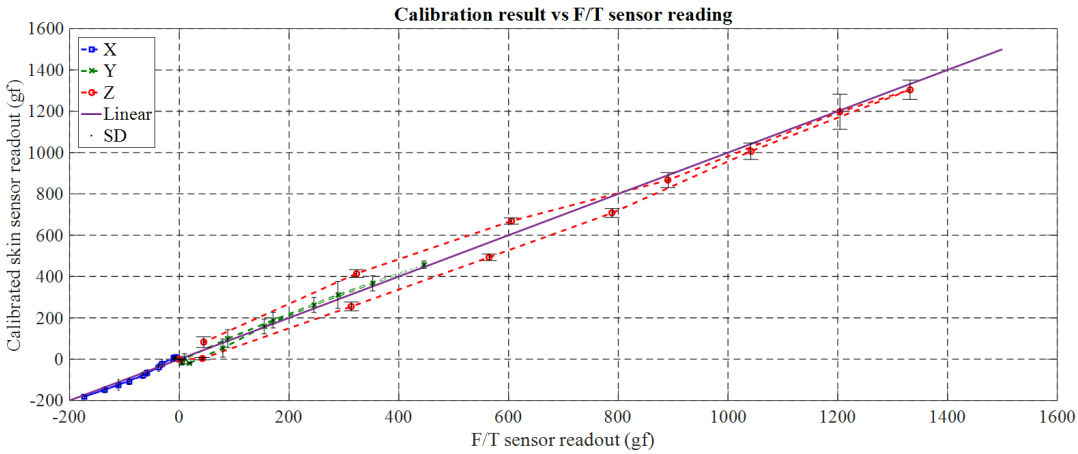

FIGURE 3.9: A calibrated sensor response when the normal and shear force applied (chip 4 on SDA1).

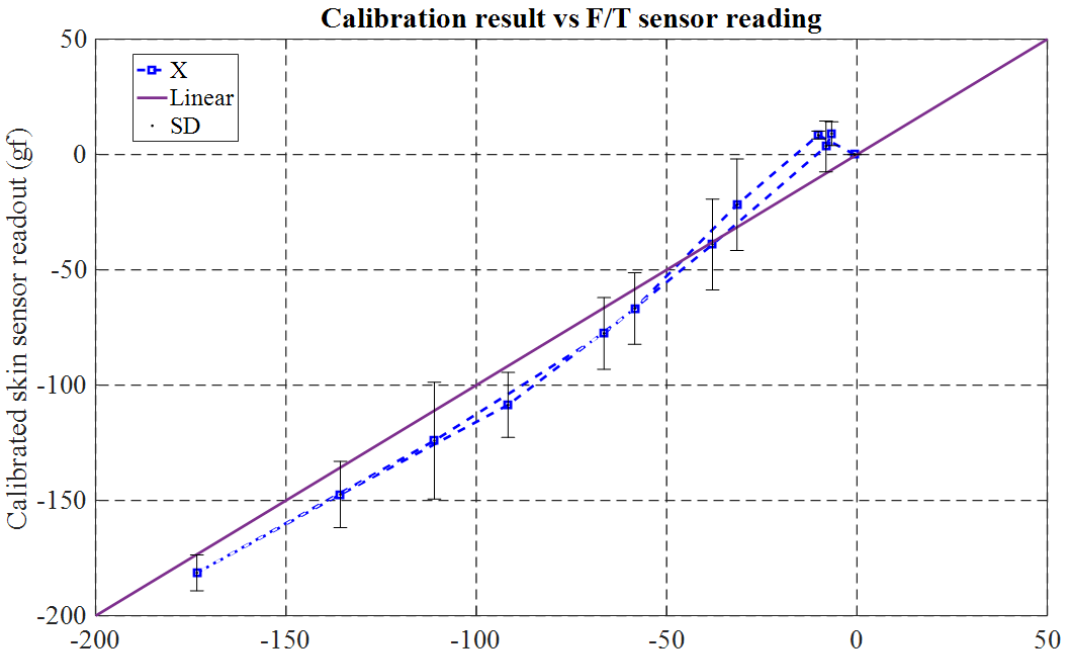

FIGURE 3.10: A calibrated sensor response when the shear force applied. (Sensor 4 on SDA1, x-axis only).

The calibrated skin sensor readout displays a similar value as the F/T sensor readout. This result verifies that the skin sensor can measure normal and shear forces. The R-squared values from the calibration results can be seen in Table 3.1. R-squared value represents how close the data are to the fitted regression line. The hysteresis of the normal force load test was 5.29%, calculated using equation (3.1).

$$Hysteresis\ \% = \left| \frac{(F_{mu} - F_{ml})}{(F_{max} - F_{min})} \right| \times 100\% \tag{3.1}$$

F_{ml} and F_{mu} are the calibrated skin force values (linear interpolation of the nearest neighbors) of the loading and unloading cycles, respectively, taken at the midpoint force of (14 N – 0 N)/2 = 7 N. F_{min} was the minimally measured average force and F_{max} the maximum measured average force.

(2) Crosstalk Evaluation Force was applied at 20 locations. Chip no. 1, 2, 3, and 4 are marked in red, blue, green, and yellow, respectively. Fig. 3.11 shows the average force value of each chip in all positions. The location of the chip no. 1, 2, 3, and 4 is at 4.7 mm, 9.4 mm, 14.1 mm, and 18.8 mm, respectively. It can be seen that the force in z-axis increases when the contact location is closer to the magnet. In contrast, the detected force becomes

TABLE 3.1: R-squared value for the normal force and shear force experiments.

	Linear + Huber	Quadratic + Huber
Normal Force	0.9211	0.9867
Shear in x-axis	0.5286	0.9723
Shear in y-axis	0.5105	0.9836

weaker with increasing distance to the contact location. This result demonstrates that my proposed skin sensor can detect the force contact location.

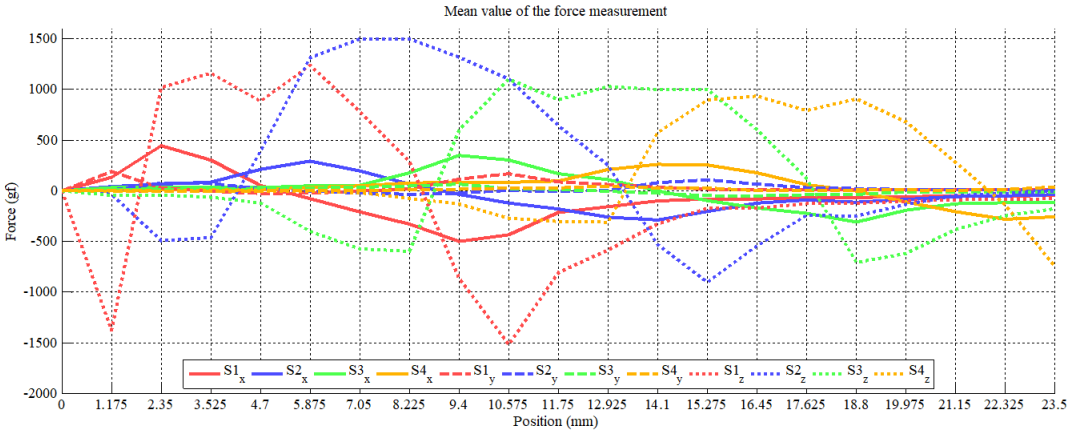

FIGURE 3.11: The average force value of individual sensor on all positions.

At certain points, the force was measured as a negative value. It happened when the silicone material was pressed next to the corresponding magnet. This and the sensor measurements in the x-axis are probably due to the fact that the silicone is incompressible. Interestingly, the distance of the two peaks in the negative z-axis corresponds to the size of the pusher plate (12mm).

Chip no. 1 is slightly more sensitive in the negative z-axis direction and the chip no. 2 more sensitive in the positive z-axis direction, but overall all 4 chips show a similar response pattern. The sensor calibration was performed with less data than in the previous section (for each taxel with only 3 time series, similar to the ones shown in Fig. 3.7 (a) and (c)), and can probably be improved with more data.

(3) Repetitive Evaluation The calibrated sensor output is shown in Fig. 3.12. The result shows that the skin sensor can reproduce a similar output during the 5 cycles. The graph also shows that the skin sensor accumulated around 0.49 N load due to the hysteresis effect of the silicone.

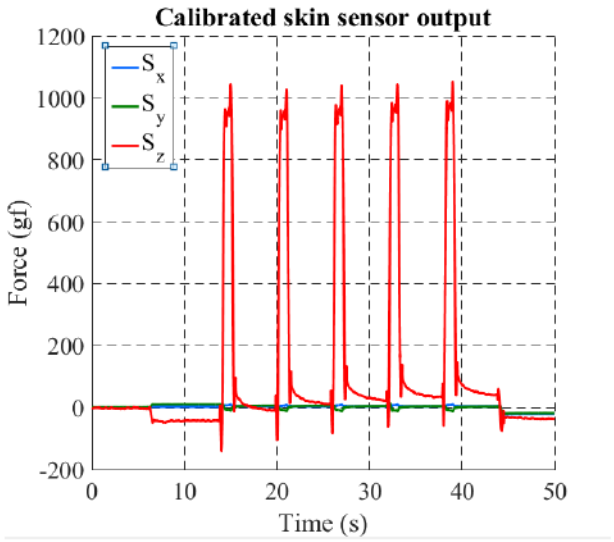

FIGURE 3.12: Repetitive test signal output (chip 3 SDA 1).

3.2.5 Discussion

A distributed 3D Hall Effect-based skin sensor was proposed in [60], [65]. The sensor required four separate Hall sensing elements and a dome to measure normal and shear forces. Due to the dome size, a minimum size of 13.8 mm diameter x 8 mm height was required in order to measure 1 force vector. As a result, the sensor could not achieve a subcentimeter (less than 1 cm) spatial density. The minimum and maximum detectable normal force were 0.094 N (9.5 gf) and 0.147 N (14.9 gf), respectively. Meanwhile, uSkin uses only a single Hall Effect sensor chip to measure normal and shear forces, and is therefore capable to measure 1 force vector within a size of less than 5 mm x 5 mm x 4 mm. In particular, the sensors had a center-to-center distance of 4.7 mm, and a thickness of 4 mm. uSkin also has a wide force measurement range, 0.01 N (1 gf) - 14 N (1400 gf), therefore being more sensitive and possessing a wider range at the same time. Furthermore, while [60], [65] implemented distributed sensing, there was no discussion about the effect caused by placing permanent magnets closely side by side. The work in this chapter investigates this effect for the first time for distributed 3D Hall Effect-based skin sensors.

Like in a human, robot fingers often have a curved shape. Therefore, a skin sensor that can cover not only flat surfaces but also a multi-curved surface is demanded. A solution could be to use a flexible PCB instead of a rigid one. To test the validity, Section 3.3 will introduce the design, manufacturing process, and the characterizations method for a curved, soft, distributed 3-axis Hall Effect-based skin sensor.

Moreover, crosstalk between the 3-axis measurements was found due to the incompressibility of silicone. Possible sources of this problem are bulk silicone structure or imprecise alignment of the magnet with the sensor. A bulk structure was used for this version of the skin sensor, meaning that there is no air gap or room for compression. As a result, the permanent magnet used for changing the magnetic field surrounding the chip was displaced to sideways in an uncontrollable way. Another possible cause is the magnet that is tilted. Although a calibration process can eliminate this effect, more time will be required for calibrating a high-density sensor. For this reason, the calibration process is preferred to be avoided if possible. However, providing training data with crosstalk information will lead to inaccuracy. For a machine learning implementation, this data will more likely severe the training result. Therefore, the crosstalk effect between 3-axis measurement should be eliminated by improving the hardware itself, the soft structure (silicone layer) in this case. The improved structure for eliminating crosstalk effect and easier magnets assembly will be introduced in Section 3.4.

3.3 uSkin - Curved Module

This section discusses uSkin's implementation for multi-curved fingertips. The experimental results revealed that uSkin has 10% hysteresis for the normal force with a maximum range of 6 N. For 0.4 N load, the Signal to Noise Ratio (SNR) value of 54 dB was achieved, which constitutes state of the art for this kind of sensors. Evaluation experiments also revealed that the distributed 3-axis load cells could produce vectors that represent the contour of objects. This result opens the possibility that the sensor can be used for classifying different shapes. Furthermore, the fingertip sensor was installed on the Allegro hand, and the changing force measurements when the robot is grasping an object are presented in Chapter 4.3. Related to this section, Wai Keat Wong made the 3D shape of the fingertip and designed a first version of the PCB under my supervision. He collected data and I analyzed it.

3.3.1 Objective

Fingertips have a multicurved shape which is difficult to cover with tactile skin sensors, but fingertips are especially important for fine manipulation. For example, fingertips are especially relevant during manipulating a small object [35]. A clear shortcoming of my previous work was that it was applied only to flat surfaces, but multicurved fingertips are beneficial [4]. In general, many soft skin sensors can be implemented for a flat or cylindrical surface, but only a few of them can be utilized to cover a multicurved surface [35][49]. The current section will introduce uSkin for the Allegro hand's fingertip. The dimension of the fingertip including the silicone skin is within 30x35x28 mm; each fingertip can measure 24 force vectors with 24 3-axis Hall-effect sensors (MLX90393). Additionally, each sensor also provides temperature measurements. An integral part of the skin sensor is 4 mm thick silicone. The output of each module is digital and requires only nine wires while providing 24x4 (3-axis magnetic field and one temperature) data. Therefore, uSkin can be connected to a microcontroller directly through I2C (Inter-Integrated Circuit) protocol without needing to amplify the signal first. My current design is based on the Allegro Hand's shape and size. However, in general, the shape of uSkin can be configured according to various robot hand forms. To summarize, the main contributions of the work in this section, both with respect to my previously published design and with respect to the literature, is that I can cover multicurved surfaces.

3.3.2 Sensor Description

In this section the structure and the manufacturing process of uSkin will be described. The whole production process is fast and effortless.

(1) Design

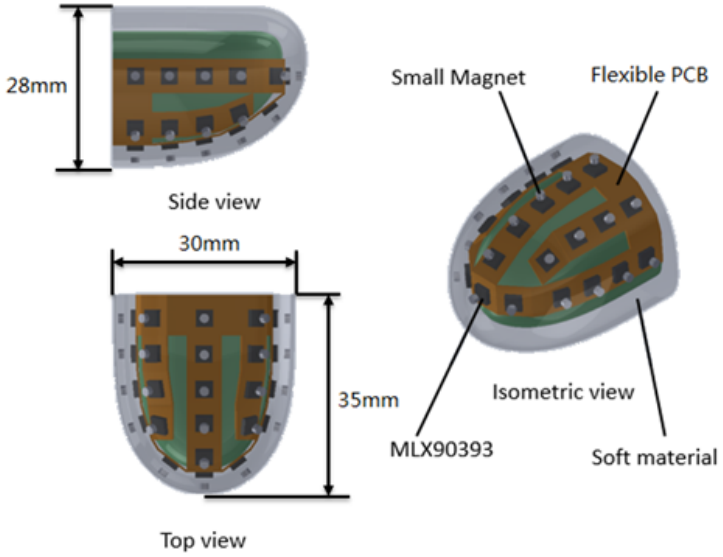

FIGURE 3.13: Conceptual design of uSkin for a fingertip.

Adopting the same concept introduced in the previous chapter, I designed a new fingertip sensor with the structure that can be seen in Fig. 4.2. Here, I am using 24 MLX90393 chips mounted on a flexible PCB (Printed Circuit Board) (Fig. 3.14). Each MLX90393 chip can provide 3-axis magnetic data and 1 temperature data. A single chip has a 7-bit I2C address where the last 2 bit can be configured by connecting two of the chip's pins to either supply voltage (VDD) or ground (VSS). As a result, one I2C bus segment (SDA) can handle four chips at the same time. my fingertip sensor has nine electrical lines in total (VDD, VSS, SCL (clock), and 6 SDAs) for transferring 96 (24 x (3+1)) measurement data.

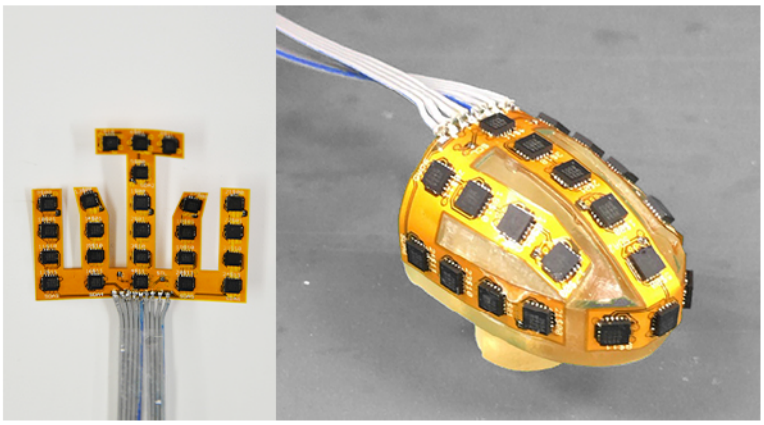

FIGURE 3.14: A flexible PCB attached to the 3D printed fingertip.

(2) Manufacturing Process

The manufacturing process was divided into two steps. I produced the fingertip based on the same shape that was previously introduced in [3].

(i) Electronics Since the fingertip does not have a flat surface, I use a flexible PCB that can conform to the contour of the surface. A 3D model of the PCB was designed in SolidWorks according to the shape of the fingertip. Later, the model was flattened producing a flat flexible PCB as in Fig. 3.14 (left). After all chips and cables had been soldered, the flexible PCB was glued to the 3D printed fingertip (Fig. 3.14 (right)).

(ii) Silicone skin First, I manufactured the silicone mold using a 3D printer. Liquid silicone rubber was poured into the molding cast, and then the hole maker for placing magnets was inserted. After the silicone skin completely cured, I removed it from the molding cast and placed all 24 magnets inside the holes. The orientation was configured so that the south pole of the magnets faces the chips. The magnets for the current implementation were neodymium (grade N50) with a 1.59 mm diameter and a 0.53 mm thickness. It had an optimal pull of 226.8 g and 729 surface gauss. Next, the skin with embedded magnets was placed into another molding cast, and more liquid silicone rubber was poured to embed all of the magnets. Fig 3.15. shows the complete manufacturing process of the uSkin fingertip silicone.

The material used was Ecoflex Supersoft with shore hardness 00-50 from Smooth-On. I also tried Ecoflex 30, but the material was too soft. A soft sensor can provide more sensitivity, however, the maximum range that can be measured will be reduced as a trade-off. In my case, with Ecoflex 30 only

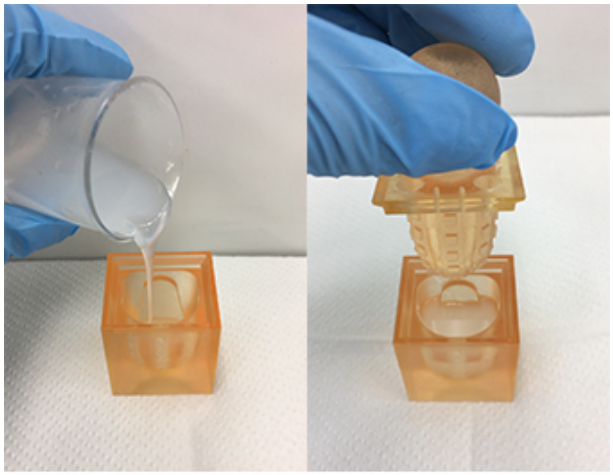

(a)

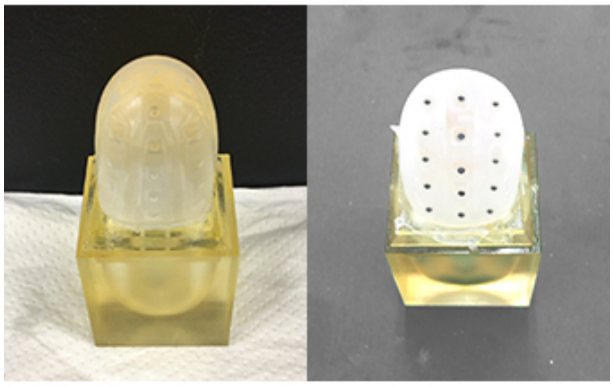

(b)

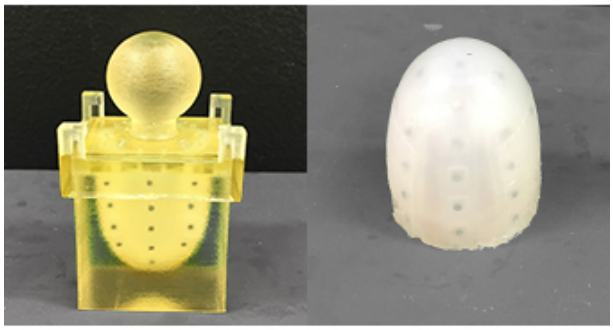

(c)

FIGURE 3.15: Fingertip molding **(a)** Liquid silicone rubber was poured, and the hole maker was placed. **(b)** 24 small magnets were placed inside the holes. **(c)** Magnets were covered with another layer of silicone.

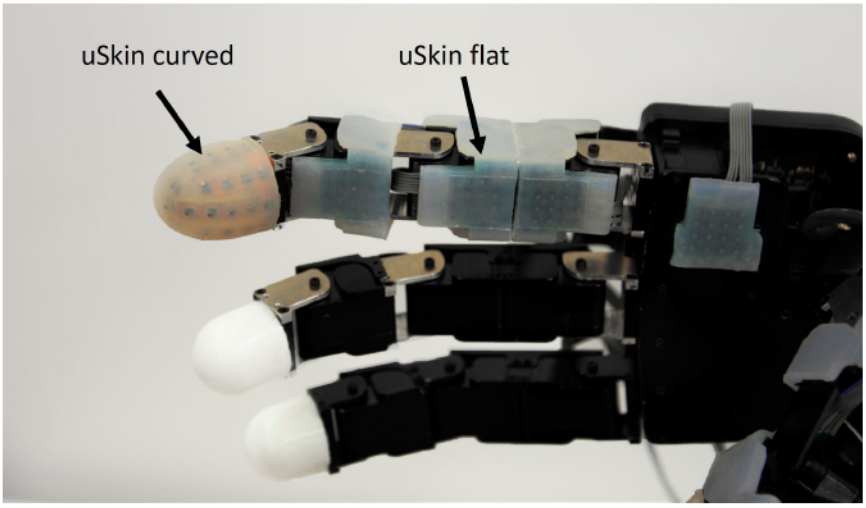

FIGURE 3.16: Allegro hand covered with uSkin on its fingertip, phalanges, and palm.

5 N was needed to saturate the Hall-effect sensor. Therefore, Ecoflex 50 was purposely chosen to provide more range.

Finally, I covered the previously made 3D printed fingertip including the PCB with the silicone skin and then mounted it to the Allegro Hand as in Fig. 3.16. The figure also shows the skin for flat phalanges that has been presented in [66].

3.3.3 Evaluation Method

Several experiments were conducted to estimate uSkin's performance. The first experiment is about calibrating and evaluating the sensor's characteristics. As uSkin has multiple sensing points distributed in 24 different locations, I presumed that this sensor can be used for identifying object shapes. I tested the distributed sensing and crosstalk response. Finally, I evaluated the sensor response while grasping objects in Section 4.3.

(1) Experimental Setup

The overall test setup used in this section can be seen in Fig. 3.28. A current controlled voice coil motor without force feedback (VM5050-190 from Geeplus) was utilized to apply varying force to the skin sensor. The load force can be changed by controlling the current of the voice coil motor using a full-bridge motor driver (LMD18245 from Texas Instruments). A 6-axis force/torque (F/T) sensor (Nano 1.5/1.5 from BL Autotech) is used for monitoring the amount of applied force. The maximum force that can be measured by this sensor is around 14 N for the x, y, and z-axis. However, the maximum

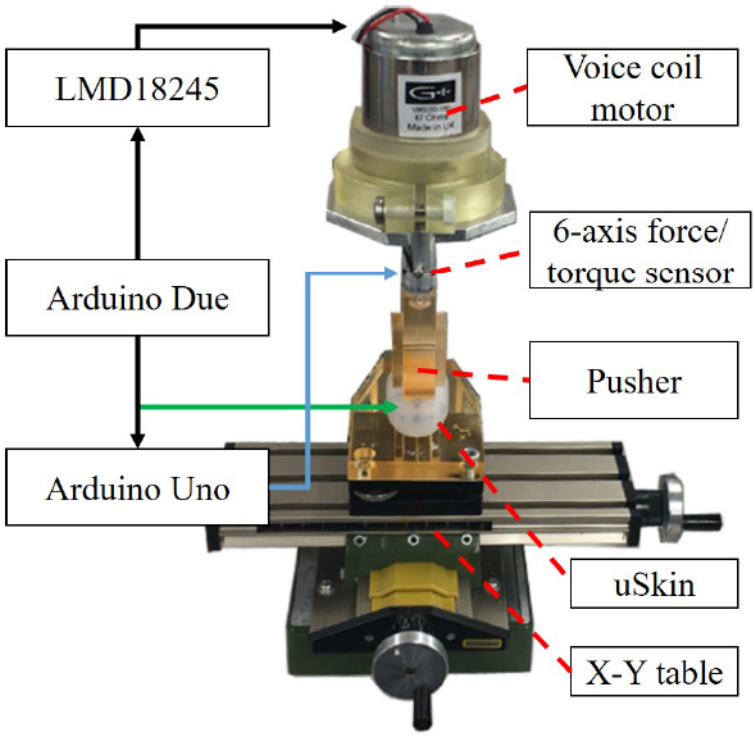

FIGURE 3.17: Test setup used in this section.

force value applied in this experiment was limited to only around 6 N. The current fingertip structure has a higher sensitivity than the one previously made (uSkin for phalanges can measure up to 14 N [66]). Applying more than 7 N causes saturation. A 3D printed push plate was attached to the F/T sensor. I used different shapes depending on the task. For the normal and shear force calibration task, I used a flat pusher with a 12x12 mm square contact area. For the shape recognition task, I used four different shapes (5x35 mm rectangle, 15x15 mm square, 10 mm diameter circle, and 7x7 mm square).

The Nano 1.5/1.5 requires 5 V supply voltage to operate. Meanwhile, uSkin requires 3.3 V. Because of these requirements, I used one Arduino Uno for recording the F/T sensor measurements and one Arduino Due for recording uSkin sensor measurements. The Arduino's were synchronized, and both data were recorded on memory cards for offline analysis.

Each load cell (MLX90393) has a sampling rate that can be configured up to around 500 Hz. As uSkin requires 6 data (SDA) lines to read all measurements, I used an I2C multiplexer (TCA9548A from Adafruit) connected to a single SDA pin of an Arduino Due.

The fingertip with the skin sensor was fixed on a sturdy X-Y table; the position where to apply the force can be adjusted with the X-Y table; also shear force can be applied by moving the X-Y table after an initial contact

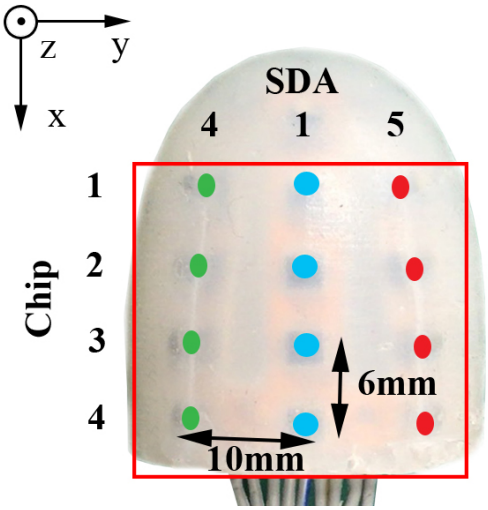

FIGURE 3.18: SDA and chip placement.

with the push plate. The sensor was mounted on a tiltable platform so that the voice coil motor applied perpendicular force to the skin surface.

The average of 1 s of each measurement when the sensor was not pushed was used as the baseline and subtracted from the measurements. Otherwise, unfiltered sensor data was used for all experiments and is shown in the plots.

(2) Calibration

The sensor was calibrated with uSkin measurements as the input and reference sensor measurements as the target when applying force only in the x, y or z-axis, respectively. In particular, three kinds of force (normal, shear in the x-axis, and shear in y-axis) were applied on the top of each load cell, resulting in three time series data to calibrate each Hall effect sensor. For the normal force, each load cell was pushed for 4 seconds, then the pusher was retracted (no force applied) for 1 minute to ensure that the silicone skin had properly returned to its initial state before higher force was applied. Four different normal forces were applied to each load cell, of around 3 N (the voice coil motor has limitations for the lowest forces it can produce), 4 N, 5 N and 6 N. Five samples before and after each load change were removed to clean the training dataset from unwanted transient signals. By conducting in such a way, I found that the prediction performance for test data can be increased. For the shear forces, I applied a constant 3 N force in the z-axis. To apply a shear force, I manually moved the X-Y table while the sensor was being pushed. I used a metronome to guide the timing. Every 4 seconds the fine adjuster knob was turned resulting in a 0.2 mm displacement either in

x or y-direction from the center of the load cell. After four steps had been performed the pusher was retracted.

In previous work, I found that calibrating my sensor with a quadratic model and Huber robust option can give a better prediction performance compared to linear regression or when using a neural network. For this reason, I also calibrated the fingertip load cells using the same method. For each chip, all three sensor measurements are used to calculate each force in the x, y, and z-axis. Nine parameters for each axis have to be calculated using this formula:

$$\begin{aligned} S_{j,c} = aS_x + bS_y + cS_z + dS_x * S_y + \\ eS_x * S_z + fS_y * S_z + gS_x^2 + hS_y^2 + iS_z^2 \end{aligned} \tag{3.2}$$

Here, $S_{j,c}$ is the calibrated sensor output of axis j (x, y, or z). S_x, S_y, and S_z are pre-calibrated skin sensor module outputs in digits. a to i are the calibration parameters. These parameters were calculated in MATLAB using the Statistics & Machine Learning Toolbox.

(3) Signal to noise ratio modeling

In this experiment, I used the calibrated sensor output of the z-axis from the previous section to calculate its SNR (signal to noise ratio) value. The calculation can be done using equation 3.3 or 3.4 [71].

$$SNR = \frac{|\mu_U - \mu_p|}{\sigma_u} \tag{3.3}$$

$$SNR_{dB} = 20 \log_{10} \left(\frac{|\mu_U - \mu_p|}{\sigma_u} \right) dB \tag{3.4}$$

In these equations, μ_U is the mean value of the uSkin measurements when not loaded, μ_p is the average uSkin measurement when loaded, and σ_u is the standard deviation value when not loaded. All SNR values were fitted using a MATLAB Curve Fitting Toolbox to create an SNR model. I used a two-term exponential model with a bisquare robust option. I found that this model can give a better fitting compared to the polynomial model.

3.3.4 Results

(1) Sensor Measurements Before Calibration

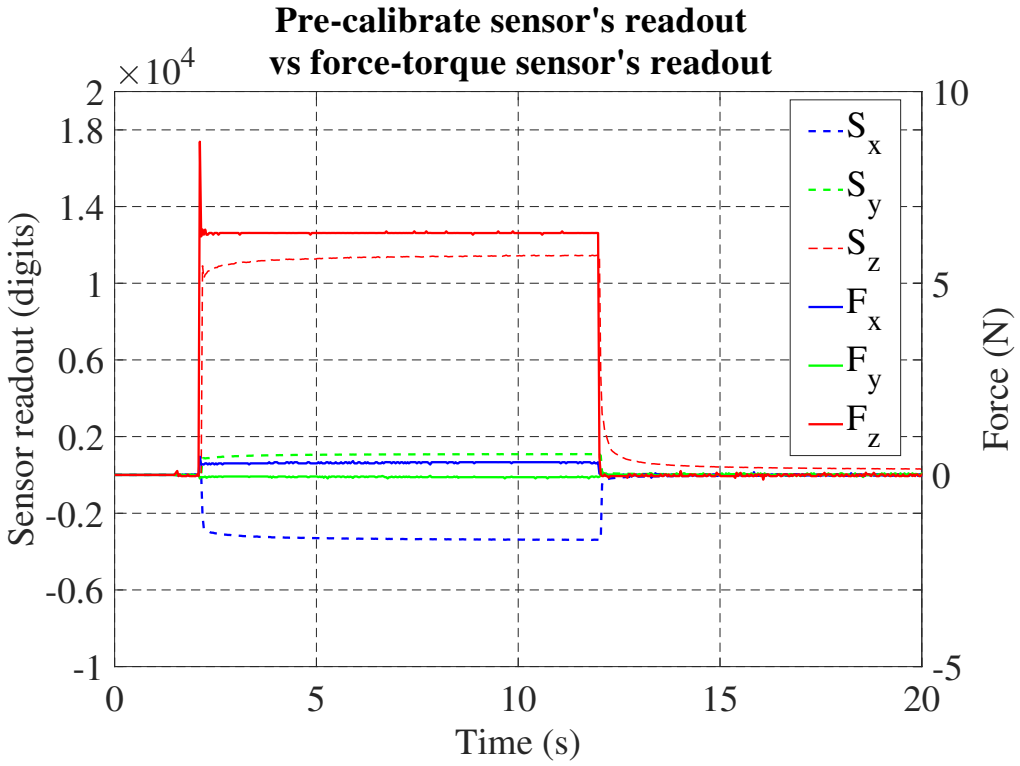

FIGURE 3.19: uSkin's readout and the corresponding force from F/T sensor when only the normal force is applied (S = sensor, F = reference sensor).

When only normal force was applied on the top of uSkin, there were also some magnet displacements in the x-axis and y-axis (details of the orientation can be seen in Fig. 4.3). This can be seen by comparing the Hall effect sensor response (SDA 1 chip 2) to the reference sensor (Fig. 3.19). It can be seen that there was no force in the y-axis in the F/T sensor (Fy, marked as green). However, a magnet displacement was measured in this axis in uSkin (Sy, marked as green). This problem happened most likely because of the magnet placement which is not perfectly centered, or due to the incompressibility of the silicone material. For this reason, uSkin needs to be calibrated.

(2) Response time

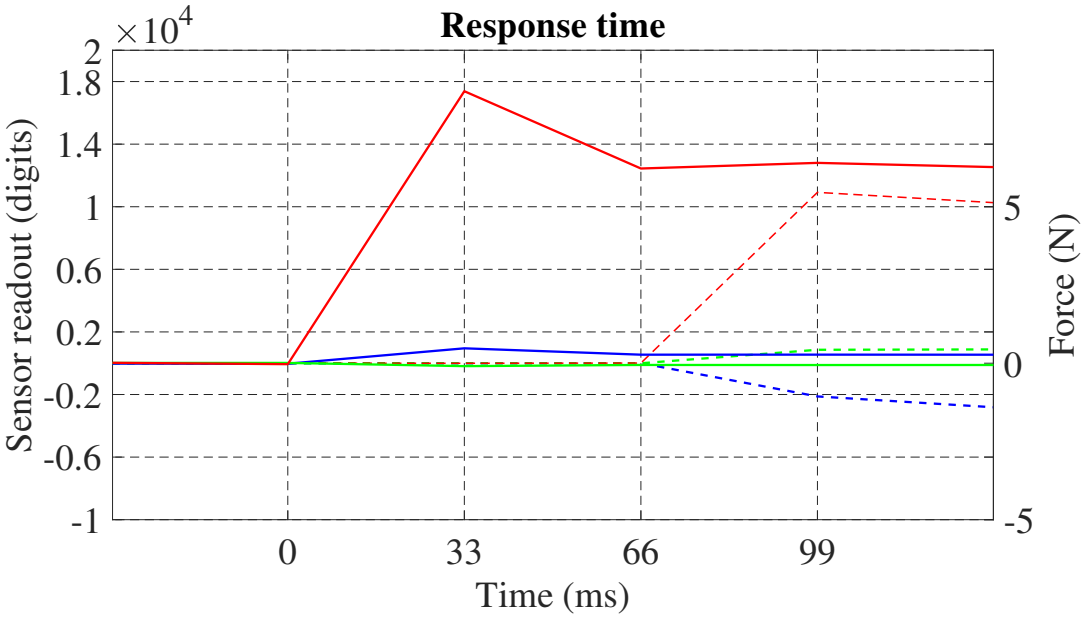

FIGURE 3.20: Closer look of the response time.

The sensor's response time can be seen in Fig. 3.20. The graph shows that uSkin can give a response in two time steps (66 ms) after it received an impact force. The sensor requires about one second to achieve its level state.

(3) Calibration and hysteresis

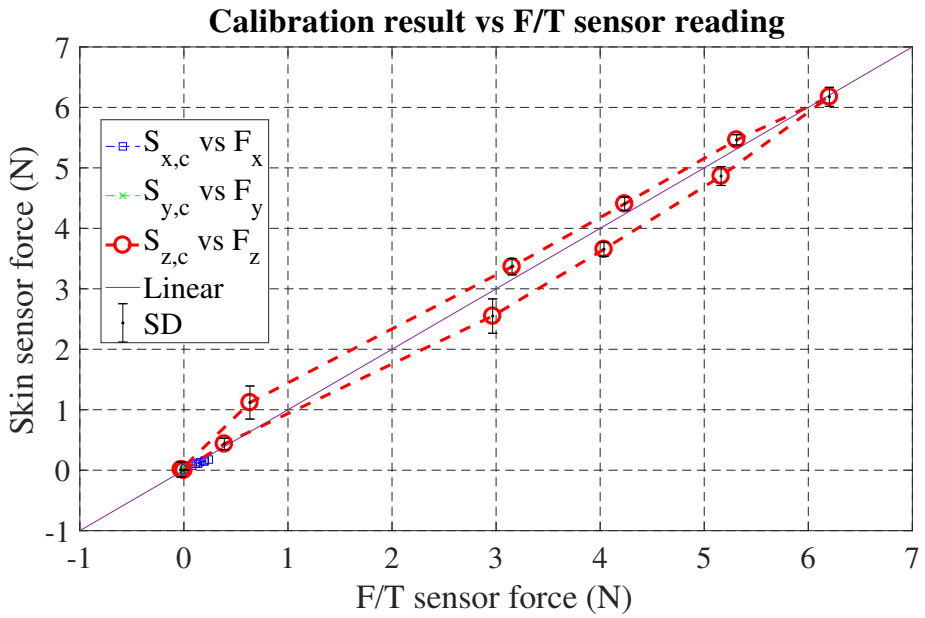

FIGURE 3.21: Calibrated sensor response when normal force is applied.

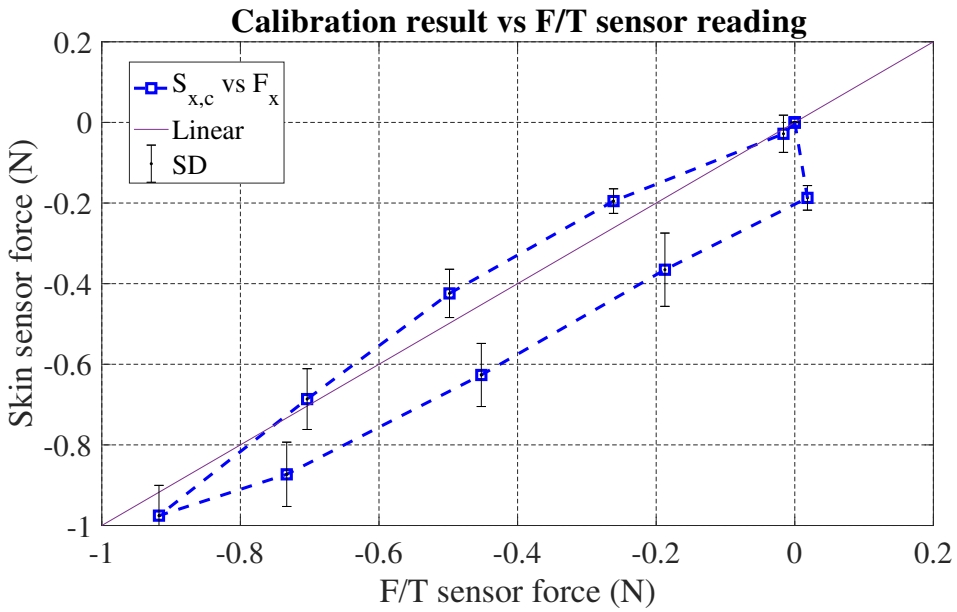

FIGURE 3.22: Calibrated sensor response when shear force is applied (x-axis only).

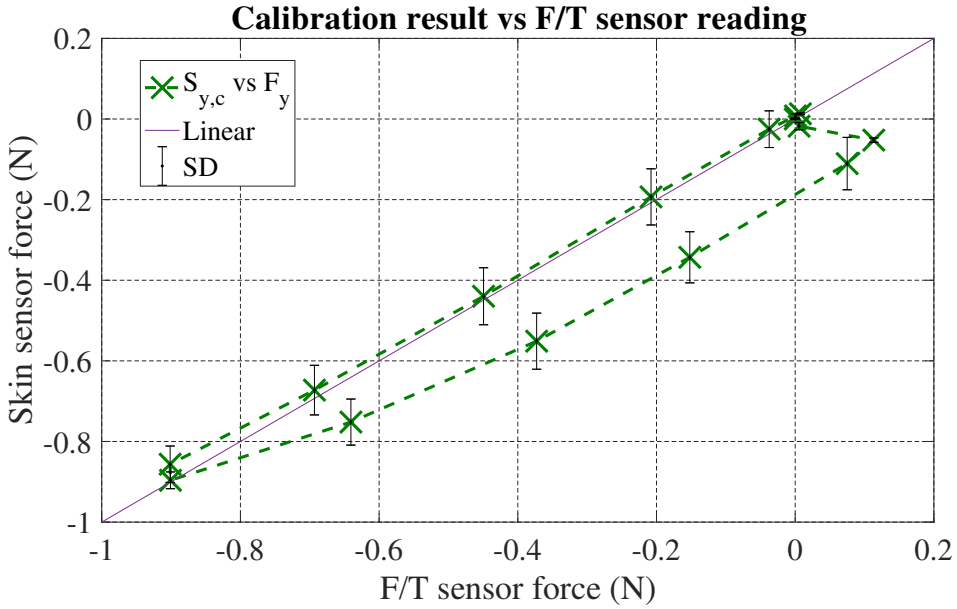

FIGURE 3.23: Calibrated sensor response when shear force is applied (y-axis only).

The normal force test data was prepared as follows. In the first four seconds, the pusher was in a retracted position (no load force). In the next four seconds, the pusher was released, touching the surface of the uSkin. Afterwards, every four seconds, using a stepwise force, I increased the load four times and then decreased again four times. Finally, the force was unloaded

(only touching the surface) for four seconds and then the pusher was retracted. In total, there were 11 steps. The input output graph of the calibrated skin sensor can be seen in Fig. 3.21. $S_{x,c}$, $S_{y,c}$, and $S_{z,c}$ are the calibrated skin sensor outputs in x, y, and z-axis, respectively. Like in the previous sections, I used chip 2 on SDA1 (see Fig. 4.3). SD is the standard deviation and shown in black for easier visibility. It can be seen that the calibrated sensor measurements correspond to the reference sensor. I found that when there was no load force under a static condition (the sensor did not move), the sensor output varied in the range of $\pm$ 0.02 N or around 2 gf (gram-force). Therefore, this is the threshold value of my current sensor. Furthermore, using equation 3.7, I found that the hysteresis of my sensor during the normal force load was 10%.

$$Hysteresis\ \% = \left| \frac{(F_{mu} - F_{ml})}{(F_{max} - F_{min})} \right| \times 100\% \tag{3.5}$$

F_{ml} and F_{mu} are the calibrated skin force values (linear interpolation of the nearest neighbors) of the loading and unloading cycles, respectively, taken at the midpoint force of (6.3 N - 0 N)/2 = 3.15 N. F_{min} was the minimum measured average force (0 N) and F_{max} the maximum measured average force (6.3 N) by the reference sensor.

For the shear forces test data, I used a similar method as for the training set preparation. However, after four steps displacing the chip from the center of the pusher, I also unload the shear force by stepwise returning the sensor to its initial position. The shear forces test results for x-axis and y-axis can be seen in Fig. 3.22 and Fig. 3.23, respectively. I can see from the graph that the skin sensor force in the end did not return to zero. This occurred most likely because of the hysteresis effect. To mitigate this, a special compensation is required. In the future, I will also use a motorized X-Y table to make the timing and movements more precise.

(4) Signal to noise ratio

Fig. 3.24 shows the SNR model of the uSkin fingertip. Here, the first point represents the force produced by the weight of the pusher (no load force from the voice coil motor). The second point is the minimum load force that the voice coil motor can produce. Therefore, there is no data in between these two values. The SNR value was higher compared to my previous work [72]. In Table 3.2, the SNR values of uSkin for the flat (i.e. my previously published design [66]) and curved (i.e. fingertip, my new design introduced

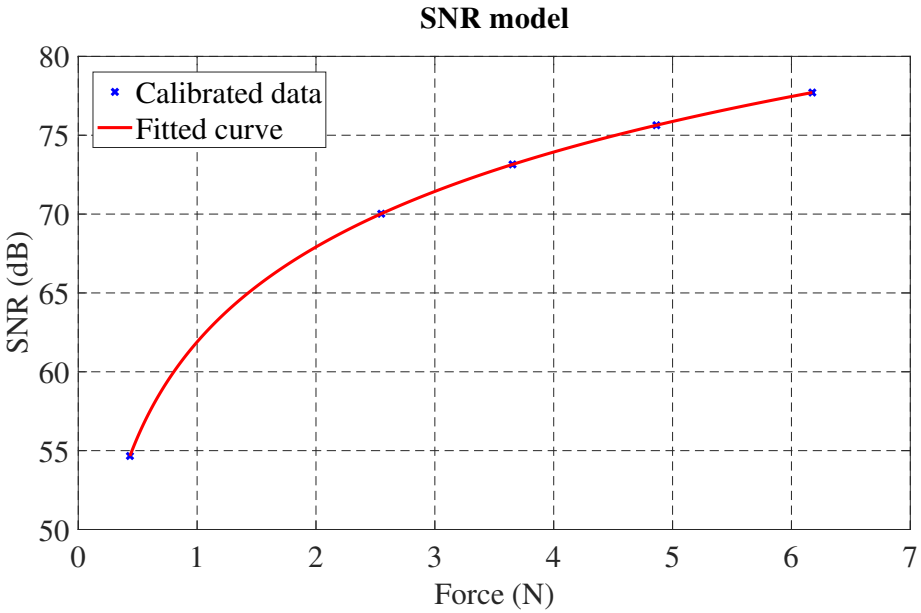

FIGURE 3.24: SNR model of the uSkin for a fingertip.

in this section) phalange are provided. The SNR value of the phalange skin was calculated using its corresponding SNR model.

TABLE 3.2: SNR comparison value.

Force (N)	SNR (dB)	
	Curved (fingertip)	Flat
0.43	54.66	29.41
2.55	70.02	52.50
3.65	73.14	54.39
4.86	75.63	55.61
6.17	77.70	56.57

(5) Visualization and crosstalk

In the previous section, I showed that a load cell of uSkin can measure a three-dimensional force vector. Here, I visualize the response vectors when the fingertip was pressed by an object with a specific shape and various load forces. The pusher was placed centered above chip no. 3 SDA 1. As the pusher only covers an area in SDA 1, 4, and 5 (Fig. 4.3), I only plot the measurements from these chips. The sensor was pushed perpendicularly to the skin surface with stepwise force from around 0.5 N to 6.3 N. The resulting

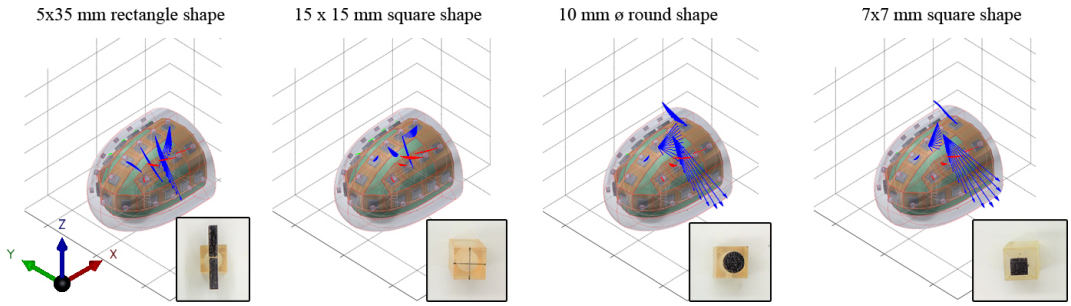

FIGURE 3.25: Response vectors when different shapes and forces are applied on the sensor. The colors of the vectors correspond to the SDAs shown in Fig. 4.3.

ten measurement vectors for each chip are shown in Fig. 3.25. The colors of the vectors correspond to the SDAs shown in Fig. 4.3. I used different scaling to plot the vector arrows. For the 5x35 mm rectangular and 15x5 mm square shapes, the output of chip no. 2-4 SDA 1 were scaled down with 1/8 ratio. For the round and 7x7 mm rectangular shapes, only the output of chip no. 3 SDA 1 was scaled down with 1/8 ratio. This is necessary to provide a clear visualization as the pressures produced by pushers with smaller contact area were higher. For the 5x35 mm rectangular shape, I can see that chip no. 2-4 on SDA 1 produced the most significant response. The response in chip no. 1 is low most likely because of the curved fingertip shape. Due to the curvature of the fingertip, the pusher could not displace the magnet above chip no. 1. I can also see that SDA 4 and 5 measured low force vectors (red and green arrows). Overall, the crosstalk effect produced from the magnetic field interference seems minimal and to not affect the performance of the sensor. The 15x15 mm square shape has a lower response because it has a larger contact area compared to the rectangular shape. As for the round shape, I can see that only chip no. 3 has a positive response. The vector arrows of chip no. 2 and 4 became negative because of the silicone skin that was being pushed upwards. If I compare the response of the round and 7x7 mm square shapes, there appears to be little difference. This makes sense as they have a similar shape and the size of the pusher is less than the distance between chip no. 2 and 4. A higher spatial density would be required to easily detect the shape of a small sized object. In conclusion, uSkin can provide force vector data that might be used for tactile object recognition. However, the minimum shape size that can be detected is limited by the distance of each load cell (in this case 6 mm between each chip in the same SDA line and 10 mm between SDA lines).

3.3.5 Discussion

Most of distributed 3-axis soft skin sensors can already cover flat surfaces [61], [65]. However, covering multicurved surfaces is still challenging with these sensors as a flat surface is required to make their sensing principle works. In contrast, distributed soft skin sensors that can cover multicurve surface usually can only measure normal force [49]. In this section, uSkin proves that its sensing principle can be used for not only covering a flat surface, but also a multicurved surface such as a fingertip. Although one fingertip can provide 24 x 3-axis force measurements, bulky electronics such as a microcontroller, a multiplexer, and a massive number of wires are required to read all skin sensor data simultaneously. It makes the overall system becomes unrealistic for the real implementation on robots. Moreover, the sampling rate is limited to only 30 Hz, lower than most skin sensors in general, especially for a dexterous manipulation purpose. At this point, a soft, distributed, 3-axis skin sensor can be achieved. But, it is not fully compact yet. As a solution, small sized microcontrollers are available; for example, the microcontroller board used for the skin sensors in iCub is about 26x18x6 mm big, can collect measurements from four I2C buses, and is connected on a daisy chain CAN (Controller Area Network) bus [49][73]. It can significantly reduce the number of wiring. A similar system will be implemented in Section 3.4 so that covering a whole hand with minimal wiring can be achieved. As the current design also implements bulk structure, the crosstalk problem remains unsolved. The solution for this will be introduced in the next section.

3.4 Improved Structure and Compact Electronics

In Chapter 3.2 I introduced uSkin, a soft skin with distributed 3-axis force sensitive elements, and a center-to-center distance between the 3-axis load cells of 4.7 mm for the flat version. This section presents a new structure for the distributed soft force transducer which reduces the crosstalk between the components of the 3-axis force measurements. 3D printing the silicone structure eased the prototype production. However, the 3D printed material has a higher hysteresis than the previously used Ecoflex. Microcontroller boards originally developed for the skin of iCub were implemented for uSkin, increasing the readout frequency and reducing the space requirements and number of wires. The sensor was installed on iCub and successfully used for shape exploration in Section 4.5.

3.4.1 Objective

Previously, I manufactured uSkin by embedding permanent magnets inside bulk silicone rubber. That means the structure did not have any cavity or room for compression. Therefore, even if only a perpendicular force was applied to the surface of the skin, the permanent magnets will also displace sideways. As a result, severe crosstalk between the three measurement axis will occur. A calibration procedure is necessary to address this issue. However, this process is time consuming, especially for a high-density sensor providing many measurements.

For specific applications such as for machine learning or for applications where the direction is more important than the force value, e.g. in a joystick-like user interface, uncalibrated data can be used. Based on this, I assume that if the measurement axes are independent (decoupled), a calibration process can be avoided. Even if calibrated force readings are required, independent sensor measurements could make the calibration procedure easier, requiring fewer calibration parameters and therefore fewer calibration data (by ignoring the crosstalk between the measurement axes), even more so when combined with a linear (instead of quadratic) calibration model.

This section will show a comparison between the conventional bulk structure and the new air gap structure. Additionally, a bump-like structure can reduce the crosstalk between neighboring 3-axis measurements and can make the assembling process easier.

The structure of uSkin in this section consists of two different materials, structured silicone and fabric. Naturally, this will result in different properties of the sensor. Another characterization process is necessary to discover the new specifications of the sensor. Especially the durability of the new structure should be tested.

Moreover, in this chapter I will use improved readout electronics, which are smaller and allow the connection of more sensors.

Thus, the main contributions of this section are that 1) I propose a design and evaluate the new structure of the skin, 2) reduce the overall size of the readout electronics (i.e. microcontroller size and the number of wires) and improve the sensor's sampling frequency, and 3) conduct a durability test.

3.4.2 Sensor Description

This section will give a short description of the sensor, followed by a comparison between the previous and the new structure including its improved readout electronics.

(1) Design

I used the same PCB layout that was previously introduced in Section 3.2 (16 MLX90393 chips with 4.7 mm of spatial distance). Sixteen permanent magnets were embedded inside bulk silicone rubber previously, meaning that the structure is deformable but incompressible. The major problem of such a structure is that the movements of permanent magnets became less independent. For example, even though only normal force is applied, permanent magnets will also move sideways. The crosstalk between the 3-axis measurements was addressed in Chapter 3.2. To minimize this effect, I designed a new structure that can be seen in Fig. 3.26. This new structure has bumps and air gaps. This deformable bump-like structure can also act like a spring. The air gap between the chip and the silicone is 1.7 mm high. The dimension of uSkin in this section is 26x27x6.05 mm (1.7 mm thick PCB, 2.85 mm silicone including magnets and chip, and 1.5 mm fabric).

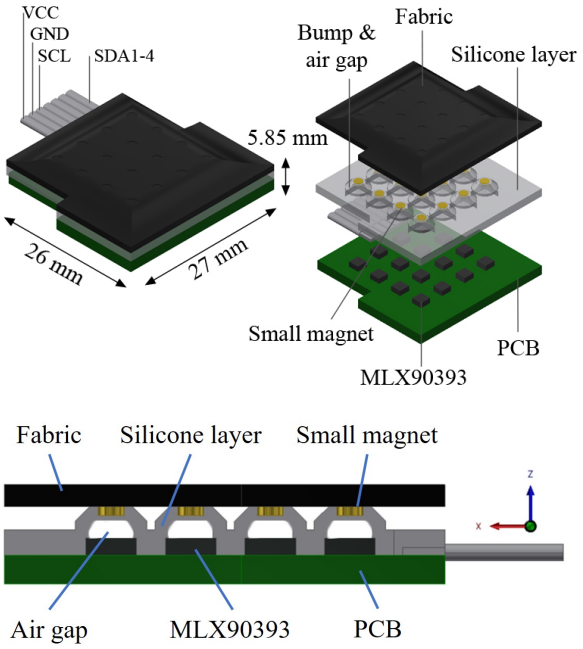

FIGURE 3.26: Design of uSkin with improved structure.

(2) Soft Skin Manufacturing Process

Two different materials constitute the soft structure of the skin sensor module (see Fig. 3.26). The first layer is silicone with cavities and bumps, mounted above the PCB, printed using Agilista 2000, a 3D printer from Keyence. I used AR-G1L as for the material. Table 3.3 provides its specification. In the previous work, I used Ecoflex 30 and 50 from Smooth-On (shore 00-30 & 00-50). Compared to Ecoflex 50, AR-G1L is stiffer. The first reason why I selected this material is that the thin wall of the bump-like structure can get deformed easily if the material is too soft. For example, the weight of the permanent magnets can already deform the structure when it was mounted on the Ecoflex 50 structure. Additionally, more than one permanent magnet were distributed every 4.7 mm center-to-center distance. These permanent magnets were pulling each other, deforming the silicone structure by default. The stiffness of AR-G1L is enough to maintain the overall shape of the structure when not loaded. Furthermore, it is still deformable and provides a reasonable force measurement range. The second reason is that a complicated structure can be 3D printed rapidly and effortlessly compared to molding thin silicone. The bump-like structures have small holes to place the permanent magnets inside. To fix the magnets and prevent them from flipping, I used a silicone glue (Sil-Poxy from Smooth-On; working time 5 minutes, cure time 12 minutes at 23°C).

TABLE 3.3: AR-G1L specifications

Details	Unit	Test	AR-G1L
Shore hardness (A)	-	JIS K6253	35
Elongation ratio at break	%	JIS K6251	160
Tensile strength	MPa	JIS K6251	0.5-0.8
Tearing strength	kg/cm	JIS K6252	3.1
Density	g/cm^3	JIS K6268	1.03
Water absorption	%	JIS K7209	less than 0.4

The second layer is a fabric (Neoprene from RS Pro, RS stock no. 733-6753, with 1.5 mm thickness) glued on the top of the silicone structure. The glue was Power Flex, a flexible super glue from Loctite (15-30 s fixture time). Afterward, this silicone layer covered with fabric was fixed on the PCB using the same super glue.

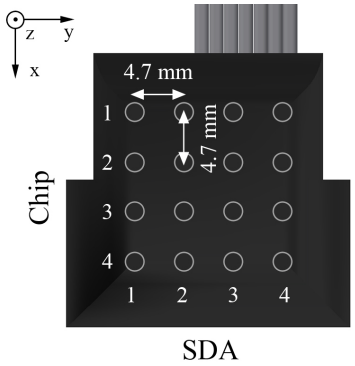

FIGURE 3.27: SDA and chip placement.

(3) Improved Readout Electronics

Previously, to read 3-axis x 16 chips measurement from one uSkin module, one Arduino Due and one I2C multiplexer are required, which is bulky. The multiplexer is necessary because Arduino Due does not have enough I2C data (SDA) buses. An MLX90393 chip only has a 2-bit configurable address. Up to four chips can be daisy-chained in one data bus. To have 16 chips in one module, they have to be split into 4 data buses. The implementation with the multiplexer limits the maximum sampling frequency to only up to 30 Hz.

This time I reduced the overall readout electronics and increased the maximum sampling rate by using a MTB3, a small microcontroller developed by

IIT (Istituto Italiano di Tecnologia) for their humanoid robot iCub [49][73]. The size of MTB3 is about 26x18x6 mm big. It has 4 data buses for I2C communication. Each microcontroller can be daisy-chained through CAN (Controlled Area Network) bus. Therefore, one MTB3 is enough to handle all 16 MLX90393 chips' measurements with a higher sampling rate. A single MLX90393 chip can provide 3-axis magnetic field and one temperature measurement. Depending on the configuration of the built-in digital filter, up to 500 Hz of sampling rate can be achieved. However, a higher frequency will have more noise as a trade-off. Therefore, this time I configured my sensor with a digital filter setting to achieve a maximum frequency of about 125 Hz. The MTB3 was set to collect measurements with 100 Hz.

As a comparison to the previous work, the sampling frequency has significantly improved from 30 Hz to 100 Hz (and possibly more). Additionally, the required number of wires is reduced to only seven wires (1 VCC/ 3.3 V of power, 1 GND/ ground, 4 SDAs, and 1 SCL/ clock) for the communication between the uSkin module and the MTB3. For the communication between two microcontrollers or the serial communication of the MTB3 with the CAN-USB or CAN-ethernet converter to PC, only four wires are needed. In short, the readout electronics became more compact.

3.4.3 Characterization Method

This section will provide the means to characterize the sensor.

(1) Experimental Setup

The overall experimental setup used in this section can be seen in Fig. 3.28. I mounted uSkin to the x-y table using a thin double sided sticky tape from 3M. A cylindrical 3D printed plastic pusher was attached to a 6-axis F/T sensor (Nano 1.5/1.5 from BL Autotech). The diameter was 10 mm. Meanwhile, the sensor was attached to a voice coil motor (VM5050-190 from Geeplus). The motor was used to apply various perpendicular load forces. The knobs of the x-y table can be rotated to displace the skin sensor in x and y-axis. These movements will generate shear forces when the pusher is in contact with the skin sensor. Compared to the previous work, instead of using an Arduino Due to producing analog output (DAC) for controlling the current for the VCM, I use an Mbed LPC1786 instead. The reason is that I could not produce forces less than 1 N with the voice coil motor using an Arduino Due due to its DAC minimum output that cannot be zero. Although

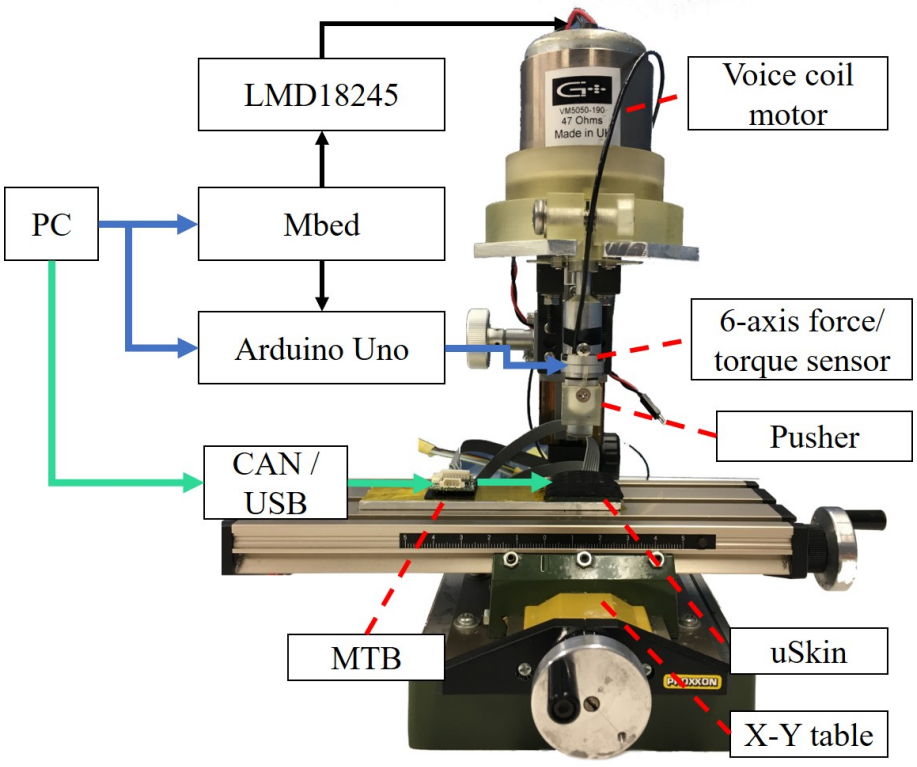

FIGURE 3.28: Test setup

Mbed's resolution is only 10-bit, it is enough to produce a step force of about 0.25 N starting from 0 N. To log the measurements from 6-axis F/T sensor and uSkin, I used 100 Hz as the sampling rate. I removed 50 samples before and after each force change. The average of the first second of measurements were used to calculate the baseline of each sensor axis. No further filters were used this time except the built-in filter in the chip.

(2) Calibration

This section describes how to convert uSkin's raw measurements into 3-axis force.

(i) Training set preparation

The chip 3, SDA 3 was used a representative data for this experiment. To find the calibration parameters, five datasets consisting of input (uSkin's raw measurements) and target (the reference sensor's 3-axis force measurements) were provided. More specifically, these datasets are the normal force and shear forces in +x, -x, +y and -y direction. The five datasets were combined, i.e. all data was used to find the calibration parameters for all axes. The data collection for the shear force is currently done manually and is very time-consuming. For that reason, only one chip was investigated this time. However, through a rough analysis, I found that some taxels could be about twice as sensitive as others in the z-axis. Comparative analyses between the taxels will be conducted in the future. This can be done by using a motorized x-y stage to perform and to provide automated calibration. Moreover, the sensor production (in particular gluing the textile and assembling the permanent magnets) could be outsourced to reduce the differences between taxels. For the normal force, I increased the force in steps of 0.5 N every 5 + 10 seconds (5 s pushing, 10 s no contact of the pusher with skin). In total, there are 5 different forces applied. For the +x shear force, before displacing the table, first 3.5 N of a normal force was applied. Afterward, every 4 s the skin sensor was displaced by 0.2 mm by manually turning the knob of the x-y table. I applied 7 steps of shear force in total. I used the same procedure for the other three shear forces.

(ii) Calibration methods

Methods such as curve fitting and neural network can be used to find the calibration parameters. In my previous works, I found that the best method for calibrating the sensor was linear regression with a quadratic model (and the robust Huber option). However, the previous structural design of uSkin

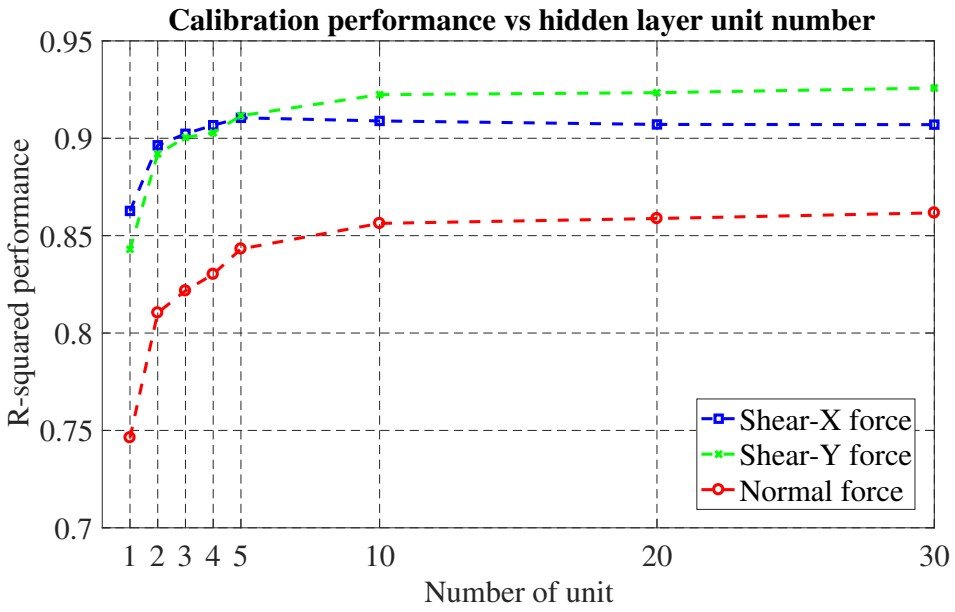

FIGURE 3.29: Neural network performance.

is entirely different from the one introduced here (without an air gap). The new structure and materials introduced here may have a different response. Therefore, several calibration methods should be compared again to find an appropriate one for this particular design. I selected three different methods, linear regressions with and without quadratic model (both with Huber robust option) and a feed-forward neural network (FNN) with one hidden layer.

As for the FNN method, I divided the data into 70 % for training and 30 % for validation. I compared eight different hidden layer sizes (1, 2, 3, 4, 5, 10, 20, and 30 neurons) to investigate their performances one by one. Each MLX90393 chip has 3-axis measurement. Therefore, one chip will have 3 FNN models, where 1 FNN model was used to calibrate one axis. The inputs were the raw x, y, z measurements of the chip while the target output was either the x, y, or z-axis of the reference sensor. The parameters calculation was conducted using the Matlab Neural Network Toolbox. I selected the BFGS quasi-Newton backpropagation algorithm where the iteration was limited to 1000 steps.

Fig. 3.29 shows the R-squared value for the 3 axes for different number of hidden units. New data (not included during training) collected for 3 axes in the same fashion as the training data was used for this figure. The R-squared value of the x-axis calibration starts to slightly decrease with more than five hidden units while there is no significant improvement for other axes.

Table 3.4 shows the calibration performance results for all methods. New

TABLE 3.4: R-squared comparison value.

Calibration method	R-squared value		
	z-axis	x-axis	y-axis
Quadratic + Huber	0.1091	0.7158	0.4129
Linear + Huber	0.8532	0.9179	0.9028
FNN (1 HL with 5 units)	0.8420	0.9100	0.9105

data (not used for calculating the calibration parameters) collected for 3 axes in the same way as the training set was used for this table. Compared to the other methods, the simple linear model already provided nearly the best results. In another preliminary experiment, I used foam as the deformable material as it has compressibility like this new structure. Again, the linear model provided nearly the best results in all cases. On the other hand, the bulk silicone in Section 3.2 and 3.3 has better results when calibrated using the quadratic model rather than the linear model. I conclude that a linear model is adequate for a compressible structure or material, while a quadratic model does better in the incompressible case. However, it should also be mentioned that the R-squared values for calibrating the z-axis with the linear model for the current version of uSkin (0.8532) are comparable or even slightly lower than in the previous works (0.8634 for the flat module with bulk silicone and a linear model, and 0.8938 for the curved fingertip). The hysteresis in the current sensor is higher than the previous works. This could be the reason why the force calculation less precise in general. Subsequently, I selected the linear model for calibrating the current version of uSkin. (3.6) shows the calibration model.

$$S_{j,c} = aS_x + bS_y + cS_z \tag{3.6}$$

Here, $S_{j,c}$ is the calibrated sensor output of axis j (x, y, or z). S_x, S_y, and S_z are pre-calibrated skin sensor module outputs in digits. a, b, and c are the calibration parameters calculated in MATLAB using the Statistics & Machine Learning Toolbox.

(3) Hysteresis test

Soft material tends to have hysteresis. It is the reason why the output of the sensor during the loading cycle can be different than during the unloading cycle. Usually, the soft material requires some time to return to its initial

state completely. Moreover, in Fig 3.33 and 3.34 the z-axis force measurement of uSkin increases by about 1 N, even though the actual force is somewhat stable or even decreases (variations in the applied force are due to limitations in the force control of the voice coil motor, i.e. friction). To calculate the hysteresis value of this version of uSkin, I used equation 3.7.

$$Hysteresis\ \% = \left| \frac{(F_{mu} - F_{ml})}{(F_{max} - F_{min})} \right| \times 100\% \tag{3.7}$$

F_{min} was the minimum and F_{max} the maximum measured average force by the reference sensor. F_{ml} and F_{mu} are the calibrated skin force values (linear interpolation of the nearest neighbors) of the loading and unloading cycles, respectively. These two values were taken at the midpoint of the cycle (X_m) as calculated using (3.8).

$$X_m = \left(\frac{F_{max} - F_{min}}{2} \right) + F_{min} \tag{3.8}$$

(4) Signal to noise ratio

The SNR (signal to noise ratio) value in decibel (dB) of each taxel for different loads can be calculated using equation 3.4.

where μ_U and σ_u are the average and standard deviation value of the calibrated uSkin measurements when there was no force applied. μ_p is the average value of the calibrated uSkin measurement when the skin was pushed.

3.4.4 Results

(1) Sensor Response before Calibration

In this section, I compared two kinds of uSkin structure: bulk silicone (as in Section 3.2 and 3.3) and the new structure with bumps and air gaps. Fig. 3.30 (top) shows the response with bulk silicone. There is a reading in x-axis even though only z-axis force was applied. The main reason why this happened is most likely because the permanent magnet was displaced sideways due to the incompressibility of the silicone material. Fig. 3.30 (bottom) shows the response of uSkin with bumps and air gaps. This time the graph shows less response in x and y-axis. I calculated the crosstalk between the 3 axes measurements as $mean(abs(S_x/S_z) + abs(S_y/S_z))$ (mean of all time steps when being pushed with z-axis force). The data are taken from Fig. 3.30 and from [67] for the curved sensor, respectively). Table 3.5 shows the

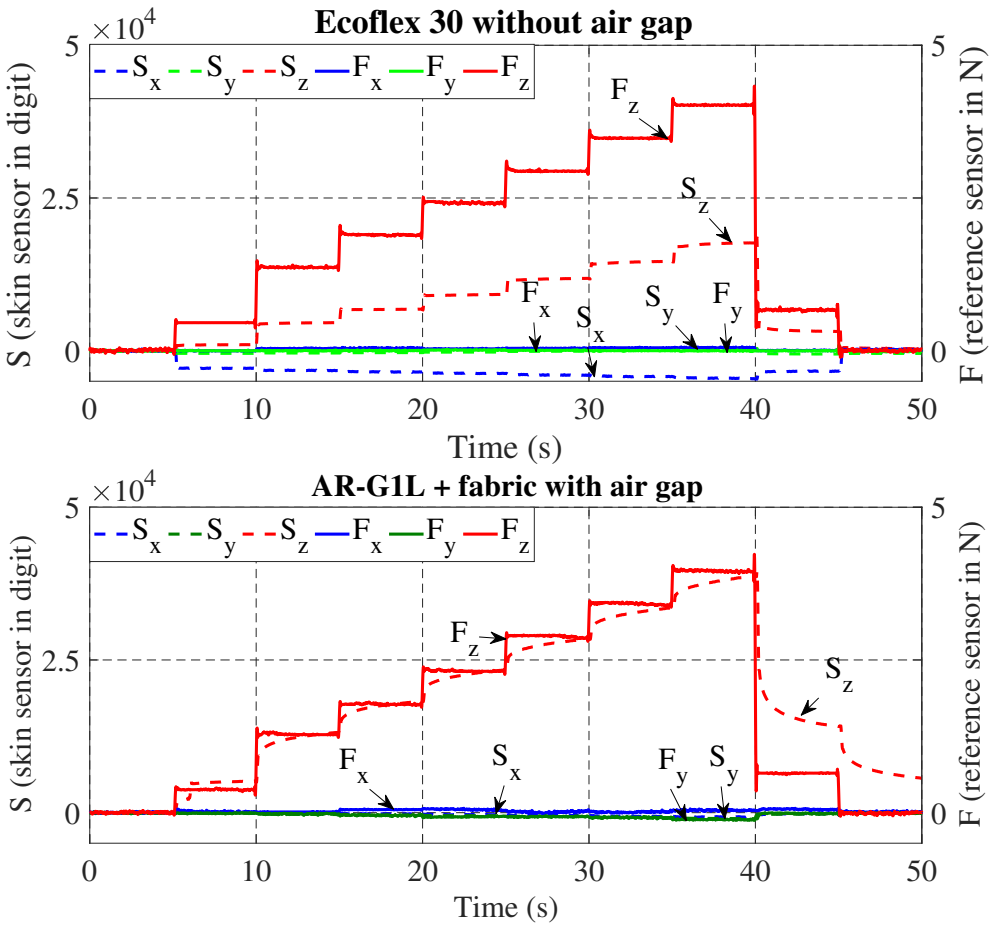

FIGURE 3.30: Sensor response when subject to stepwise z-axis force with bulk silicone (top) and new structure (bottom).

result. The crosstalk between the 3-axis measurements in % decreased about ten times less (from around 40% to around 4%).

(2) Durability

Fig. 3.31 shows the response of uSkin when the motor applied a high load force to demonstrate its durability. There was no load in the first 5 s. Afterward, the motor pushed uSkin with around 50 N of normal force (about 637 kPa) for 10 s. The uSkin measurement had an overflow as the distance of the permanent magnet got too close to the chip. After uSkin was unloaded, all axis readings gradually return towards zero. Even though uSkin received high pressure, the sensor is still working normally.

(3) Calibration result

The calibrated z-axis measurement of uSkin can be seen in Fig. 3.32. The response for x-axis and y-axis can be seen in Fig. 3.33 and 3.34 respectively. Unlike the training set for the calibration parameters, in which the force was

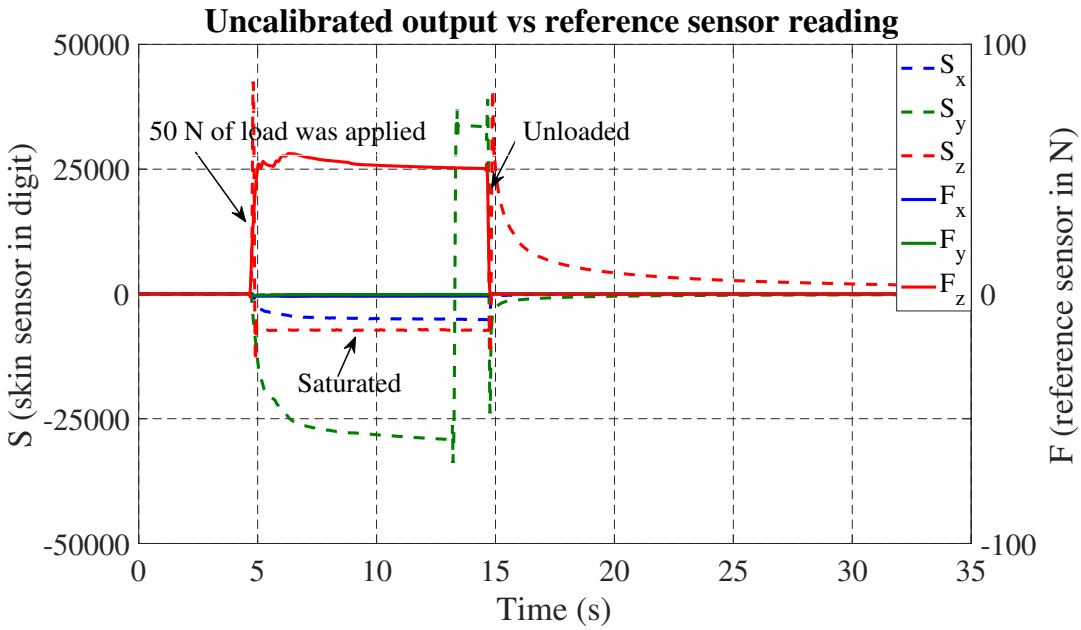

FIGURE 3.31: Overloading test.

only stepwise increasing, the force in the respective axis was stepwise increased and then decreased for all three figures. Also, the data for Fig. 3.32 has no 10s breaks between the increasing z-axis force steps.

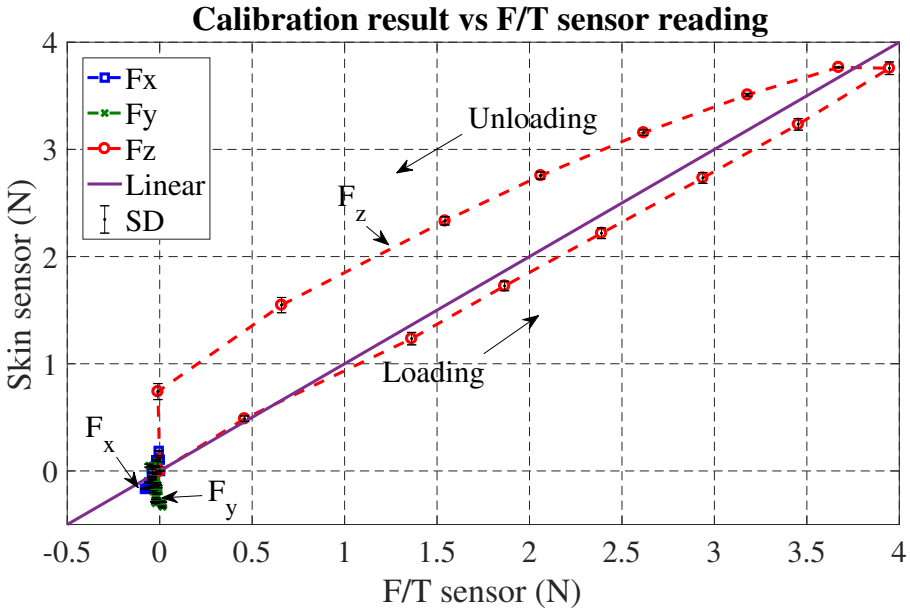

FIGURE 3.32: Calibrated sensor response when normal force is applied.

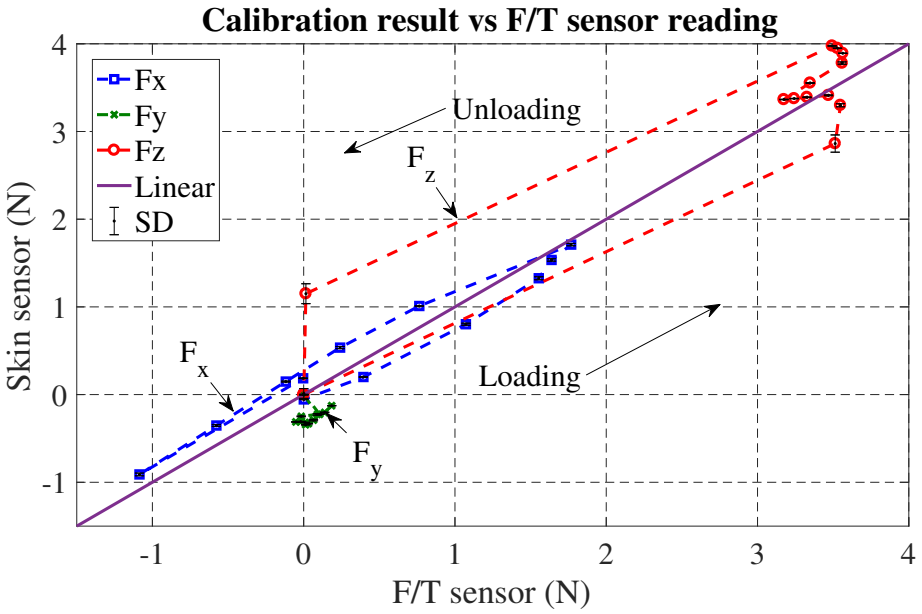

FIGURE 3.33: Calibrated sensor response when shear force is applied.

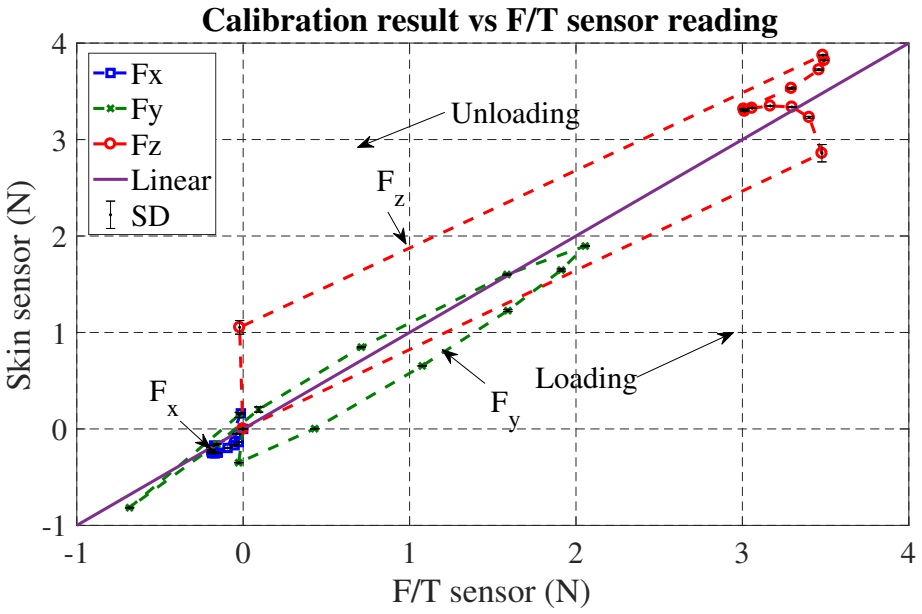

FIGURE 3.34: Calibrated sensor response when shear force is applied.

(4) Hysteresis evaluation

I found that the hysteresis was about 20.5 % for the z-axis, 12.2 % for the x-axis, and 16.8 % for the y-axis. It was measured using the loading and unloading cycle in Fig. 3.32, 3.33 and 3.34.

(5) Signal to noise ratio result

TABLE 3.5: Comparison Table

	flat	curved	new structure
Pressure (kPa)	SNR (dB)		
4.5	48.04	47.62	39.06
7.6	53.35	51.51	47.44
9.4	55.49	52.61	50.67
12.6	58.89	53.29	54.56
Hysteresis z-axis (%)	5.29	10	20.5
Range (N)	14	6	14
Thickness (mm)	4	4	5.85
Crosstalk during z-axis pushing (%)	41.48	38.48	3.86

Table 3.5 presents The SNR results of one sensor for different pressures together with an overview of other relevant results. Table 3.5 also shows a comparison to the results with bulk silicone for flat [66] and curved modules [67]. New data was taken using the new measurement electronics presented here to calculate the SNR values for those sensors. Additionally, the measurement frequency and the pusher size are also the same (100 Hz and 10 mm of diameter respectively). The SNR values are overall similar and lie within the normal variation that can be observed in my experiments between different loadcells (the noise, as well as sensitivity, varies between sensors).

3.4.5 Discussion

A soft layer with an air gap structured for skin sensors were introduced in [65], [69]. The work in [65] proposes a dome-like structure. [60], [65] claimed that such kind of structure can improve the sensitivity to the shear forces measurement. The difference to the work in this section is that uSkin has an additional layer that covers the bump structure to maintain the surface as flat as possible. A flat surface is more preferred to cover robot parts. Additionally, this cover can give an extra protection to the sensor and also can be replaced for the ease of maintenance. This can be achieved because the gap between each bump is very small. In [69], instead of using a dome structure, a

conventional bulk structure with additional cavity above the chip was used to allow the silicone to compress. The main intention is for increasing the sensitivity of the sensor. The additional benefits of the structure introduced in this section is that the permanent magnets are easier to be assembled as they do not need to be implanted inside the silicone. Implanting magnets inside a silicone has some drawbacks. First, two layers molding process is required (as explained in Fig. 3.2), consuming more manufacturing time, labor cost, and efforts. Second, the whole silicone skin needs to be replaced if a maintenance is necessary.

Both works mentioned above were not investigating the importance of an air gap structure to reduce the crosstalk between 3-axis for a 3D Hall Effect-based skin sensor. This section investigates for the first time and shows that an air gap structure can reduce the crosstalk for about ten times lower than the conventional bulk structure. Data without too much crosstalk information can be used straightforwardly for a machine learning purpose without any further calibration. Unfortunately, the hysteresis becomes higher than the conventional bulk structure (about 20% from 5%) due to the characteristic of the material (AR-G1L). A low hysteresis value is important to minimize the measurement inaccuracy and give a faster response to reach a quasi-static state. Therefore, optimizing the materials to lower the hysteresis is required and will be presented in the next section.

Finally, in the previous section, uSkin required an Arduino Due and a multiplexer to read 16 x 3-axis force data, limiting the maximum readout frequency to 30 Hz. The work in this section proofs that the same amount of data can be read at 100 Hz (possibly up to 250 Hz) using an MTB3, a small microcontroller from the IIT [73]. This improved network enables multiple uSkin modules to be mounted on robot hands such as Allegro Hand and iCub Hand in a daisy-chained link with only four final output wires. As a comparison with other distributed skin sensors, Twendy-One [35] requires bulky and heavy electronics mounted on the back side of the hand, causing the maintenance to be work-intensive. Compared to the iCub skin [49], uSkin can measure shear forces. In short, a compact, soft, distributed, 3-axis skin sensor is achieved already at this stage.

3.5 Sensor Optimization

3.5.1 Objective

In the previous section, the silicone structure of uSkin was printed using AR-G1L material from the Keyence for a rapid prototyping purpose. Although the crosstalk between 3-axis measurement could be reduced to about 4%, the hysteresis is about four times higher than the Ecoflex series. To determine which material can give the best performance, several liquid silicone rubbers will be compared. Moreover, the new uSkin specification after it has been optimized will be presented here.

3.5.2 Sensor structure

Initially, Ecoflex 30 and 50 (shore 00-30 and 00-50 respectively) from Smooth-on were used. However, the improved structure has bumps with a 0.5 - 0.8 mm thin wall as in Fig. 3.35.

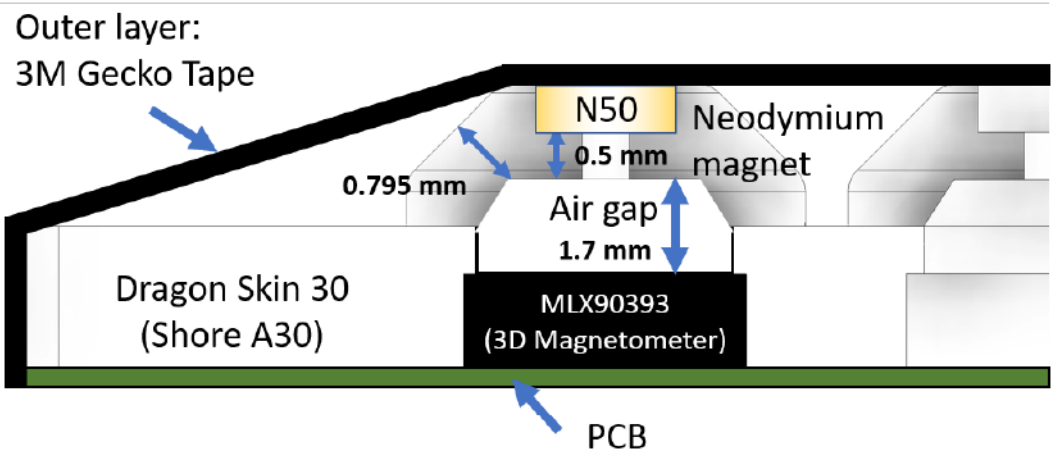

FIGURE 3.35: Detailed structure of uSkin with optimized materials.

Because of this, the stiffness of the material is not enough to maintain the structure. The pulling strength of the permanent magnets are stronger causing them attracting each other. As a result, the bump structure gets deformed by default. For this reason, a material that is harder than shore 00-50 is required. The shore A is harder than 00 in general. A silicone rubber with the shore A17 was confirmed to be enough to maintain the structure from deforming due to the permanent magnet's weight or its pulling strength. A

softer material can provide a higher sensitivity but has a lower maximum detectable force as a trade-off. A wider sensing range is important to manipulate various daily objects. For that reason, a shore hardness of about A30 was selected. Even though some silicone rubbers have the same stiffness level, they may have different response characteristics such as hysteresis. This can be seen in Fig. 3.36, where three different materials (DY, RBB, and DragonSkin) were compared. As we can see, DragonSkin 30 has the lowest hysteresis value outperforming the others. Based on this result, DragonSkin 30 from Smooth-On was chosen for manufacturing the air gap structure of uSkin.

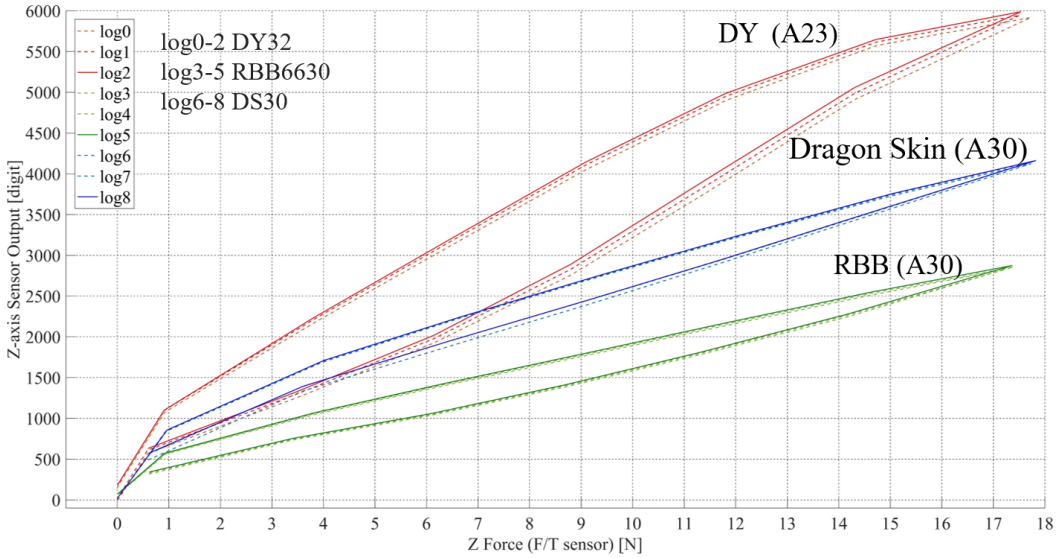

FIGURE 3.36: Uncalibrated sensor response when normal force is applied.

Initially, the outer layer covering the silicone structure was a Neoprene fabric. The surface friction was somewhat low, resulting the shear forces were difficult to be measured as the objects tend to slip. To increase the grasping stability and shear forces detection, a gecko tape from 3M is selected.

3.5.3 Characterization Method

An experiment to characterize uSkin with optimized materials was conducted. The experimental procedures are similar as in the previous section. A Nano 17 force-torque sensor is used this time as it has more force measurement range. The maximum force generated by the voice coil motor is 18 N. All 16 chips were pressed simultaneously with a pusher that has a contact area similar to the sensor module size. The procedure for training and validation

is the same as in 3.4. As expected, a linear model has the best fitting to find the calibration parameters.

3.5.4 Result

The test result can be seen in Fig. 3.37, representing one out of 16 sensors during z-axis (normal force) load.

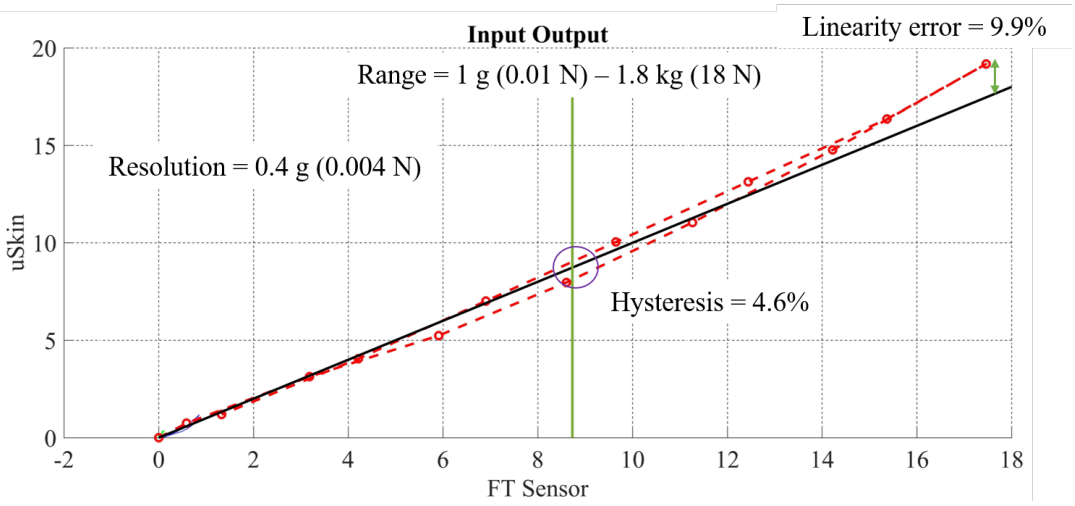

FIGURE 3.37: The response of uSkin with Dragon Skin measured at 50 Hz when normal force was applied. (Unit is in Newton)

(1) Sensitivity

The sensitivity of a sensor can defined as follows:

$$Sensitivity = \Delta S / \Delta F \tag{3.9}$$

There are 14 load points in total (7 loading and 7 unloading), including two where the sensor was not pushed. The differences between each load/unload point were calculated, resulting 13 values of ΔS (uSkin) and ΔF (Reference sensor). Using equation 3.9, 13 sensitivity values were calculated then averaged. The average value of the sensitivity is calculated as 1.1233 with a standard deviation of 0.1785.

(2) Range

The range is the minimum and the maximum detectable forces that can be measured by the sensor. For the minimum detectable force, a piece of paper cut in a square shape (about 30 mm x 30 mm) was used. The shape

is slightly bigger than the skin sensor so that it can cover the whole surface. It was confirmed that the skin sensor could measure a 1 g of paper. For the maximum detectable force, the highest load that can be generated by the voice coil motor (18 N) was used for the test. Although the sensor is not yet saturated at the maximum load, we can see that the output starts to significantly deviate from an ideal line. As a conclusion, the current design of uSkin has a range of 1 - 1800 gf. Further test with a higher load will be conducted in the future to determine its saturation point.

(3) Resolution

The resolution (minimum detectable force for a given bandwidth) is calculated as:

$$Resolution = NL/Sensitivity \tag{3.10}$$

NL is the RMS noise of calibrated sensor measurement at 50 Hz when there is no load applied. 200 samples were averaged to calculate NL. Later, the value was found as 0.0052 N or 0.52 gf. Using the sensitivity value calculated previously, the resolution of the sensor is 0.004 N or 0.4 gf.

(4) Accuracy

The accuracy can be seen in Fig. 3.38 and was measured using equation:

$$Accuracy(\%) = 100 - \frac{|S_{avg}/F_{avg}|}{F_{avg}} \times 100 \tag{3.11}$$

where S_{avg} and F_{avg} are the average value of skin sensor output and reference sensor output at one load point respectively.

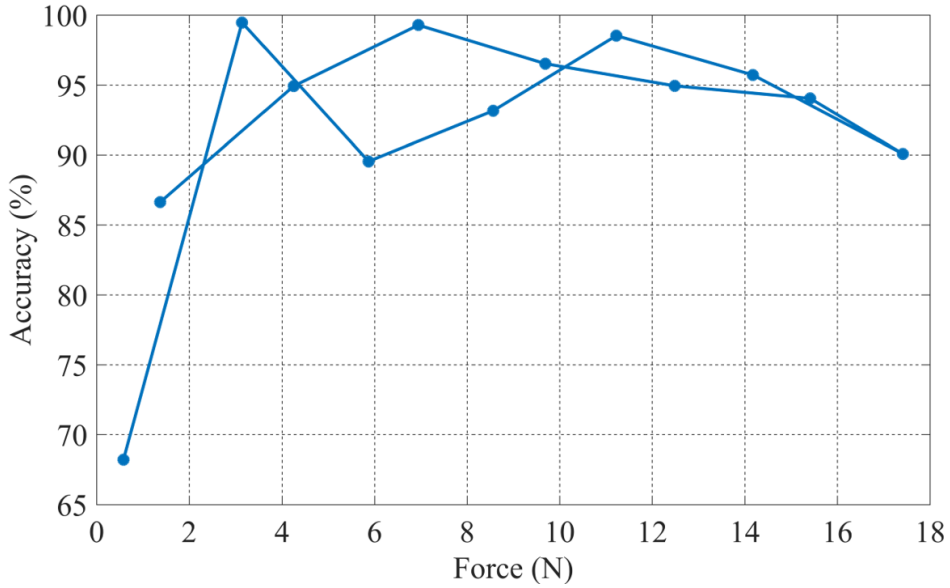

FIGURE 3.38: Sensor's accuracy during different load forces.

Please note that the first data point when there is no load applied is removed from the plot as there is no meaningful information. In overall, the accuracy of the sensor is above 90% when more than 2 N of forces were applied.

(5) Linearity

The linearity expresses how much the sensor output value deviated from the ideal curve. It can be calculated as:

$$Nonlinearity(\%) = \frac{D_{in(max)}}{IN_{f.s.}} \times 100 \tag{3.12}$$

$D_{in(max)}$ is the maximum input deviation and $IN_{f.s.}$ is the maximum, full-scale input. By looking at Fig. 3.37, we can see that uSkin starts to deviated from the ideal curve at around 14 N of normal force. The linearity error of uSkin is 9.9% at around 18 N under the normal force load.

(6) Hysteresis

The hysteresis value was calculated as 4.6% using Equation 3.1, slightly improved compared than the conventional bulk structure (5%) and about four times lower than the AR-G1L material (20%).

(7) Response Time

The response time here is defined by measuring the rise-time (T_r) and fall-time (T_d), a period of time required to change into a quasi-static state value. At 50 Hz, it was found that 22 time step is required to reach a quasi-static state. Therefore, the response time of the sensor is 440 ms. However, the required time for the sensor to give an actual feedback after an impact is presumed to be lower than that. A test with a higher sampling rate to determine the response time of the overall system (required time for the sensor to give a feedback using an actuator) will be presented in the next chapter.

3.5.5 Discussion

Many skin sensors had been successfully implemented on the robots to perform tasks [35], [49], [65], [69]. uSkin was developed to cover robot hands as the main motivation. Although the sensor specification is much more mature than the earliest design, it has not been used yet for conducting tasks. In the Chapter 4, some tasks will be demonstrated to show uSkin capability.

The major drawback of uSkin compared than non magnetic sensors such as [35], [49] is that it can get influenced by external magnetic sources such as ferromagnetic objects and the earth magnetic field. However, compensating a magnetic influence is possible. For example, by having extra reference sensors, the difference before and after the sensor gets influenced can be measured. The idea to nullify an influence from other magnetic source will be demonstrated in Chapter 4.3. This limitation will be discussed further in Chapter 5.

3.6 Conclusion of this Chapter

(1) Section 3.2 presented the design of a skin sensor with 16 Hall effect sensors. Load tests were performed by applying normal and shear forces on the proposed sensor. The tests revealed that when only normal force was applied, displacements in the x-axis and y-axis were detected. However, after performing a calibration, a similar result as the reference sensor force measurement could be achieved. The test also revealed that the shear forces in x and y-direction could be measured. Further tests were performed to measure the distributed sensor response when being pushed in different locations. It was concluded that the sensor

can be used to detect the distributed force vector. Furthermore, grasping experiments with the hand will be performed to evaluate the sensor measurements during real use in Section 4.3.

(2) Section 3.3 presented the design of a skin sensor for robot fingertips with 24 Hall effect sensors. Load tests were performed by applying normal and shear forces on the proposed sensor. The tests revealed that even though it has a round shape, uSkin can successfully be used to measure 3-axis force. Further tests were performed to measure the distributed sensor response when being pushed with different shapes. It was concluded that the sensor can be used to detect the distributed force vector.

(3) Section 3.4 presented a new structure for the soft skin of uSkin. Table 3.5 shows the most important characteristics and compares them to the previous versions of uSkin. Most importantly, the crosstalk between the 3-axis (due to the incompressibility of silicone material) was reduced (from around 40 to about 4%). Even without a time consuming calibration of the sensor, the 3-axis components are therefore more independent. The SNR was comparable and lies within the normal variation between different loadcells that I observed in my experiments. The range was also similar to the previous flat version. The sensor was thicker, but this does not constitute an inherent weakness of the current sensor, as it was partially due to the rather thick Neoprene (1.5 mm thickness) and partially due to the PCB (I used a 1.7 mm thick PCB, which is otherwise identical to the 0.5 mm thick PCB in [66], to increase the stability, as the iCub hand does not provide a flat support for the sensors). Therefore, the sensor thickness can be easily reduced in future work. The hysteresis was increased. This is due to the material, which has a visibly high hysteresis also when used in bulk form. Future work could use the new structure with a material with less hysteresis. However, currently few soft materials can be 3D printed, and 3D printing facilitates the prototype production compared to molding. Furthermore, I could show that despite using structured silicone, the sensor was robust to overloading with 50 N (about 637 kPa). Overall, I proved that it is easy to configure uSkin for different requirements. Using a textile as the top layer can be beneficial depending on the application.

(4) Section 3.5 presented material optimization to reduce the hysteresis and

to achieve the optimal measurement range. Dragon Skin 30 is considered to be the best material option compared to RBB and DY as it has the lowest hysteresis (4.6 %). Using the current design and materials, the dynamic range of 1 gf - 1800 gf can be achieved. The accuracy of the sensor may vary under different loads. For example, about 90% of accuracy can be achieve when the sensor was loaded with normal forces between 2 - 18 N. The sensor becomes less accurate when it measures lower forces.

3.7 Chapter Summary

This chapter investigates the sensor's behavior when the Hall Effect sensing elements and permanent magnets are distributed in less than one centimeter from center to center distance. The method introduced here such as structural design and materials selection proofs that a compact, distributed, soft, and 3-axis skin sensor can be achieved. Furthermore, the sensor can be used to cover many kinds of robot shapes (flat and multi-curved). The next work that needs to be done is to proof that the sensor can be truly implemented on robots for conducting tasks. Therefore, the next chapter will demonstrate uSkin's capability when it is used for real use cases.

Chapter 4

Implementation

4.1 Background

Tactile sensing gives us humans better perception for controlling force while grasping and manipulating an object. Likewise, tactile sensing is also crucial for robots to enable a robust interaction with a dynamic environment. In this chapter, I covered an EzGripper from Sake Robotics, an Allegro Hand, and an iCub Hand with uSkin to demonstrate the capabilities that distributed 3-axis soft skin sensors can deliver.

I found that the earth magnetic field may influence the sensor's readout. Through a compensation method, I successfully nullified this effect. As the skin sensor can also measure shear forces, I took advantage of this information for implementing feedback control to prevent an object from slipping as it got heavier. The gripper could grasp with a low force, but enough to prevent the object from slipping. The response time of the sensor is fast, 5 ms at 200 Hz sampling frequency. The sensor is also sensitive. It could detect an object with 5 g of weight. Meanwhile, the minimum detectable weight is 1 g.

A visualization software was also developed to enable seeing the sensor's response while grasping objects. Four different objects were grasped using an EzGripper, and they produced distinctly different force visualizations. A similar situation also occurred when an object shape exploration task was performed using a humanoid robot iCub.

4.2 Objectives

The objectives of this chapter are:

1. To prove that uSkin can be integrated into various robots.
2. To discuss that other magnetic sources can influence the sensor yet compensation is possible.

3. To show the importance of 3-axis force data and its fast response time for preventing objects from slipping.

4. To give an idea that the data of uSkin can be used for machine learning purpose such as classifying object shapes.

4.3 Implementation on the Allegro Hand

In this section, I will show uSkin's response when it is implemented on the Allegro Hand.

4.3.1 Method

uSkin used in this section is based on the one introduced in Chapter 3.2 and 3.3. The sensor was mounted into Allegro Hand's fingertip and phalanges. To show the 3-axis force measurement from the sensor, a 40 s long experiment was conducted. The sequence of the experiment can be described as follows:

1. At 0 to 10 s, there is no object grasped.

2. At 10 to 20 s, the Allegro Hand will grasp an empty plastic cup.

3. At 20 to 30s, an object with 175 g of weight will be dropped into the cup.

4. At 30 to 40s, the Allegro Hand will release the cup.

   One load cell (SDA 1 chip 2) on the fingertip will be used as a representative data. uSkin in this section can cover flat (phalange) and multi-curved surface (fingertip). Although it shows that the shear forces information can be useful for detecting weight changes, feedback control is still not implemented here. Therefore, the next section will demonstrate the reactive grasping using uSkin data.

4.3.2 Result

The output of one load cell (SDA 1 chip 2) corresponding to different grasping conditions can be seen in Fig. 4.1. Initially, the Allegro Hand did not grasp anything so there was no response from the sensor. When the hand grabbed the cup, measurements in x, y, and z-axis changed. Later, I dropped a 175 g heavy roll of wires into the cup, which caused a visible vibration and the cup slightly moved due the weight of the object. The output of uSkin

changed accordingly as shown in the plot. Finally, the cup was released and the output of the sensor eventually returned to zero.

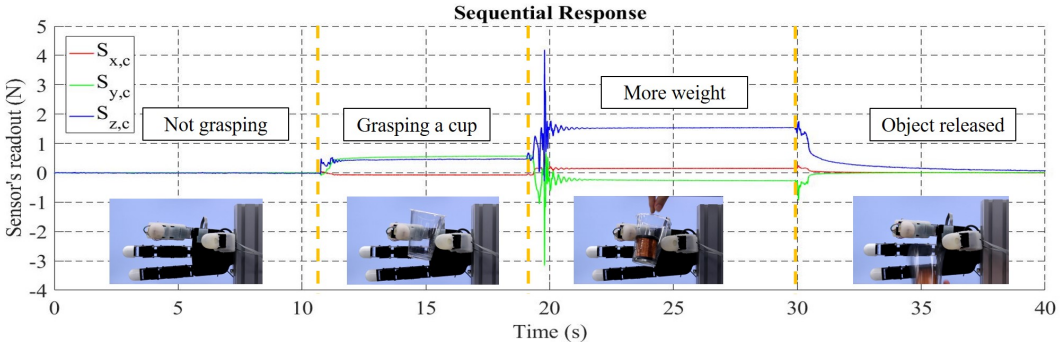

FIGURE 4.1: Sequential response.

4.3.3 Discussion

uSkin in this section can cover flat (phalange) and multi-curved surface (fingertip). Although it shows that the shear forces information can be useful for detecting weight changes, feedback control is still not implemented here. Therefore, the next section will demonstrate the reactive grasping using uSkin data.

4.4 Reactive Grasping

4.4.1 Hardware Description

In this section, a short description of the general working principle of the sensor and the specifications of the gripper will be provided.

(1) Sensor

In a 27 x 28 mm area, there are 16 load cells that individually can measure 3-axis force. There are 16 small permanent magnets embedded inside a silicone structure, floating above 16 3-axis hall-effect sensor chips. These permanent magnets will displace in x-y-z direction corresponding to the direction of the contact force or the shape of the objects. Through a calibration process, the output of the sensor can be converted from a magnetic field (mT) into pressure (Pa). A microcontroller is used to collect the data from the sensor through I2C (inter-integrated circuits) communication and send it to the PC via CAN (controlled area network) protocol. The communication from the sensor module to the microcontroller requires only 7 wires, and from the microcontroller to the PC only 4 wires, adding to the space efficiency of the sensor system. The maximum sampling frequency I can achieve is 250 Hz per axis.

(2) Gripper

The gripper I used in this section is an EzGripper from Sake Robotics. The gripper is tendon driven, and its servo head needs to rotate for about 180 degrees in order to fully close the gripper. It can be connected to the PC through serial communication. By default, the latency time of the COM port in Microsoft Windows is 16 ms. I changed it to 1 ms so that the gripper can provide a faster response. uSkin was attached to one side of the gripper as shown in Fig. 4.2. I used a Python software as an interface to integrate the sensor and gripper. The details of the gripper are provided in Table 4.1. I mounted the gripper on a sturdy aluminum profile as shown in Fig. 4.3.

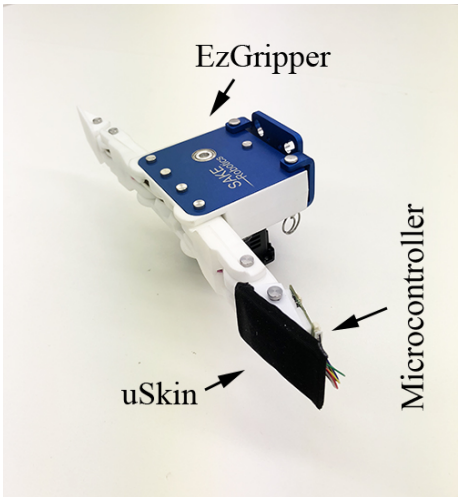

FIGURE 4.2: uSkin mounted on the EzGripper.

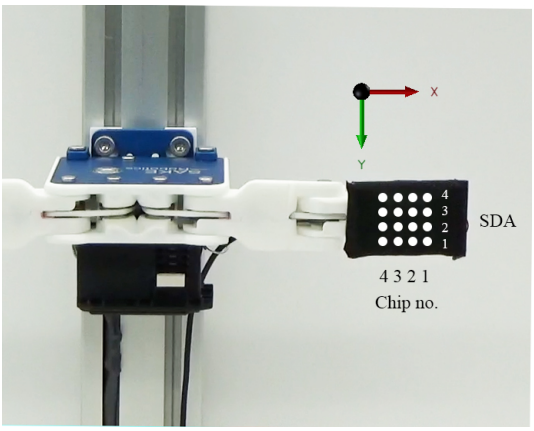

FIGURE 4.3: SDA and chip placement.

TABLE 4.1: EZGripper specifications

Grasp Width	145 mm
Payload	2.5 kg - 5 kg
Gripper Weight	365 g + 35 g (mount)
Grasp Force	35 N
Servo	MX-64AR from Robotis
Operating Voltage	12 V

4.4.2 Method

(1) Grasping Algorithm

My grasping algorithm can be described as follows: First, I calculated the baseline of 3x16 axes by averaging the first 100 samples of the sensor's raw (initial) value. Afterwards, I subtracted those baseline values from the sensor readings. Thus, all axes values are around zero when the sensor is not touching an object. Next, I calculated the average value of each axis ($S_{avg,x}$, $S_{avg,y}$, $S_{avg,z}$) from all 16 load cells. For grasping an object, I continuously rotated the servo motor head to close the gripper until the $S_{avg,z}$ met a desired threshold value. This value was determined empirically to achieve an as low as possible normal force but enough to avoid the object from slipping. In the next stage, I am implementing the slip prevention algorithm by comparing the current $S_{avg,x}$ value with the previous sensor value ($S_{avg,x,t-1}$). Like before, I slightly close the gripper by rotating the servo motor about 0.2 degree/ digit if the comparison value surpassed the pre-determined threshold.

(2) Earth Magnetic Field Compensation

As my skin sensor measures the magnetic field changes to detect pressure, an external magnetic field (i.e. earth magnetic or electromagnetic) can potentially influence the sensor's reading. In general, an electric motor generates a magnetic force to rotate the rotor that can affect my sensor's reading. In [66], I tested the sensor by placing it on the top of a rotating servo motor and no influence was detected. However, this time I measured some small changes in uSkin's reading due to the orientation changes as in Fig. 4.5 (top). All axes started from nearly zero as the gripper was opened and no electrical current was applied (the motor did not rotate). After about three seconds, the motor started to rotate to close the gripper. Here we can see that the raw value of x-axis ($S_{x,raw}$) increased about 25 digit. To investigate the source of this influence, I conducted two experiments. First, I tried to manually close the gripper without actuating the motor. Second, I tried to rotate the motor without pulling the wire so that the orientation of the skin sensor will not change. As a result, the skin sensor's reading changed only when its orientation changed. I concluded that the source of the influence came from the earth magnetic field, not from the servo motor. Therefore, the sensor needs to be compensated according to its orientation.

The orientation of the end-effector can be estimated through the kinematics calculation. Therefore, the joint angle information can be used to acquire the compensation offset. In this section, I am assuming that the gripper is

attached to a stationary base. For this reason, I only used the EzGripper's servo angle to calculate the compensation offset. The skin sensor I used in this section has 16 load cells which individually can measure 3-axis force. Thus, 48 offset compensation parameters are needed. To calculate these parameters, I compared several methods such as linear regression, quadratic regression, and feed forward neural network (FNN) using a MATLAB Statistic & Machine Learning and Neural Network Toolbox. In general, the first order exponential model can already fit the training data very well. For ease of implementation I used a FNN with only the servo angle as input, one neuron in the hidden layer, and 48 outputs. The BFGS Quasi-Newton backpropagation algorithm was used.

To train the network, I recorded 887 samples of skin sensor measurements and servo angle from the fully opened position to fully closed position. Each sample consists 48 axes of skin sensor data and 1 EzGripper servo angle. The servo angle values were used as an input, while the target output is the 48 values of skin sensor's reading. The training was limited to 1000 iterations. The data was divided into 70% for training and 30% for validation. The R-squared value of the predicted result for new independent test data was 0.9999.

(3) Feedback Control

In this section, I evaluate the sensor's performance in a real-time situation.

(i) Increasing Weight

In this experiment, I demonstrate that the shear forces information can be used for increasing the grasping force to prevent the object from slipping. The object I used for this experiment was a 37 mm diameter cylindrical plastic bottle with a funnel attached on the top as shown in Fig. 4.4 (top). The overall weight of the object was 15 g. After the plastic bottle was securely gripped, I gradually increased the weight by pouring small balls inside. I used a metronome to guide the timing for increasing the weight. The weight was increased by about 5 g in each step.

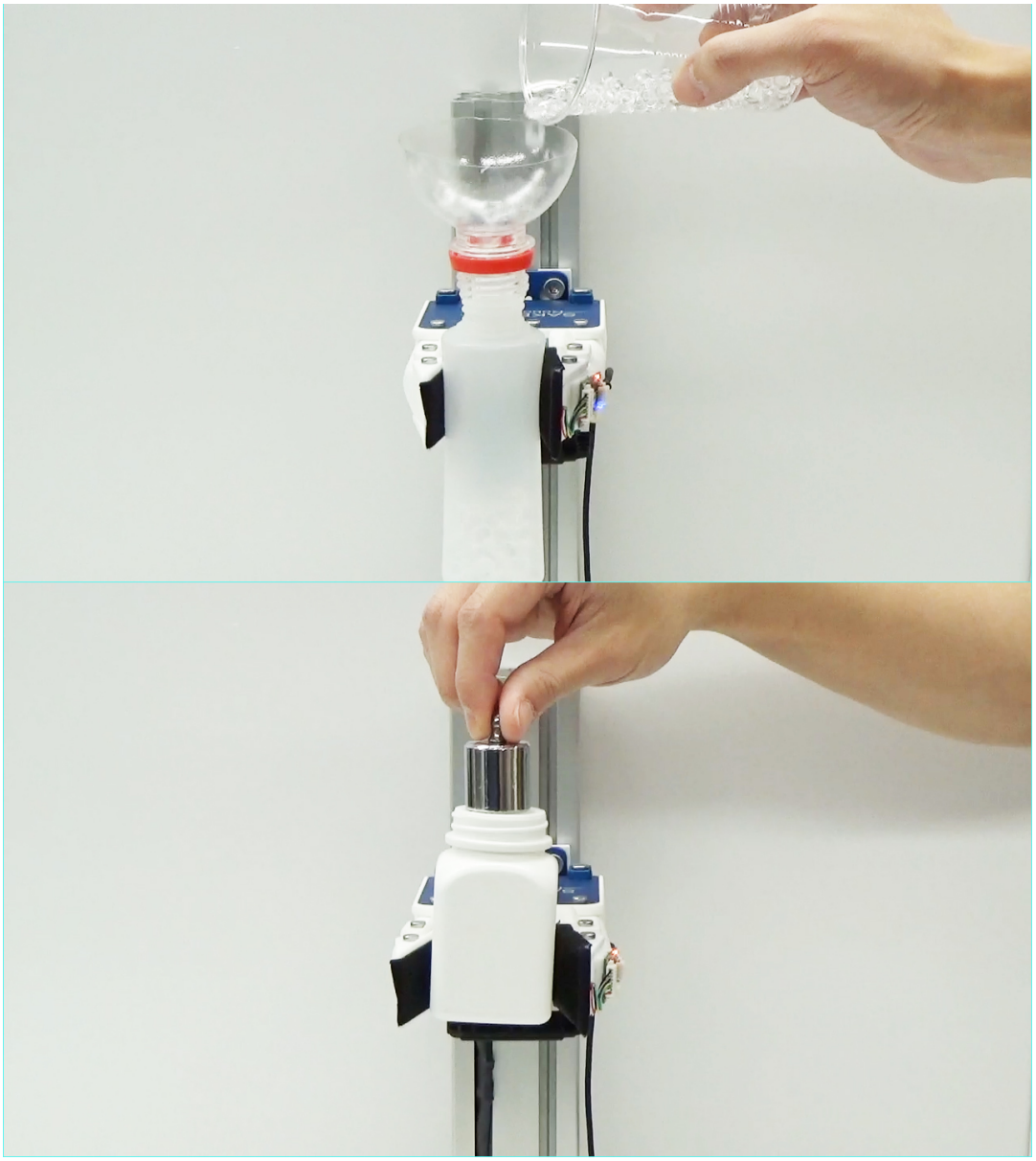

FIGURE 4.4: Some small pellets were poured into the cylindrical plastic bottle to increase its weight (top) and a 100 g of weight was dropped into the flat plastic bottle (bottom).

(ii) Response Time

A skin sensor with fast response is crucial for a safe manipulation. In this experiment, I investigate whether the skin sensor is fast enough to give an immediate response to the gripper. Similar to the previous experiment, this time I used a 43 x 43 mm plastic container with a flat surface as in Fig. 4.4 (bottom). The weight of the container is 17 g. I dropped a 100 g weight inside the container to produce a sudden shear force change in y-axis direction.

(4) Real-time Visualization

The visualization software was developed using a Siv3D Engine for Visual Studio 2015. The communication between the skin sensor and visualization software was done through TCP/IP. A python server was run to trigger the sensor and collecting all data at 100 Hz. The visualization software was running as a client. In Fig. 4.9, 4x4 black squares represent the tactile arrays of uSkin. In the center of each square, there is a yellow circle visualizing the 3D force. The diameter of the circle represents the amount of normal force applied and the circle displacements in x and y-axis represent the shear forces. Four objects with different shapes (30 mm ϕ ball, 20 mm ϕ bearing, 25 x 25 x 25 mm cube, and 20 mm ϕ x 100 mm cylinder) were used in this experiment.

4.4.3 Result

(1) Earth Magnetic Field Compensation

Fig 4.5 (bottom) shows the graph with the compensation algorithm. As can be seen, the external magnetic field influence generated by the earth magnetic field could be nullified.

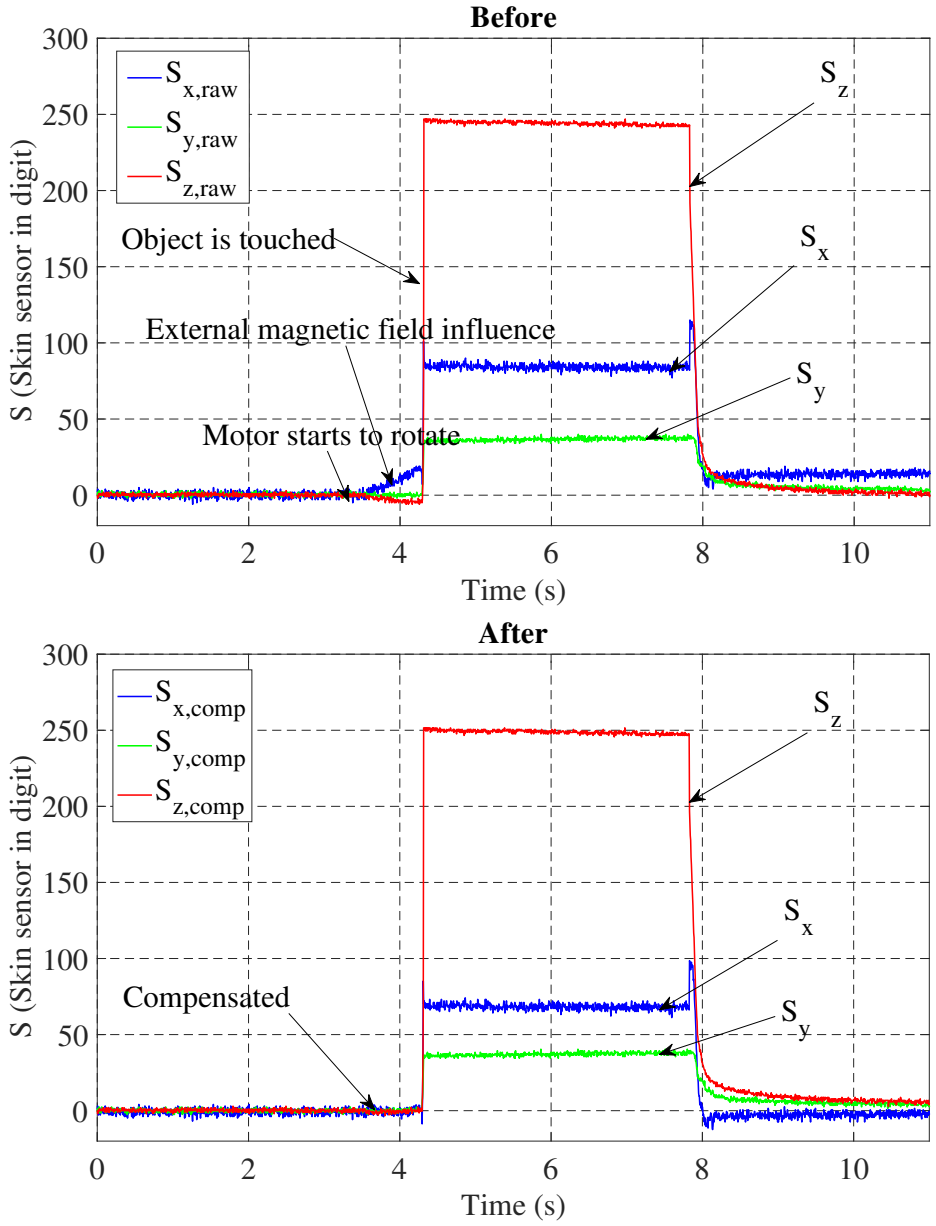

FIGURE 4.5: Skin sensor response before (top) and after compensation algorithm was implemented (bottom).

(2) Feedback Control

The experiment result can be seen in Fig. 4.6. The gripper successfully increased the normal force ($S_{avg,z}$) every time a change in $S_{avg,y}$ was detected, as can be seen in the graph. From this experiment I concluded that the skin sensor was sensitive enough to detect very small weight changes.

(3) Response Time

The correlation between the skin sensor and servo motor response can be seen in Fig. 4.7. After about 3 s, the gripper started to close until the plastic

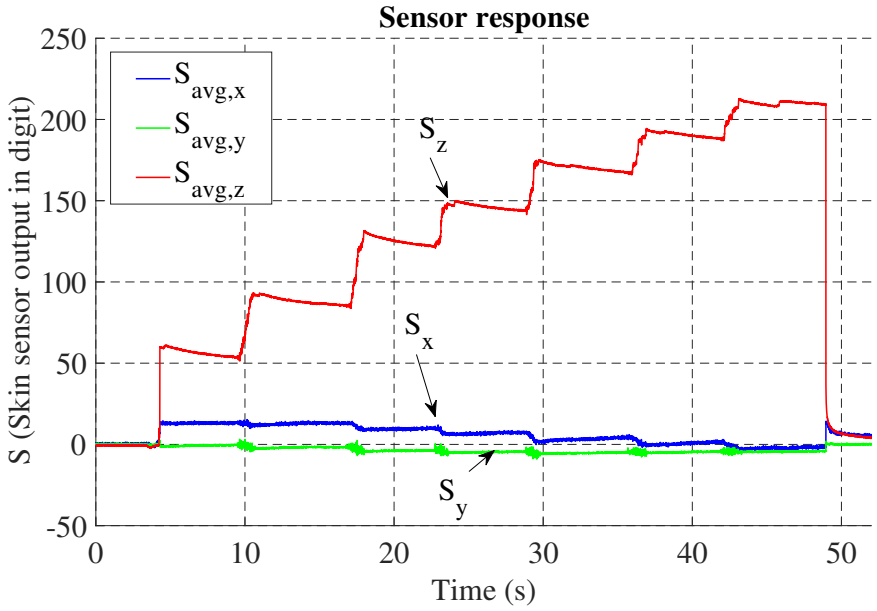

FIGURE 4.6: The response of the skin sensor when small balls were poured into the plastic bottle.

container was touched. We can see that even though the orientation of the skin sensor changed, $S_{avg,x}$, $S_{avg,y}$, $S_{avg,z}$ remained the same thanks to the compensation algorithm explained previously. At around 12 s, the weight was dropped. A closer look of the graph during this moment can be seen in Fig. 4.8. Time t = 0 ms is the moment where the weight was slightly touching the upper part of the plastic container. At t = 50 ms, a major change in y-axis was detected. Supposedly, at this moment the weight firstly landed at the bottom of the container. 5 ms after that, the servo motor started to rotate for increasing the grasping force. However, the servo motor requires 130 ms to reach the goal position. EzGripper employs an MX-64AR servo from Robotis. This servo motor has PID parameters that can be tuned for optimization. I presume that by tuning these parameters, a faster response from the servo motor can be possibly achieved. Meanwhile, by using the default PID parameters and maximum speed of the motor, the slip still could be prevented. I concluded that the new response time of my skin sensor at 200 Hz sampling rate is 5 ms. On overall response time of less than about 10 ms was also confirmed by analyzing a slow motion video. We can also see that all axes immediately returned to zero after the object was released. The skin sensor has a low hysteresis. In the figure we can see that x-axis change is higher than y-axis. The reason is because during the slipping, the object was rotating to the front as its center of gravity was shifted.

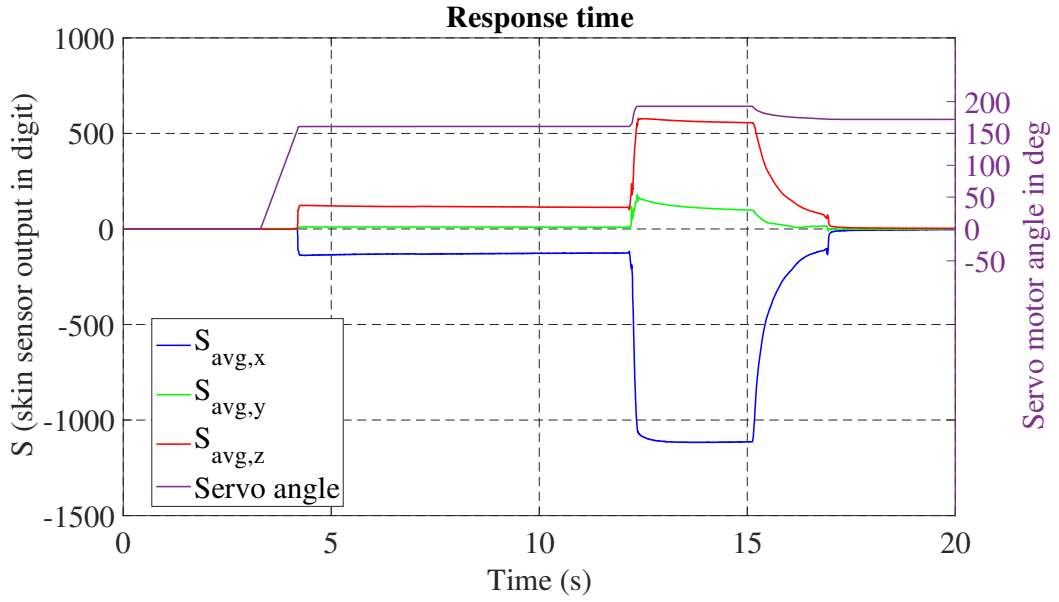

FIGURE 4.7: Servo motor response when a 100 g of weight was dropped

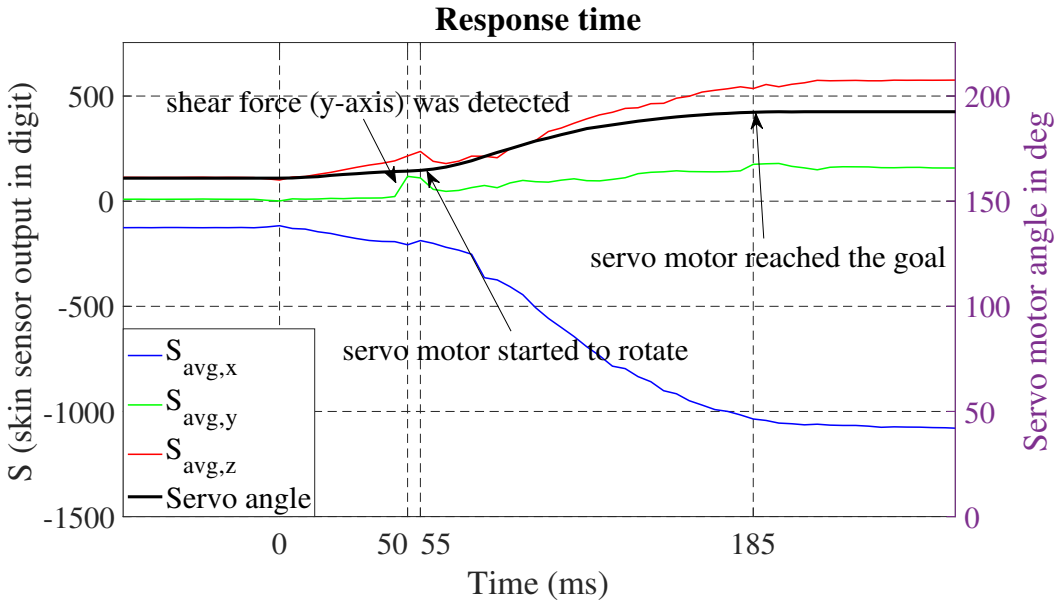

FIGURE 4.8: Closer look of Fig. 4.7

(4) Real-time Visualization

The sensor response can be seen in Fig. 4.9. In Fig. 4.9 (a), the chip no. 2 on SDA 2 has the most response compared to the rest. This is because the contact area of the spherical object is very small. However, we can also see that chip no. 1 on SDA 1 is slightly shifted from the center due to the shear force. The responses for objects with flat surface can be seen in Fig 4.9 (b) and (c).

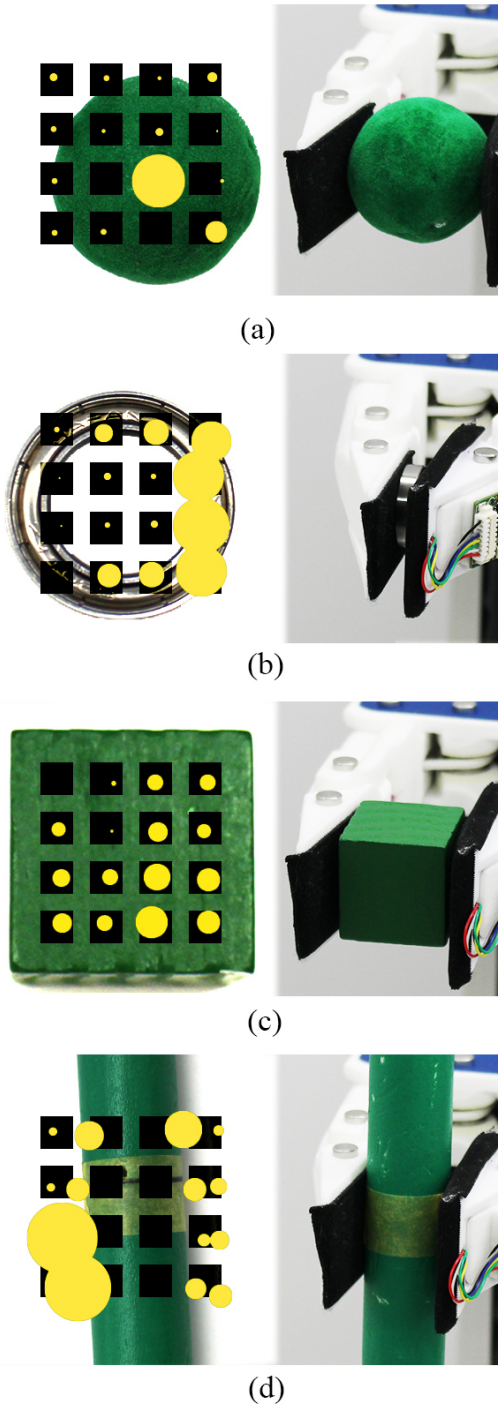

FIGURE 4.9: The skin sensor response when four different objects were grasped.

As the bearing has a hole in the middle, the outer sensors are more active. The pressures are distributed more to the front side due to the closing mechanism of the gripper (not parallel). This explains why the right side of the sensor is more active. Finally, in Fig. 4.9 (d) we can see that the curvature shape of the cylinder created shear forces displacing the circles to the left

and right side. From this experiment, we can see that shear forces can give more information such as identifying the contour of the object. Although object classification is not the main concern of this research, this result indicates that my skin sensor data can potentially be used for this kind of tasks.

4.4.4 Discussion

The sensor I used in this chapter is similar to the one I introduced in Chapter 3.5. However, this time I integrate the sensor to EzGripper from Sake Robotics[1] and slightly adjust the shape to fit the gripper. Here, the full implementation of uSkin to perform a feedback control using a servo motor is demonstrated for the first time. Tactile sensors based on a magnetic field sensing are usually sensitive enough to detect the earth magnetic field. Therefore, the sensor's measurement can change in respect to its orientation.

The main contributions of this work are that 1) I implement an algorithm for compensating the sensor from earth magnetic field influence, 2) improve the sensor's sampling frequency to achieve a faster response time, 3) integrate the sensor in a robot gripper and implement a slip prevention algorithm using a distributed 3-axis skin sensor.

[1] https://sakerobotics.com/

4.5 Implementation in iCub

4.5.1 Hardware Description

The PCB module covered with the skin (uSkin module presented in Section 3.4) was mounted into iCub's hand. I used VHB, a strong double-sided sticky tape from 3M. The thickness of this tape is about 1 mm thick. The iCub with uSkin can be seen in Fig. 4.10.

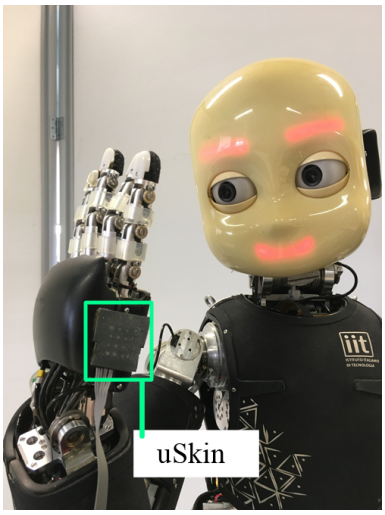

FIGURE 4.10: Humanoid robot, iCub, and uSkin mounted on its hand.

4.5.2 Evaluation Method

Object shapes exploration was conducted by using uSkin mounted on iCub's hand. iCub was configured to push objects in eight different locations with a particular force within the optimal measurement range of the skin sensor. I utilized a compliance control for the three shoulder joints (pitch, roll, yaw) and on the elbow joint. A position control was implemented for other joints. There are four objects with different shapes (named as arc, flat, wave, and saw) used in this experiment. All objects have the same length and width (5 x 3 cm) when seen from above. Fig. 4.11 (bottom) shows the whole pushing procedure. The overlap of the displacement is 50% of the module size, resulting in all chips on SDA4 will always be on top of SDA1 of the previous step. For this reason, I remove all data from SDA1.

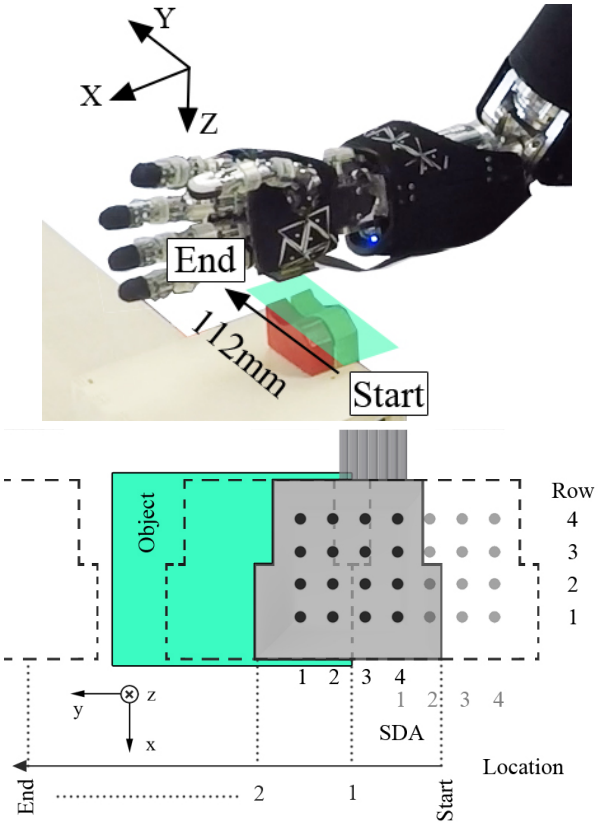

FIGURE 4.11: Experimental setup for shape exploration task (top). Illustration of exploration procedure (bottom).

4.5.3 Result

Fig. 4.12 shows the exploration results. Although the sensor measures 3-axis, only the data from z-axis will be provided here for easier comprehensibility. The graph shows the raw sensor measurements from eight exploration steps for four different objects. Based on this figure, we can see that the response from row no. 3 and 4 were the most significant. Furthermore, the result from flat object shows that SDA 2 and 3 responded stronger than SDA 1. Perhaps, two factors caused this phenomenon. First, when the iCub hand pushed the object, it was not perfectly perpendicular. Second, the skin sensor was uncalibrated, resulting in some taxels are more sensitive than others. Moreover, the y-axis displacement shown in the plots is only indicative, as iCub has compliance in its arms, which would explain some of the differences in the locations of the sensor response and the corresponding object features such as corners. Since the skin sensor has a T-shape, sometimes the edge of the sensor module was in contact with the object. When this happened, none of the sensors responded, which would explain the response of arc shape.

Despite all these factors, the first three objects provided very notable results. Wave and saw shapes have a similar result, which is understandable, as their shapes look similar. However, we can see that the saw shape has two peaks in the 30 - 50 mm. Meanwhile, the wave shape only has one. Perhaps, the sharp edge of the saw shape produced a higher pressure and could be detected.

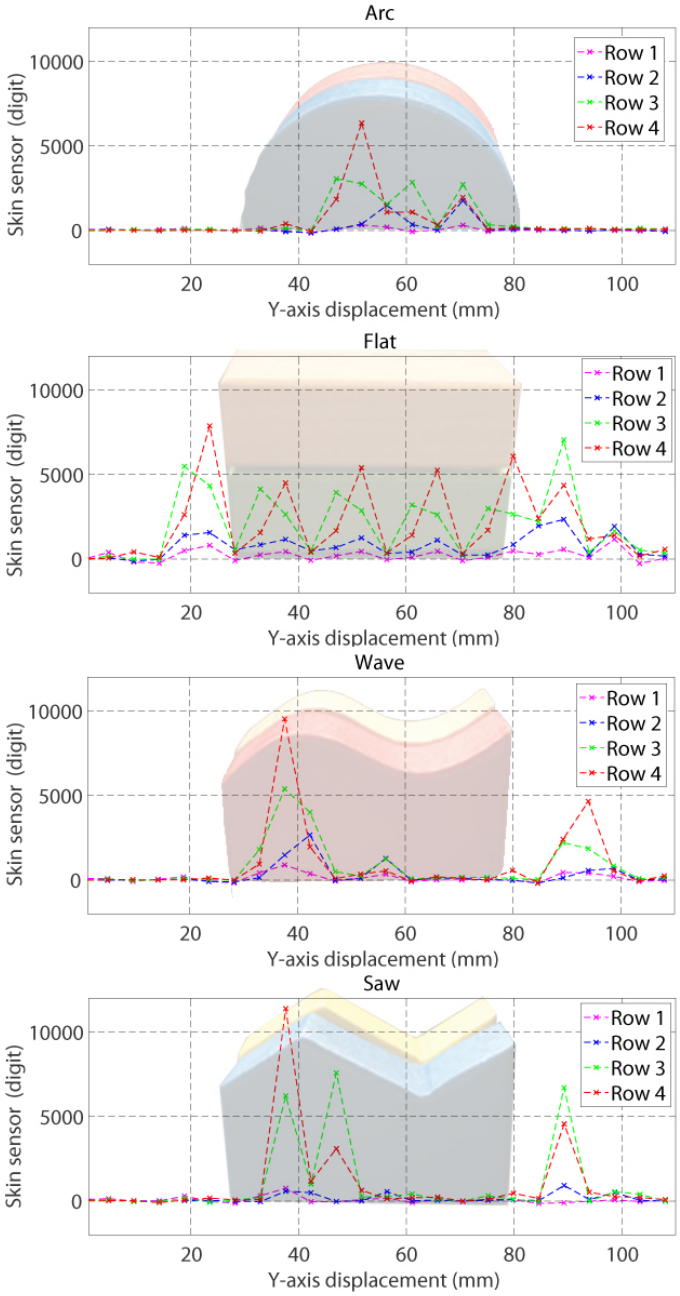

FIGURE 4.12: Shape exploration response (uncalibrated z-axis measurements at different positions: 0 mm - SDA 4, 4.7 mm - SDA 3, 9.4 mm - SDA 2, 14.1 mm - SDA 4 of second exploration step, and so on.

4.5.4 Discussion

Although iCub is already equipped with compact and distributed skin sensors [49], they can only measure 1-axis. Meanwhile, uSkin provides 3-axis force measurements. uSkin that is used in this section is originally designed for Allegro Hand. However, this section proofs that it can be easily adapted for iCub without further hardware modification. This is possible because uSkin has compact readout electronics, few numbers of wires, and lightweight. The previous section also shows that it can be integrated into EzGripper. Therefore, it could be demonstrated that easy integration is one of the features that uSkin has.

4.6 Conclusion of this chapter

1. This chapter proofs that uSkin can be integrated on various robots (Allegro Hand, EzGripper, and iCub).

2. I found that the earth magnetic field could affect the sensor's readout. However, a compensation algorithm could be implemented to nullify the influence.

3. This chapter shows that shear forces information is vital to prevent an object from slipping. Most importantly, uSkin's response time is fast enough for preventing objects from slipping (5 ms at 200 Hz of the sampling rate). I confirmed that the sensor could achieve 250 Hz of sampling rate per axis. I showed that the grasping force of the gripper could be increased corresponding to the weight of the object using the shear force information. The skin sensor in this section was not calibrated, but could be by using the technique presented in the previous chapter.

4. uSkin was used for tactile exploration tasks. Four different objects were used, and all of them show a distinct result. It gives an idea that the data can be possibly used for a machine learning purpose such as a classification task.

Chapter 5

Conclusion

5.1 Background

This section will explain achievements from each chapter, the limitation of this research, and possible future works.

5.2 Research achievements

This thesis presented the development of uSkin, a compact, distributed, 3-axis soft skin sensor.

In Chapter 2, the sensor was successfully developed using MLX-90393, a small 3D Hall Effect sensor that is commercially available from Melexis. The manufacturing process is straightforward, making the production low cost and efficient. A mature characterization is conducted for the first time for such kind of tactile sensor. In Chapter 3, it was shown that the sensor can be used for distributed 3-axis sensing with a sub-centimeter spatial density. uSkin was develop both for flat as well as curved surfaces, in particular uSkin sensors were also integrated in the multicurved Allegro hand fingertip.

Initially, uSkin was developed using silicone in a bulk structure, resulting in severe crosstalk between the measurement axes due to the incompressibility of the silicone. Therefore, the air gap structure was developed and the crosstalk could be reduced to about 4%. The structure is also like a bump which can increase the sensitivity of the sensor to measure shear forces.

Aside from the new skin structure, I also implemented iCub's MTB3 microcontrollers for uSkin to increase the sampling frequency, reduce the size of the readout electronics, and to minimize the required wires.

Finally, I did first tests with uSkin mounted on an iCub, and showed that the sensors can be used to differentiate object shapes.

5.3 Current Limitations

As the sensor uses magnetic field changes as its sensing principle, other magnetic fields (including the earth magnetic field), nearby magnets, or nearby ferromagnetic materials can influence the sensor measurements. Reference measurements could be used to offset such influences, and I had preliminary success with offsetting the influence of the earth magnetic field. Furthermore, the purpose of the sensor was to grasp and manipulate everyday objects, and most of them do not include ferromagnetic materials or magnets, and therefore uSkin can already be used for a wide variety of relevant objects.

5.4 Future Works

In future work I plan to calibrate all sensors using a motorized x-y stage. This improved calibration setup could be also used for more detailed analysis of the response of the sensor to shear forces.

Furthermore, I would like to improve the sensor's performance such as lowering the hysteresis and crosstalk. A proper material selection needs to be conducted for this. Moreover, a simulation can also be done.

Currently, uSkin has 4.7 mm spatial density. However, this can be reduced even more by using a smaller magnetometer. For example, by using an MMC341 (1.6x1.6x0.6 mm) from MEMSIC, a 2.4 mm spatial distance can be possibly achieved. Therefore, in 21x26 mm area, 64 3D magnetometer chips can be mounted.

Magnetic compensation will be implemented in the future to eliminate interference from magnetic objects. Magnetic shielding could be implemented for this. Alternatively, another reference sensor (magnetometer) can be mounted on the skin sensor module to generate compensation parameters.

Lastly, uSkin performance for manipulating an object will also be evaluated. This can be done through a collaboration with other Sugano Laboratory members for example.

Bibliography

[1] R. D. Howe, "Tactile sensing and control of robotic manipulation", *Advanced Robotics*, vol. 8, no. 3, pp. 245–261, 1993.

[2] K. Or, A. Schmitz, S. Funabashi, M. Tomura, and S. Sugano, "Development of robotic fingertip morphology for enhanced manipulation stability", in *2016 IEEE International Conference on Advanced Intelligent Mechatronics (AIM)*, 2016, pp. 25–30. DOI: 10.1109/AIM.2016.7576738.

[3] K. Or, M. Tomura, A. Schmitz, S. Funabashi, and S. Sugano, "Position-force combination control with passive flexibility for versatile in-hand manipulation based on posture interpolation", in *2016 IEEE/RSJ International Conference on Intelligent Robots and Systems (IROS)*, 2016, pp. 2542–2547. DOI: 10.1109/IROS.2016.7759395.

[4] K. Or, S. Morikuni, S. Ogasa, S. Funabashi, A. Schmitz, and S. Sugano, "A study on fingertip designs and their influences on performing stable prehension for robot hands", in *2016 IEEE-RAS 16th International Conference on Humanoid Robots (Humanoids)*, 2016, pp. 772–777. DOI: 10.1109/HUMANOIDS.2016.7803361.

[5] A. Schmitz, Y. Bansho, K. Noda, H. Iwata, T. Ogata, and S. Sugano, "Tactile object recognition using deep learning and dropout", in *2014 IEEE-RAS International Conference on Humanoid Robots*, 2014, pp. 1044–1050. DOI: 10.1109/HUMANOIDS.2014.7041493.

[6] K. Kojima, T. Sato, A. Schmitz, H. Arie, H. Iwata, and S. Sugano, "Sensor prediction and grasp stability evaluation for in-hand manipulation", in *2013 IEEE/RSJ International Conference on Intelligent Robots and Systems*, 2013, pp. 2479–2484. DOI: 10.1109/IROS.2013.6696705.

[7] S. Funabashi, A. Schmitz, T. Sato, S. Somlor, and S. Sugano, "Robust in-hand manipulation of variously sized and shaped objects", in *2015 IEEE/RSJ International Conference on Intelligent Robots and Systems (IROS)*, 2015, pp. 257–263. DOI: 10.1109/IROS.2015.7353383.

[8] S. Funabashi, T. Sato, A. Schmitz, and S. Sugano, "Feature extraction by deep learning for improved in-hand manipulation", *The Abstracts of the international conference on advanced mechatronics : toward evolutionary fusion of IT and mechatronics : ICAM*, vol. 2015.6, pp. 31–32, 2015. DOI: 10.1299/jsmeicam.2015.6.31.

[9] R. S. Dahiya, G. Metta, M. Valle, and G. Sandini, "Tactile sensing—from humans to humanoids", *IEEE Transactions on Robotics*, vol. 26, no. 1, pp. 1–20, 2010.

[10] M. R. Cutkosky, R. D. Howe, and W. R. Provancher, "Force and tactile sensors", in *Springer Handbook of Robotics*, Springer, 2008, pp. 455–476.

[11] H. R. Nicholls and M. H. Lee, "A survey of robot tactile sensing technology", *The International Journal of Robotics Research*, vol. 8, no. 3, pp. 3–30, 1989. DOI: 10.1177/027836498900800301.

[12] S. C. Jacobsen, I. McGammon, K. B. Biggers, and R. P. Phillips, "Design of tactile sensing systems for dextrous manipulators", *IEEE Control Systems Magazine*, vol. 8, no. 1, pp. 3–13, 1988.

[13] P. Puangmali, K. Althoefer, L. D. Seneviratne, D. Murphy, and P. Dasgupta, "State-of-the-art in force and tactile sensing for minimally invasive surgery", *IEEE Sensors Journal*, vol. 8, no. 4, pp. 371–381, 2008.

[14] B. D. Argall and A. G. Billard, "A survey of tactile human–robot interactions", *Robotics and Autonomous Systems*, vol. 58, no. 10, pp. 1159 – 1176, 2010, ISSN: 0921-8890. DOI: https://doi.org/10.1016/j.robot.2010.07.002. [Online]. Available: http://www.sciencedirect.com/science/article/pii/S0921889010001375.

[15] D. Silvera-Tawil, D. Rye, and M. Velonaki, "Artificial skin and tactile sensing for socially interactive robots: A review", *Robotics and Autonomous Systems*, vol. 63, pp. 230 –243, 2015, Advances in Tactile Sensing and Touch-based Human Robot Interaction, ISSN: 0921-8890. DOI: https://doi.org/10.1016/j.robot.2014.09.008. [Online]. Available: http://www.sciencedirect.com/science/article/pii/S0921889014001833.

[16] Z. Kappassov, J.-A. Corrales, and V. Perdereau, "Tactile sensing in dexterous robot hands—review", *Robotics and Autonomous Systems*, vol. 74, pp. 195–220, 2015.

[17] R. S. Dahiya, P. Mittendorfer, M. Valle, G. Cheng, and V. J. Lumelsky, "Directions toward effective utilization of tactile skin: A review", *IEEE Sensors Journal*, vol. 13, no. 11, pp. 4121–4138, 2013.

[18] D. Göger, N. Gorges, and H. Wörn, "Tactile sensing for an anthropomorphic robotic hand: Hardware and signal processing", *2009 IEEE International Conference on Robotics and Automation*, pp. 895–901, 2009.

[19] B. Choi, S. Lee, H. R. Choi, and S. Kang, "Development of anthropomorphic robot hand with tactile sensor : Skku hand ii", in *2006 IEEE/RSJ International Conference on Intelligent Robots and Systems*, 2006, pp. 3779–3784. DOI: 10.1109/IROS.2006.281763.

[20] J. Jockusch, J. Walter, and H. Ritter, "A tactile sensor system for a three-fingered robot manipulator", in *Proceedings of International Conference on Robotics and Automation*, vol. 4, 1997, 3080–3086 vol.4. DOI: 10.1109/ROBOT.1997.606756.

[21] K. Hosoda, Y. Tada, and M. Asada, "Anthropomorphic robotic soft fingertip with randomly distributed receptors", *Robotics and Autonomous Systems*, vol. 54, no. 2, pp. 104 –109, 2006, Intelligent Autonomous Systems, ISSN: 0921-8890. DOI: https://doi.org/10.1016/j.robot.2005.09.019. [Online]. Available: http://www.sciencedirect.com/science/article/pii/S092188900500148X.

[22] T. Minato, Y. Yoshikawa, T. Noda, S. Ikemoto, H. Ishiguro, and M. Asada, "Cb2: A child robot with biomimetic body for cognitive developmental robotics", in *2007 7th IEEE-RAS International Conference on Humanoid Robots*, 2007, pp. 557–562. DOI: 10.1109/ICHR.2007.4813926.

[23] "Touchense.", [Online; accessed 8-February-2019].

[24] "ShokacChip^{TM}Product outline.", [Online; accessed 8-February-2019].

[25] S. Saga, T. Morooka, H. Kajimoto, and S. Tachi, "High-resolution tactile sensor using the movement of a reflected image", in *Proceedings of Eurohaptics*, 2006, pp. 81–86.

[26] W. Yuan, R. Li, M. A. Srinivasan, and E. H. Adelson, "Measurement of shear and slip with a gelsight tactile sensor", in *2015 IEEE International Conference on Robotics and Automation (ICRA)*, 2015, pp. 304–311. DOI: 10.1109/ICRA.2015.7139016.

[27] M. Ohka, A. Tsunogai, T. Kayaba, S. C. Abdullah, and H. Yussof, "Advanced design of columnar-conical feeler-type optical three-axis tactile sensor", *Procedia Computer Science*, vol. 42, pp. 17 –24, 2014, Medical and Rehabilitation Robotics and Instrumentation (MRRI2013), ISSN: 1877-0509. DOI: https://doi.org/10.1016/j.procs.2014.11.

028. [Online]. Available: http://www.sciencedirect.com/science/article/pii/S1877050914014665.

[28] "TacTip.", [Online; accessed 8-February-2019].

[29] T. Yoshikai, M. Hayashi, Y. Ishizaka, H. Fukushima, A. Kadowaki, T. Sagisaka, K. Kobayashi, I. Kumagai, and M. Inaba, "Development of robots with soft sensor flesh for achieving close interaction behavior", *Advances in Artificial Intelligence*, vol. 2012, p. 8, 2012.

[30] K. Yamada, K. Goto, Y. Nakajima, N. Koshida, and H. Shinoda, "A sensor skin using wire-free tactile sensing elements based on optical connection", in *Proceedings of the 41st SICE Annual Conference. SICE 2002.*, vol. 1, 2002, 131–134 vol.1. DOI: 10.1109/SICE.2002.1195198.

[31] "OnRobot OMD 3 Axis Sensors.", [Online; accessed 8-February-2019].

[32] H. Iwata and S. Sugano, "Whole-body covering tactile interface for human robot coordination", in *Proceedings 2002 IEEE International Conference on Robotics and Automation (Cat. No.02CH37292)*, vol. 4, 2002, 3818–3824 vol.4. DOI: 10.1109/ROBOT.2002.1014315.

[33] G. Cannata and M. Maggiali, "An embedded tactile and force sensor for robotic manipulation and grasping", in *5th IEEE-RAS International Conference on Humanoid Robots, 2005.*, 2005, pp. 80–85. DOI: 10.1109/ICHR.2005.1573549.

[34] G. Cannata and M. Maggiali, "Design of a tactile sensor for robot hands", in *Sensors: Focus on Tactile Force and Stress Sensors*, InTech, 2008.

[35] H. Iwata and S. Sugano, "Design of human symbiotic robot twendy-one", in *Robotics and Automation, 2009. ICRA'09. IEEE International Conference on*, IEEE, 2009, pp. 580–586.

[36] H Liu, P Meusel, N Seitz, B Willberg, G Hirzinger, M. Jin, Y. Liu, R Wei, and Z. Xie, "The modular multisensory dlr-hit-hand", *Mechanism and Machine Theory*, vol. 42, no. 5, pp. 612–625, 2007.

[37] L. B. Bridgwater, C. A. Ihrke, M. A. Diftler, M. E. Abdallah, N. A. Radford, J. M. Rogers, S. Yayathi, R. S. Askew, and D. M. Linn, "The robonaut 2 hand - designed to do work with tools", in *2012 IEEE International Conference on Robotics and Automation*, 2012, pp. 3425–3430. DOI: 10.1109/ICRA.2012.6224772.

[38] R. Platt, C. Ihrke, L. Bridgewater, D. Linn, R. Diftler, M. Abdallah, S. Askew, and F. Permenter, "A miniature load cell suitable for mounting on the phalanges of human-sized robot fingers", in *2011 IEEE International Conference on Robotics and Automation*, 2011, pp. 5357–5362. DOI: 10.1109/ICRA.2011.5980169.

[39] C. M. Oddo, M. Controzzi, L. Beccai, C. Cipriani, and M. C. Carrozza, "Roughness encoding for discrimination of surfaces in artificial active-touch", *IEEE Transactions on Robotics*, vol. 27, no. 3, pp. 522–533, 2011, ISSN: 1552-3098. DOI: 10.1109/TRO.2011.2116930.

[40] H. Takahashi, A. Nakai, N. Thanh-Vinh, K. Matsumoto, and I. Shimoyama, "A triaxial tactile sensor without crosstalk using pairs of piezoresistive beams with sidewall doping", *Sensors and Actuators A: Physical*, vol. 199, pp. 43 –48, 2013, ISSN: 0924-4247. DOI: https://doi.org/10.1016/j.sna.2013.05.002. [Online]. Available: http://www.sciencedirect.com/science/article/pii/S0924424713002069.

[41] K. Noda, K. Hoshino, K. Matsumoto, and I. Shimoyama, "A shear stress sensor for tactile sensing with the piezoresistive cantilever standing in elastic material", *Sensors and Actuators A: Physical*, vol. 127, no. 2, pp. 295 –301, 2006, MEMS 2005 Special Issue, ISSN: 0924-4247. DOI: https://doi.org/10.1016/j.sna.2005.09.023. [Online]. Available: http://www.sciencedirect.com/science/article/pii/S0924424705005534.

[42] K. Noda, K. Matsumoto, and I. Shimoyama, "Flexible tactile sensor sheet with liquid filter for shear force detection", in *2009 IEEE 22nd International Conference on Micro Electro Mechanical Systems*, 2009, pp. 785–788. DOI: 10.1109/MEMSYS.2009.4805500.

[43] T. Liu, Y. Inoue, and K. Shibata, "Design of low-cost tactile force sensor for 3d force scan", in *Sensors, 2008 IEEE*, IEEE, 2008, pp. 1513–1516.

[44] L. Viry, A. Levi, M. Totaro, A. Mondini, V. Mattoli, B. Mazzolai, and L. Beccai, "Flexible three-axial force sensor for soft and highly sensitive artificial touch", *Advanced materials*, vol. 26, no. 17, pp. 2659–2664, 2014.

[45] J. A. Dobrzynska and M. Gijs, "Polymer-based flexible capacitive sensor for three-axial force measurements", *Journal of Micromechanics and Microengineering*, vol. 23, no. 1, p. 015 009, 2012.

[46] M.-Y. Cheng, C.-L. Lin, Y.-T. Lai, and Y.-J. Yang, "A polymer-based capacitive sensing array for normal and shear force measurement", *Sensors*, vol. 10, no. 11, pp. 10 211–10 225, 2010.

[47] H.-K. Lee, J. Chung, S.-I. Chang, and E. Yoon, "Normal and shear force measurement using a flexible polymer tactile sensor with embedded multiple capacitors", *Journal of Microelectromechanical Systems*, vol. 17, no. 4, pp. 934–942, 2008.

[48] P. Maiolino, M. Maggiali, G. Cannata, G. Metta, and L. Natale, "A flexible and robust large scale capacitive tactile system for robots", *IEEE Sensors Journal*, vol. 13, no. 10, pp. 3910–3917, 2013, ISSN: 1530-437X. DOI: 10.1109/JSEN.2013.2258149.

[49] A. Schmitz, P. Maiolino, M. Maggiali, L. Natale, G. Cannata, and G. Metta, "Methods and technologies for the implementation of large-scale robot tactile sensors", *IEEE Transactions on Robotics*, vol. 27, no. 3, pp. 389–400, 2011.

[50] S. Somlor, A. Schmitz, R. S. Hartanto, and S. Sugano, "First results of tilted capacitive sensors to detect shear force", *Procedia Computer Science*, vol. 76, pp. 101–106, 2015.

[51] S. Somlor, R. S. Hartanto, A. Schmitz, and S. Sugano, "A novel triaxial capacitive-type skin sensor", *Advanced Robotics*, vol. 29, no. 21, pp. 1375–1391, 2015.

[52] S. Somlor, A. Schmitz, R. S. Hartanto, and S. Sugano, "A prototype force sensing unit for a capacitive-type force-torque sensor", in *2014 IEEE/SICE International Symposium on System Integration*, 2014, pp. 684–689. DOI: 10.1109/SII.2014.7028121.

[53] P. Mittendorfer and G. Cheng, "Integrating discrete force cells into multimodal artificial skin", in *2012 12th IEEE-RAS International Conference on Humanoid Robots (Humanoids 2012)*, 2012, pp. 847–852. DOI: 10.1109/HUMANOIDS.2012.6651619.

[54] K. Kim, Y. Sun, R. M. Voyles, and B. J. Nelson, "Calibration of multiaxis mems force sensors using the shape-from-motion method", *IEEE Sensors Journal*, vol. 7, no. 3, pp. 344–351, 2007, ISSN: 1530-437X. DOI: 10.1109/JSEN.2006.890141.

[55] P. Mittendorfer and G. Cheng, "Humanoid multimodal tactile-sensing modules", *IEEE Transactions on robotics*, vol. 27, no. 3, pp. 401–410, 2011.

[56] C. Ledermann, S. Wirges, D. Oertel, M. Mende, and H. Woern, "Tactile sensor on a magnetic basis using novel 3d hall sensor-first prototypes and results", in *Intelligent Engineering Systems (INES), 2013 IEEE 17th International Conference on*, IEEE, 2013, pp. 55–60.

[57] L. Jamone, G. Metta, F. Nori, and G. Sandini, "James: A humanoid robot acting over an unstructured world", in *Humanoid Robots, 2006 6th IEEE-RAS International Conference on*, IEEE, 2006, pp. 143–150.

[58] L. Jamone, L. Natale, G. Metta, and G. Sandini, "Highly sensitive soft tactile sensors for an anthropomorphic robotic hand", *IEEE sensors Journal*, vol. 15, no. 8, pp. 4226–4233, 2015.

[59] L. Natale and E. Torres-Jara, "A sensitive approach to grasping", in *Proceedings of the sixth international workshop on epigenetic robotics*, 2006, pp. 87–94.

[60] S. Youssefian, N. Rahbar, and E. Torres-Jara, "Contact behavior of soft spherical tactile sensors", *IEEE sensors Journal*, vol. 14, no. 5, pp. 1435–1442, 2014.

[61] W. Yuan, R. Li, M. A. Srinivasan, and E. H. Adelson, "Measurement of shear and slip with a gelsight tactile sensor", in *Robotics and Automation (ICRA), 2015 IEEE International Conference on*, IEEE, 2015, pp. 304–311.

[62] J. J. Clark, "A magnetic field based compliance matching sensor for high resolution, high compliance tactile sensing", in *Robotics and Automation, 1988. Proceedings., 1988 IEEE International Conference on*, IEEE, 1988, pp. 772–777.

[63] W. C. Nowlin, "Experimental results on bayesian algorithms for interpreting compliant tactile sensing data", in *Robotics and Automation, 1991. Proceedings., 1991 IEEE International Conference on*, IEEE, 1991, pp. 378–383.

[64] T. P. Tomo, S. Somlor, A. Schmitz, L. Jamone, W. Huang, H. Kristanto, and S. Sugano, "Design and characterization of a three-axis hall effect-based soft skin sensor", *Sensors*, vol. 16, no. 4, p. 491, 2016.

[65] E. Torres-Jara, I. Vasilescu, and R. Coral, "A soft touch: Compliant tactile sensors for sensitive manipulation", 2006.

[66] T. P. Tomo, W. K. Wong, A. Schmitz, H. Kristanto, A. Sarazin, L. Jamone, S. Somlor, and S. Sugano, "A modular, distributed, soft, 3-axis sensor system for robot hands", in *2016 IEEE-RAS Humanoids*, IEEE, 2016.

[67] T. P. Tomo, A. Schmitz, W. K. Wong, H. Kristanto, S. Somlor, J. Hwang, L. Jamone, and S. Sugano, "Covering a robot fingertip with uskin: A soft electronic skin with distributed 3-axis force sensitive elements for robot hands", *IEEE Robotics and Automation Letters*, vol. 3, no. 1, pp. 124–131, 2018. DOI: 10.1109/LRA.2017.2734965.

[68] T. P. Tomo, M. Regoli, A. Schmitz, L. Natale, H. Kristanto, S. Somlor, L. Jamone, G. Metta, and S. Sugano, "A New Silicone Structure for uSkin - a Soft, Distributed, Digital 3-axis Skin Sensor - and its Integration on the Humanoid Robot iCub", *IEEE Robotics and Automation Letters*, 2018.

[69] T. Paulino, P. Ribeiro, M. Neto, S. Cardoso, A. Schmitz, J. Santos-Victor, A. Bernardino, and L. Jamone, "Low-cost 3-axis soft tactile sensors for the human-friendly robot vizzy", in *IEEE International Conference on Robotics and Automation*, 2017.

[70] "Triaxis micropower magnetometer (magnetic field sensor).", [Online; accessed 8-February-2019].

[71] B. Davison, "Techniques for robust touch sensing design", *AN1334 Microchip Technology Inc*, p. 53, 2010.

[72] T. P. Tomo, W. K. Wong, A. Schmitz, H. Kristanto, S. Somlor, J. Hwang, and S. Sugano, "Snr modeling and material dependency test of a low-cost and simple to fabricate 3d force sensor for soft robotics", in *SII, 2016 IEEE*, IEEE, 2016.

[73] G. Cannata, M. Maggiali, G. Metta, and G. Sandini, "An embedded artificial skin for humanoid robots", in *Multisensor Fusion and Integration for Intelligent Systems, 2008. MFI 2008. IEEE International Conference on*, IEEE, 2008, pp. 434–438.

List of Publication

Related Publications

1. **T. P. Tomo**, M. Regoli, A. Schmitz, L. Natale, H. Kristanto, S. Somlor, L. Jamone, G. Metta and S. Sugano, "A New Silicone Structure for uSkin-a Soft, Distributed, Digital 3-axis Skin Sensor-and its Integration on the Humanoid Robot iCub," IEEE Robotics and Automation Letters, vol. 3, no. 3, pp. 2584-2591, July 2018, doi: 10.1109/LRA.2018.2812915.

2. **T. P. Tomo**, A. Schmitz, W. K. Wong, H. Kristanto, S. Somlor, J. Hwang, L. Jamone and S. Sugano, "Covering a Robot Fingertip with uSkin: a Soft Electronic Skin with Distributed 3-axis Force Sensitive Elements for Robot Hands," IEEE Robotics and Automation Letters, vol. 3, no. 1, pp. 124-131, Jan. 2018, doi: 10.1109/LRA.2017.2734965.

3. **T. P. Tomo**, S. Somlor, A. Schmitz, L. Jamone,W. Huang, H. Kristanto and S. Sugano, "Design and characterization of a three-axis hall effect based soft skin sensor," Sensors, vol. 16, no. 4, p. 491, 2016, doi:10.3390/s16040491.

4. **T. P. Tomo**, W. K. Wong, A. Schmitz, H. Kristanto, A. Sarazin, L. Jamone, S. Somlor and S. Sugano, "A modular, distributed, soft, 3-axis sensor system for robot hands," 2016 IEEE-RAS 16th International Conference on Humanoid Robots (Humanoids), Cancun, 2016, pp. 454-460, doi: 10.1109/HUMANOIDS.2016.7803315.

5. **T. P. Tomo**, W. K. Wong, A. Schmitz, H. Kristanto, S. Somlor, J. Hwang and S. Sugano, "SNR modeling and material dependency test of a low-cost and simple to fabricate 3D force sensor for soft robotics", 2016 IEEE/SICE International Symposium on System Integration (SII), Sapporo, 2016, pp. 428-433, doi: 10.1109/SII.2016.7844036.

6. **T. P. Tomo**, S. Somlor, A. Schmitz, S. Hashimoto, S. Sugano and L. Jamone "Development of a hall-effect based skin sensor", 2015 IEEE SENSORS, Busan, 2015, pp. 1-4, doi: 10.1109/ICSENS.2015.7370435.

Others

1. **T. P. Tomo**, A. Schmitz, G. Enriquez, S. Hashimoto and S. Sugano, "Wayang Robot with Gamelan Music Pattern Recognition," Journal of Robotics and Mechatronics, vol. 29, no. 1, pp. 137-145, Feb. 2017, doi: 10.20965/jrm.2017.p0137.

2. **T. P. Tomo**, G. Enriquez, and S. Hashimoto, "Indonesian puppet theater robot with gamelan music emotion recognition", 2015 IEEE International Conference on Robotics and Biomimetics (ROBIO), Zhuhai, 2015, pp. 1177-1182, doi: 10.1109/ROBIO.2015.7418931.

3. **T. P. Tomo**, G. Enriquez, S. Hashimoto, "Development of Wayang Puppet Theater Robot,"The 33rd annual conference of the Robotics Society of Japan (RSJ), AC2G1-02, 2015.

4. **T. P. Tomo**, A. Schmitz, W. K. Wong, H. Kristanto, S. Somlor, J. Hwang, L. Jamone, S. Sugano, "Implentation of a Soft, Distributed 3-Axis Skin Sensor System on a Robotic Hand," 2017 IEEE International Conference on Robotics and Automation (ICRA), Workshop on "Innovative Haptic Interfaces Emerging from Soft Robotics", Singapore, 2017.

5. H. Kristanto, P. Sathe, A. Schmitz, **T. P. Tomo**, S. Somlor and S. Sugano, "A Wearable Three-Axis Tactile Sensor for Human Fingertips," IEEE Robotics and Automation Letters, vol. 3, no. 4, pp. 4313-4320, Oct. 2018, doi: 10.1109/LRA.2018.2864669.

6. S. Funabashi, S. Morikuni, A. Geier, A. Schmitz, S. Ogasa, **T. P. Tomo**, S. Somlor and S. Sugano, "Object recognition through active sensing using a multi-fingered robot hand with 3D tactile sensors," 2018 IEEE/RSJ International Conference on Intelligent Robots and System (IROS), Madrid, 2018.

7. A.C. Holgado, J.A. Alvarez Lopez, A. Schmitz, **T. P. Tomo**, S. Somlor, L. Jamone, S. Sugano, "Electromagnet for a Soft, Distributed, Digital 3-Axis Skin Sensor," 2018 IEEE/RSJ International Conference on Intelligent Robots and Systems (IROS), Madrid, 2018.

8. K. Nakajima, K. Inoue, Y. Kuniyoshi, S. Somlor, **T. P. Tomo**, A. Schmitz, "Soft Keyboard: A Novel User Interface for Soft Devices," Proceedings of International Symposium on Nonlinear Theory and its Applications (NOLTA2018), pp. 147-150, 2018.

9. S. Somlor, A. Schmitz, H. Jinsun, T. P. Tomo and S. Sugano, "Development of a capacitive-type 6-axis force-torque sensor," 2017 IEEE SENSORS, Glasgow, 2017, pp. 1-3, doi: 10.1109/ICSENS.2017.8234153.

10. 小笠 駿，森國 秀，船橋 賢，アレクサンダー シュミッツ，ティト トモ，菅野 重樹，"多指ロボットハンドの動作情報と3 軸分布型触覚センサによる物体認識手法の提案"，日本機械学会，ROBOMECH2018.

11. H. Kristanto, **T. P. Tomo**, A. Schmitz, C. Wei, Y. Huang, C. Kuo, S. Sugano, “A Wearable Sensor for Fingertips That Can Measure 3-Axis Force”, ロボティクス・メカトロニクス講演会講演概要集, 2017, doi: 10.1299/jsmermd.2017.1A1-O03.

12. 黄 振善, ソムロア ソフォン, シュミッツ アレクサンダー, トモ ティト, 菅野 重樹, 新しいセンサ配置を取り入れた小型静電容量式6軸力センサの開発, ロボティクス・メカトロニクス講演会講演概要集, 2017, doi: 10.1299/jsmermd.2017.1A1-N03.

13. 黄 偉傑, 黄 振善, H. Kristanto, **T. P. Tomo**, S. Somlor, A. Schmitz, 菅野 重樹, (2016) ロボットハンド用マルチモーダ, 柔軟性を有する分散型3軸触覚センサの開発, 第１７回ＳＩＣＥシステムインテグレーション部門講演会 (SI 2016), Sapporo, Japan.